2 mf

NASA TECHNICAL MEMORANDUM

NASA TM X-71515

NASA TM X-71515

WIDE AREA COVERAGE RADAR IMAGING SATELLITE FOR EARTH APPLICATIONS

by Grady H. Stevens and James R. Ramler
Lewis Research Center
Cleveland, Ohio
February 1974

This information is being published in preliminary form in order to expedite its early release.

WIDE AREA COVERAGE RADAR IMAGING
SATELLITE FOR EARTH APPLICATIONS

CONTENTS

WIDE AREA COVERAGE RADAR IMAGING SATELLITE FOR EARTH APPLICATIONS

by Grady H. Stevens and James R. Ramler

Lewis Research Center
Cleveland, Ohio

ABSTRACT

A preliminary study was made of a radar imaging satellite for earth applications. A side-looking synthetic-aperture radar was considered and the feasibility of obtaining a wide area coverage to reduce the time required to image a given area was investigated. Two basic approaches were examined; low altitude sun-synchronous orbits using a multibeam/multifrequency radar system and equatorial orbits up to near-synchronous altitude using a single beam system. Surveillance and mapping of ice on the Great Lakes was used as a typical application to focus the study effort.

E-7903

INTRODUCTION

The National Aeronautics and Space Administration's continued interest in and support of space applications has resulted in recent years in significant advancements in developing technology for earth observations including resource surveys, meteorology, geology, oceanography, and environmental monitoring, all on a global scale. Weather imaging satellites, such as TIROS and NIMBUS, have been extremely useful to the advancement of the meteorological sciences. The first Earth Resources Technology Satellite (ERTS-1) launched on July 23, 1972 is providing impressive data on the earth's environment and its resources. Such programs are demonstrating the technology required for eventually establishing an operational system of earth observation satellites.

To date, observation satellites have operated in the UV, visible or IR spectrums. It is logical to consider complementing these systems with observations in the RF spectrum, in particular using radar systems. Some activities have already started in this area. For example, a microwave experiment operating at about 14 GHz was recently flown on Skylab to measure radar scattering cross section and passive microwave emissivity of land and sea and to determine signal correlation properties. Satellites in early mission definition phases include SEASAT to be launched about 1978 to demonstrate and test remote sensing instrumentation for use on oceanographic satellites; Earth Observatory Satellite (EOS) to be launched about 1978 as a follow-on to ERTS; and SEOS, an experimental synchronous earth observation

satellite to be launched about 1980 with active and passive microwave scanners for observing phenomena, such as flood situations, sea state and anomalous snow packs. The U.S. Navy is studying the feasibility of using radar imaging satellites to provide sea state and fleet status information.

While radar has been used for some time for a variety of detection and tracking applications, it has only been recently that its application to fine-resolution aerial mapping has been fully developed. The well-known capability of airborne radar to generate imagery at night and through cloud cover enhances the attractiveness of this technique.

Side-looking radar in which the earth is viewed at oblique angles is particularly suited for discerning surface features. It has been developed to the point where it is now a proven instrument for all-weather reconnaissance and ground mapping.

Concurrent with the development of side-looking airborne radar has been a growing interest in its potential for a wide variety of earth applications. These include surveillance and mapping of ice in shipping areas, such as the Great Lakes and Alaskan ports, scientific observation of the Arctic ice fields, ocean state surveillance, pollution detection and disaster assessment.

An investigation of the Great Lakes ice cover by the Radar and Optics Laboratory of the University of Michigan (ref. 1) using synthetic aperture radar suggested that a suitably designed radar system may have the capability to discriminate among a large variety of ice types. Such a system could potentially impact shipping and ice clearing operations in a major way and enhance the economics of the entire region.

The Lewis Research Center is currently conducting a demonstration program to develop a rapid all-weather ice information system for determining ice type and coverage on the Great Lakes for shipping and navigation purposes. This study is part of a multiagency demonstration program in response to Public Law 91-611 passed by Congress in 1970 which authorized a 3-year demonstration program for determining the feasibility of extending the Great Lakes shipping season.

During the 1972-73 winter season an AN/APS-94C Side-Looking Airborne Radar (SLAR) installed in a Lewis Research Center OV-1B aircraft was flown over Lake Erie and the adjacent Great Lakes to obtain radar imagery of the ice cover (ref. 2). Results to date have been excellent and it is planned to continue this project through the 1973-74 winter season. It is anticipated that visual and automatic methods will be developed for interpreting this imagery for ice type, distribution, thickness, and motion. As an aid for developing these interpretive methods, extensive "ground truth" and low altitude visual and thermal imagery are acquired simultaneously with the radar imagery. The eventual use of a radar imaging satellite to collect such information is a clear possibility.

Any serious attempt to extend the general shipping season beyond the present duration of about 8 months must begin with a modern updated system which provides, as often as needed, a map of the ice coverage and ice type distribution everywhere on the lakes. At present, only the most primitive means are used to provide this information and, unfortunately, no agency exists which recognizes as part of its mission, the upgrading of existing methods. Such an upgrading requires the type of technology already developed and being developed by NASA.

This report covers the results of a preliminary feasibility study of a radar imaging satellite for earth applications. The purpose of this study was to scope the problems associated with radar imaging from orbital altitudes, to grossly define the requirements of a radar imaging satellite and to assess the technical feasibility of such a system.

A side-looking, synthetic aperture radar was considered and the feasibility of obtaining a wide area coverage (large swath width) to reduce the time required to image a given area was investigated. Two basic approaches were examined; low altitude sun-synchronous orbits using a multi-beam radar system and equatorial orbits up to near-synchronous altitude to reduce the beams required. While such a satellite would likely have a multi-application role, surveillance and mapping of ice on the Great Lakes was used to focus the study effort.

Future studies will be needed to identify other potential users of the imagery and to determine what applications are practical. The costs and benefits associated with these applications will need to be defined along with the capabilities of alternate approaches such as aircraft, in situ observations, etc. to completely assess the merits of a radar imaging satellite.

SUMMARY

A preliminary study was made of a radar imaging satellite for earth applications. A side-looking, synthetic aperture radar was considered and the feasibility of obtaining a wide area coverage (large swath width) to reduce the time required to image a given area was investigated. Short response time would be necessary for a number of applications, such as ice surveillance in shipping areas, ocean state surveillance and pollution monitoring.

This study was conducted in support of the Lewis Research Center's participation in a multiagency demonstration program to determine the feasibility of extending the Great Lakes shipping season. Lewis is currently flying an AN/APS-94C Side-Looking Airborne Radar (SLAR) over Lake Erie and the adjacent Great Lakes to develop a rapid all-weather ice information system for determining ice type and coverage on the Great Lakes for shipping and navigation purposes. Consequently, surveillance and mapping of ice on the Great Lakes was used as a typical application to focus the satellite study effort. For ice imaging the conditions being surveyed can be quite changeable due to current, winds, temperature, etc. and it would be necessary to obtain a complete image in as short a time as possible (daily if possible) to effectively aid navigation and ice control operations. However, it is obvious that this single application would not justify a dedicated satellite and that it would likely perform a multiapplication role.

The purpose of this study was to scope the problems associated with wide swath radar imaging from orbital altitudes, to grossly define the requirements of such a satellite and to assess its technical feasibility.

Two basic approaches were examined; low altitude sun-synchronous orbits using a multibeam/multifrequency radar system and equatorial orbits up to near-synchronous altitude to reduce the number of beams required. Equatorial orbits do not appear to be a practical solution. Two equatorial orbits were considered in some detail; one at about 6400 km altitude and another at about 14,000 km.

The 6400 km orbit "laps" the earth five times daily thus allowing a daily image to be constructed from a mosaic of five consecutive passes. Radar beam swath widths of about 250 km are achievable at the latitude of the Great Lakes with such an equatorial satellite so that an area the size of the Great Lakes (about 900 km north to south) could be mapped in five or even four passes. For the single application of mapping the Great Lakes (or any area at the same latitude) a single beam/single frequency synthetic aperture radar system would be required with an average power requirement of about 400 watts.

However, an equatorial orbit at 6400 km altitude would place the satellite in the midst of the most intense trapped proton radiation belt and a power source other than solar cells (e.g., an RTG) would be required. Other electronic components would need radiation protection, thus incurring a weight penalty. This system is judged to be relatively complex and costly and does not appear to be an attractive solution. However, this approach would need more detailed study than can be given in this report to adequately assess its feasibility.

An alternate approach was studied in which the orbit altitude would be high enough so that solar cells could be adequately shielded. An altitude of about 14,000 km was chosen. At this altitude, daily imaging with a single beam/single frequency radar is no longer possible without resorting to

antennas in excess of 30 meters. The required average power for imaging at the latitude of the Great Lakes would be increased to about 2.3 kw. The satellite would "lap" the earth twice daily. At the Great Lakes, swath widths of 280-420 km appear feasible depending on antenna size. It would take from 3-4 days to map an area the size of the Great Lakes with the mosaic technique. Battery backup power does not appear practical for eclipse periods due to the high daily energy demand.

Equatorial orbits do not allow global coverage thus limiting other potential applications. Coverage of a range of latitudes would require a multibeam/multifrequency synthetic aperture radar and a slewed antenna. In addition, coverage at the lower latitudes results in high radar beam incidence angles. In order to maintain a constant range resolution as the latitude is decreased the power would need to be increased markedly up to the multikilowatt range. Thus, the lowest latitude covered would determine the power requirement.

Sun-synchronous orbits around 1000 km altitude appear to be the best approach to obtaining wide swath coverage. However, a multibeam/multifrequency synthetic aperture radar system will need to be developed. Daily coverage of an area the size of the Great Lakes does not appear practical since the large number of beams required (approximately 12) is not consistent with the required antenna range dimension of about 3 meters. Coverage at 2-day or 3-day intervals appears feasible. This would require six beams and four beams respectively. The average power required would be about 600 and 400 watts respectively.

The 3-day and 2-day coverage cases are summarized below for an X-band radar with a resolution of 100 meters x 100 meters and a receiver effective noise temperature of 500°K.

Sun-Synchronous Orbits

Coverage Period	3-day	2-day
Altitude, km	1011.5441	1072.2403
Period, hours	1.75610	1.77778
Inclination, deg	99.5310	99.8105
Average power, watts	400	600
Orbits per 24 hours	13-2/3	13-1/2
Orbit track separation in longitude, deg	8.7805	13.3333
Orbit track separation at equator, km	952.0	1443.5
Orbit track separation at 45 deg latitude, km	655.5	995.2
Beams required	4	6
Total achievable swath width, km	436	654
Antenna size, length x width, meters	10 x 3	10 x 3

Sun-synchronous orbits can obtain global coverage, thus allowing potentially more applications than an equatorial orbit. Antenna slewing would not be required since all targets eventually come into view.

Future studies are needed to define this system in more depth. Particular attention should be given to assessing the feasibility of a multibeam/multifrequency synthetic aperture radar and the possibility of using a large number of beams such as 12 to allow daily coverage of an area the size of the Great Lakes. In addition, studies are needed to identify other potential users and to determine what applications are practical. The costs and

benefits associated with these applications need to be defined along with the capabilities of alternate approaches such as aircraft, in situ observation, etc. to adequately assess the merits of a radar imaging satellite.

ORBIT CONSIDERATIONS

A. General

Radar imaging from a satellite is basically a different and in many ways technically more demanding application than using aircraft mounted radar. Because of the higher altitude, considerably higher RF power levels are required. In addition, some satellite orbits result in a much higher ground velocity than an aircraft which can severely limit the maximum ground area covered on any one pass for a given set of parameters such as image resolution, RF power, etc.

Initial rough estimates of the radiated RF power required indicated that it could easily be on the order of several kilowatts so that it is important that a reasonably optimum system be devised to limit the power required to a practically achievable value. In general, the lower the altitude the lower will be the power required (all other things being equal). This suggested that one class of orbits to be considered should be low earth orbits and in particular, sun-synchronous orbits. Sun-synchronous orbits allow the satellite to remain in more or less continuous sunlight so that the relatively high power levels required can be obtained from solar cells on a nearly continuous basis. One major problem that low sun-synchronous orbits have, however, is that the velocity of the satellite (or radar beam) relative to the earth's surface is quite high (approximately orbital velocity). This severely limits the ability of the radar system to obtain a good image resolution unless the radar beam is restricted to a fairly small swath as it sweeps across the earth's surface. This is discussed in detail in the section dealing with Radar Considerations. This swath could be extended by using a multi-beam system with an associated increase in the RF power required. However, such a system may be complex and costly to implement.

One possible means for avoiding these problems is to reduce the satellite's velocity relative to the earth's surface thereby improving the ability of the radar system to cover a much wider swath while retaining the desired image resolution. This would suggest relatively high equatorial orbits up to near-geosynchronous altitude where the earth-relative velocity could be tailored to some desired value. (A geosynchronous equatorial orbit has no earth-relative velocity and could not be used since the radar depends on a Doppler effect for resolution.) As the orbit altitude is increased a wide swath width can be obtained with fewer beams or even a single beam system thus reducing the power required as the number of beams is reduced. However, at the same time the power will increase as the altitude is increased. It then becomes a matter of trading off these effects to find an optimum equatorial orbit.

The following sections will discuss some of the factors to be considered for the two basic types of orbits that seem feasible: (1) low sun-synchronous and (2) equatorial.

B. Sun-Synchronous Orbits

A sun-synchronous orbit is defined as an orbit which has a nodal precession rate equal in magnitude and direction to the earth's mean rate of revolution about the sun, 1.991×10^{-7} rad/sec (0.9856 deg/day). The earth-sun-satellite geometry is shown in Figure 1. This figure depicts a geocentric coordinate system in which the X-axis is directed toward the vernal equinox, the Z-axis is directed toward the north celestial pole, and the Y-axis lies in the equatorial plane forming a right-handed coordinate system with the X and Z axes. The orientation of the orbit plane is described by:

a. The node (Ω_a) in the equatorial plane measured eastward from the vernal equinox to the ascending node of the orbit plane.

b. The inclination (I) measured in a counterclockwise direction at the ascending node from the equatorial plane to the orbit plane.

The ecliptic plane is the plane of the motion of the sun as seen from the center of the earth. The obliquity of the ecliptic (ϵ) is the angle between the ecliptic and equatorial planes. The position of the sun in the ecliptic plane is described by the celestial longitude of the sun (λ) which is measured eastward from the vernal equinox to the sun. The position of the satellite in the orbit plane is described by the argument of latitude (u) which is measured from the ascending node to the satellite in the direction of motion.

The desired nodal precession of the satellite orbit can be accomplished by utilizing the effects of earth's oblateness. An analytical expression for the secular rate of change of nodes of an orbit can be obtained by considering only the terms through the second harmonic in the potential function of the oblate earth. The following expression is obtained:

$$\dot{\Omega}_a \approx -\sqrt{\mu}\, J R_e^2 \,(R_e + h)^{-7/2} \cos I \quad \text{for } 0 \leq I \leq 2\pi \qquad (1)$$

where

μ = gravitational constant of earth, 398601.2 $\frac{km^3}{sec^2}$

J = coefficient of second harmonic in gravitational potential function, 1.62405×10^{-3}

R_e = earth equatorial radius, 6378.160 km

h = altitude of satellite above equatorial radius

I = orbit inclination

For inclinations greater than $\frac{\pi}{2}$ rad (retrograde orbits), $\dot{\Omega}_a$ is positive, which results in a precession (eastward movement) of the node. This is the desired direction to keep the orbit plane in a proper position relative to the sun. Inclinations less than $\frac{\pi}{2}$ (posigrade orbits) will result in a regression (westward movement) of the orbit plane. Perturbations due to the oblateness of the earth on other orbital elements such as inclination, eccentricity, and semimajor axis are small and periodic with no resultant secular change.

A plot of equation (1) is shown in Figure 2 for the desired precession rate of 1.991×10^{-7} rad/sec. Sun-synchronous orbits about the earth do not exist above 5974.7 km (3226.1 n mi). It is obvious that for relatively low earth orbits (altitudes less than 2000 km say) the orbits will be nearly polar.

Consider the geometry (Figure 3) of a satellite in a nearly polar retrograde circular orbit about the earth. The orbital angular velocity vector is defined as the orbit perpendicular. The longitudinal position or right ascension of the orbit perpendicular (Ω) is measured positively counterclockwise from the vernal equinox to the projection of the orbit perpendicular in the equatorial plane. Note that $\Omega = \Omega_a + 3\pi/2$. The sun (sunline) may in general be on either side of the orbit plane. For this analysis it was taken to be on the same side as shown in Figure 3. The opposite side analysis is similar. The orientation of the sunline is described by angles obtainable from an ephemeris:

a. The right ascension of the sun (α) measured positively counterclockwise from the vernal equinox to the projection of the sunline in the equatorial plane.

b. The declination of the sun (δ) measured positively above the equator and negative below.

The longitudinal relation between the sunline and the orbit perpendicular can be taken as $\Psi = \alpha - \Omega_\odot$. A so-called noon-midnight sun-synchronous orbit is one in which Ψ is nominally $\pi/2$ or $3\pi/2$. Some sun-synchronous satellites such as the ITOS meteorological satellite, use an orbit in which the satellite always crosses the equator at 3p.m. northbound and 3a.m. southbound local time (Ψ = approximately $\pi/4$). This type of orbit provides oblique illumination angles suitable for photographic purposes.

In the case of a radar imaging satellite, illumination of the earth is not required and the orbit may be chosen to provide maximum illumination of the satellite's solar cells. Twilight orbits where Ψ is nominally zero are ideally suited for this purpose since the satellite would be illuminated over all or almost all of the orbit. Any desired Ψ may be established by simply launching at the proper time of day.

1. Orbit Eclipse

By assuming only circular orbits and a spherical earth, the geometry of the orbit with respect to illumination from the sun is simplified. The existence of a penumbra region of shadow can be neglected with negligible error thus assuming that the rays of the sun are parallel, causing a cylinder shaped umbra region behind the earth. Shown in Figure 4 is an edgewise view of the orbit plane and its geometrical relation to the position of the sun. The angle between the orbit perpendicular and the sunline is η. It can be

seen from Figure 4 that as long as η is less than the critical value, η_c, the entire orbit will be in sunlight. The situation depicted in Figure 4 is a limiting case in which the orbit is just on the edge of the cylindrical shadow and η equals η_c. From Figure 4, η_c is defined by

$$\cos \eta_c = \frac{R_e}{R_e + h} \quad \text{for } 0 < \eta_c < \frac{\pi}{2} \tag{2}$$

This means that for an orbit to be in continuous sunlight, the orbit perpendicular must remain inside a cone having the moving sunline as its axis (ref. 3). The half-angle of this cone is the η_c corresponding to the instantaneous orbit altitude. An expression for η can be derived from Figure 3. For the sunline being on the same side of the orbit plane as the orbit perpendicular, it can be shown that

$$\cos \eta = \cos \Psi \sin I \cos \delta + \cos I \sin \delta \tag{3}$$

The angles η_c and η can then be evaluated from equations (2) and (3), respectively, and compared to determine whether or not the entire satellite orbit is in sunlight.

If the orbit is eclipsed, the fraction of the orbit in shadow can be simply found from the equation

$$f = \frac{\frac{\pi}{2} + \sin^{-1}\left[\frac{\sin \eta_c}{\sin \eta}\right]}{\pi} \quad \text{for } \eta > \eta_c \tag{4}$$

However, in order to determine battery requirements, charge/discharge rates and duty cycles it is also necessary to know when or at what point in the orbit the satellite will enter and leave the eclipsed segment. From reference 4 it can be shown that

$$\cos\left(\pi/2 + \eta_c\right) = \sin u \left[\sin\lambda \left(\sin\epsilon \sin I + \cos\epsilon \cos I \cos\Omega_a\right) - \cos\lambda \left(\cos I \sin\Omega_a\right)\right] + \cos u \left[\sin\lambda \left(\cos\epsilon \sin\Omega_a\right) + \cos\lambda \left(\cos\Omega_a\right)\right] \quad (5)$$

where $\sin\lambda = \dfrac{\sin\delta}{\sin\epsilon}$

$$\cos\lambda = \frac{\cos\delta - \sin\lambda \sin\alpha \cos\epsilon}{\cos\alpha}$$

Two solutions for u may be obtained from these equations corresponding to the satellite orbital positions at entrance to and exit from the shadow.

Continuously sunlit orbits only exist over an altitude range from about 1500 km (800 n mi) to 3300 km (1800 n mi). For other altitudes the eclipse time varies depending on the time of year. This is depicted in figure 5 for the range of altitudes from 185 km to 1296 km (100 n mi to 700 n mi). Some shadowing occurs when the satellite is over the northern hemisphere for altitudes below about 280 km (150 n mi).

It should be noted at this point that if the sun were assumed to be on the opposite side of the orbit plane from that depicted in figure 3, the shadowing characteristics would be opposite to that shown in figure 5. That is, the major eclipsing would occur in the northern hemisphere during the winter instead of in the southern hemisphere during the summer. For this reason, the "opposite-side" case is not a desirable geometry for ice imaging in the northern hemisphere.

2. Atmospheric Drag

a. Orbit Decay: Atmospheric drag causes a satellite to decay or lose altitude. For all practical purposes, the orbit remains circular and the

inclination remains constant. Atmospheric drag decreases with increasing altitude until it is virtually zero at a thousand kilometers or so. However, for relatively low orbits (several hundred kilometers), which are being considered here, atmospheric drag can be a major perturbation.

The most accurate estimate of the effects of orbit perturbations on the motion of a satellite is obtained by integrating the differential equations of motion for an orbiting spacecraft while considering all perturbing forces such as atmospheric drag, gravitational perturbation of other bodies, solar pressure etc., as precisely as possible. However, this requires extensive input data and computer time. A number of techniques have been developed to yield approximate results making certain simplifying assumptions. The accuracy of these other techniques when considering relatively low orbits depends primarily on the assumptions made with regard to upper atmosphere density and its variation with solar activity. For the purposes of this study the effects of solar activity have been averaged.

Atmospheric drag effects have been estimated assuming an atmosphere model based on the 1962 U.S. Standard Atmosphere (ref. 5). This model depicts a typical mid-latitude, year-round condition averaged for the range of solar activity that occurs between sunspot minimum and maximum. The altitude range of interest lies above 200 km. The 1962 U.S. Standard Atmosphere model in the altitude range from 90 to 700 km is termed speculative. Although the model does not extend beyond 700 km this is sufficient for our purposes. Atmospheric density is presented in figure 6 for an altitude range from 200 to 700 km.

Following the analysis of Billik (ref. 6) and that of reference 4, an exponential atmosphere will be assumed.

$$\rho = \gamma e^{-\beta h} \tag{6}$$

where $\gamma = 1.58423 \times 10^{-9}$, kg/m^3

$\beta = 1.33812 \times 10^{-5}$, m^{-1}

ρ = density, kg/m^3

h = altitude, m

This assumed fit is shown in figure 6. Note that this is an approximation to the actual density but is reasonably close for the altitude range being considered.

For $h << R_e$, Billik has derived an expression involving h, t and known constants

$$86400 \left(\frac{t}{W/C_D A}\right) \beta \gamma \sqrt{\mu R_e} + e^{\beta h} = e^{\beta h_o} \tag{7}$$

where $W/C_D A$ is the ballistic coefficient involving: W, the satellite weight (kgf), C_D, the satellite drag coefficient (dimensionless), and A (m^2), the effective satellite area normal to the direction of motion and consistent with the definition of C_D. The factor 86400 allows t to be input in days.

Equation (7) may be solved for h,

$$h = \frac{1}{\beta} \ln \left[-86400 \; B \left(\frac{t}{W/C_D A}\right) + e^{\beta h_o} \right] \tag{8}$$

where $B = \beta \gamma \sqrt{\mu R_e}$ = constant

A plot of equation (8) is presented in figure 7 for various initial altitudes. As an example, for a satellite having a weight of 1000 kgf, an area of $10 m^2$ and a drag coefficient of 2.0 (ballistic coefficient equals 50) it would take about 320 days to decay from an initial altitude of 500 km down to 400 km.

To determine the amount of de-synchronization as the satellite decays it is useful to consider the longitudinal relation between the sunline and the orbit perpendicular (Ψ). An equation for Ψ in terms of t and known constants is derived in Appendix A. A plot of $\frac{\Psi_o - \Psi}{W/C_D A}$ versus $\frac{t}{W/C_D A}$ is shown in figure 8 for various initial sun-synchronous orbits (ho = 300 to 800 km). Intermediate altitudes are noted on the curves down to 200 km. As an example, consider the effects of decay from ho = 600 km to h = 400 km. From figure 8, $\frac{\Psi_o - \Psi}{W/C_D A} = 0.0235 \frac{\text{rad}}{\text{kgf/m}^2}$ and $\frac{t}{W/C_D A} = 31 \frac{\text{days}}{\text{kgf/m}^2}$. If a ballistic coefficient of 50 is assumed, $\Psi_o - \Psi = 1.175$ rad (63.3 deg) and t = 1550 days (4.25 years).

As an orbit decays, the eclipse fraction will tend to increase. This effect is illustrated in figures 9(a)-9(e) for initial altitudes of 400-800 km and an assumed ballistic coefficient of 50 kgf/m^2. The time that the satellite would spend in shadow on each orbit is shown as it varies throughout the year. The mission is shown starting on January 1 with $\Psi_o = 0$. If the orbit altitude is maintained (by thrusting to cancel drag) the eclipse pattern will simply repeat itself year after year without getting any worse (assuming sun-synchronization is also maintained). If no drag compensation is provided, the orbit will decay with a consequent increase in the time spent in shadow each year.

For a ballistic coefficient of 50 kgf/m^2 the orbit will completely decay and reenter the earth's atmosphere in less than 5 years for initial altitudes

up to slightly beyond 600 km (see figure 7). However, the situation rapidly improves beyond this point so that at h_o = 700 km the altitude would decay to only about 675 km after 5 years and the effect on the eclipse history would not be significant (figure 9(d)).

b. Drag Compensation: Based on the considerations just discussed it is clear that orbit drag can significantly affect the solar synchronization and eclipsing history of the satellite's orbit. Another consideration which will be discussed in the next section is the effect that orbit decay can have on the earth coverage pattern , i.e., the way in which the orbit tracks are phased so as to cover a desired mapping area on the earth's surface. As will be seen, this is probably the most critical aspect when considering how much orbit decay, if any, is acceptable.

Orbit drag can be virtually eliminated as a consideration over a typical satellite's lifetime by choosing an altitude of perhaps 800 km or more. This may be preferred to avoid the cost, complexity and weight associated with having to provide a velocity compensation system for drag makeup during the lifetime of the satellite. On the other hand, if satellite RF power is a critical factor it may be desirable to go to a lower orbit to conserve power in which case the satellite could either be allowed to decay with no drag compensation or a velocity correction system could be provided. Allowing the satellite to decay with no drag compensation would be acceptable only if the amount of decay over the satellite's lifetime was not in any way detrimental to its operation and mission. As will be seen in the next section, the requirement to maintain a pre-determined earth coverage pattern

would allow virtually no orbit decay over the satellite's lifetime. The question then becomes one of determining how low an orbit might be feasible assuming a drag compensation system is included on the satellite.

Orbit sustaining could be accomplished in two ways. The first method is simply a continuous application of thrust equal to drag. The second method consists of altitude gaining Hohmann transfers in between periods of altitude decay due to drag. Thrust is applied for only short periods of time and impulsive applications are assumed. In this method the altitude is allowed to vary an amount Δh whose upper limit is the desired altitude.

The continuous thrust case would require an electric propulsion system such as an ion thruster or resistance jet. It can be shown that the velocity requirements for continuous thrust orbit sustaining are given by

$$\Delta V = I_{sp}\, g \ln \left[\frac{1}{1 - \left(\frac{t}{W/C_D A}\right)\left(\frac{86400\, q}{I_{sp}}\right)} \right] \qquad (9)$$

where

I_{sp} = the specific impulse (sec) of the rocket

g = the acceleration of gravity, 9.80665 m/sec^2

$\frac{t}{W/C_D A}$ = time (sec) divided by the ballistic coefficient (defined previously)

q = the dynamic pressure, kgf/m^2

A plot of equation (9) is shown in figure 10 for various initial altitudes and three representative specific impulses. Note that for altitudes of 500 km or higher the curves for the I_{sp} range of 1000-3000 sec are very close so that only the 1000 sec curve is plotted for clarity.

The thrust required to cancel drag as a function of altitude is shown in figure 11 along with the propellant consumed over a 5-year period for I_{sp}'s of 1000, 2000 and 3000 sec. Note that the required thrust ranges from about the size tested on SERT II down to the microthruster range.

Two cesium contact ion microthrusters with several discrete thrust levels ranging from 4-20 μlb were tested on ATS IV in 1968 (ref. 7) and generally performed as expected.

It can be seen from figure 11 that the amount of propellant consumed over a 5-year lifetime would be reasonably small for altitudes of about 400 km or more. At lower altitudes the propellant could represent a significant fraction of the satellite's weight which is undesirable since it subtracts from useful payload. The feasibility of using an electric propulsion system for drag compensation and its impact on the satellite's design, cost, complexity, reliability, etc. requires much more detailed study than is possible in this report. The major problem would seem to be one of developing a sufficiently high level of confidence in the ability of the system to operate effectively over the satellite's lifetime to warrant its use.

The impulsive thrust case would require a chemical propulsion system such as a monopropellant hydrazine system. The velocity requirements in this case are determined by the Hohmann transfer maneuvers from the low altitude to which the satellite has been allowed to decay to the original starting altitude. Two impulsive velocity corrections are required for each maneuver :

(1) ΔV_1 at the low altitude to place the satellite on a transfer ellipse with an apogee at the original desired altitude and (2) ΔV_2 at the apogee of the transfer ellipse to recircularize the orbit at the desired altitude. The required velocity increments are given by

$$\Delta V_1 = \sqrt{\frac{\mu}{r_i}} \left[\sqrt{\frac{2r_f}{2r_f - \Delta h}} - 1 \right] \qquad (10a)$$

$$\Delta V_2 = \sqrt{\frac{\mu}{r_f}} \left[1 - \sqrt{\frac{2r_i}{2r_f - \Delta h}} \right] \qquad (10b)$$

where

r_i = radius of initial orbit at beginning of Hohmann transfer maneuver

r_f = radius of final desired orbit

The Hohmann transfer maneuvers are separated by periods during which the orbit is allowed to decay to some lower altitude limit so that the thrusters operate on a cyclic basis. The duty cycle depends on the starting altitude (drag encountered) and on the amount of decay allowed.

A plot of the total ΔV ($\Delta V_1 + \Delta V_2$) versus $\frac{t}{W/C_{DA}}$ is presented in figure 12(a) for various initial altitudes and for $\Delta h/h_o$ = .10, .05 and .01. ΔV_1 and ΔV_2 are nearly equal due to the proximity of the upper altitude limit (desired orbit) and the lower limit (decayed orbit). The duty cycle structure of these curves was omitted for clarity since the number of cycles gets fairly large for low altitudes. A plot of the duty cycle or time between Hohmann transfer maneuvers is shown in figure 12(b). As an example, for ho = 400 km and $\Delta h/h_o$ = .05 the duty cycle would be $\frac{t}{W/C_D A}$ = 0.53 $\frac{\text{days}}{\text{kgf/m}^2}$ so that for a ballistic coefficient of 50 kgf/m^2

the Hohmann transfer maneuver would be made every 26.5 days. Each maneuver involves two thruster firings so that for a 5-year mission the thrusters would fire about 140 times. For higher altitudes the duty cycle is increased and the number of thruster firings would be reduced as indicated in figure 12(b).

In comparing figure 12(a) with figure 10 it may be seen that the ΔV's for either system compare reasonably well. However, since the chemical system has a much lower specific impulse, the propellant requirement will be greater (compare figure 13 with figure 11).

If we were to limit the propellant consumed for drag compensation to say 5 percent of the initial satellite weight for a 5-year mission the minimum initial altitude allowable would be about 525 km for a 300 sec thruster and $\Delta h/h_o = .05$ (see figure 13).

3. Earth Coverage Patterns

The considerations discussed thus far for sun-synchronous orbits have typically been in the nature of constraints bearing upon the choice of an orbit. These constraints help to set a lower limit on the choice of altitude but are not really definitive. Theoretically, an infinite number of orbit altitudes exist from which to choose so that it is desirable to have a more definite criteria upon which a reasonable choice can be made. For a surveillance and mapping satellite one of the important criteria involves the way in which the ground areas of interest are covered or scanned. This involves consideration of the distance between successive or neighboring (not necessarily successive) orbit tracks across the surface of the earth, and the time required to completely cover an area.

To focus this discussion, the application of surveillance and mapping of ice on the Great Lakes will be considered. The Great Lakes are bounded roughly by latitudes of 41 deg north and 49 deg north and longitudes of 75 deg west and 92 deg west. This area is shown in figure 14 and would measure about 1400 km (southern edge) by 1200 km (northern edge) by 900 km (meridian).

The orbit will pass over this area twice a day, once on the up leg (south to north on a north-northwesterly heading) and once on the down leg (north to south on a south-southwesterly heading). However, only one of these passes (either one) can be considered for an orderly mapping since the two passes will cross the area out of sequence and at different angles. Only the up leg (south to north) will be considered here.

Once the orbit is established, the orbit track on the earth's surface will regress or move westward as the earth rotates. For the limited range of orbit altitudes being considered, the equator crossing will regress about .38-.45 rad/orbit (22-26 deg/orbit). For example, if we had an orbit with a period of 1.5 hours (altitude = 274.400 km) the equator crossing would regress 0.3927 rad/orbit (22.5 deg/orbit) since the earth rotates 0.2618 rad/hour (15 deg/hour). In this case, exactly 16 orbits would be completed in one day with the 17th orbit repeating the 1st.

Obviously, if we reduce the number of exact orbits completed in one day to 15, 14, etc. the orbit period will become larger and the amount each successive track moves westward will increase. In each case the required orbit altitude is unique. For example, 14 orbits/day requires an orbit period of 1.7143 hours and an altitude of 893.777 km. The orbit would regress 0.4488 rad/orbit (25.714 deg/orbit).

It is apparent that the separation between successive orbits (orbits 1 and 2, 2 and 3, etc.) would be at least 0.3927 rad (22.5 deg) in longitude. Thus as successive orbit tracks pass over the Great Lakes, for example, they will be separated by at least 1650 km minimum which is wider than the entire area. The radar would thus be required to cover a swath of 1650 km minimum to obtain an image once a day. Initial study indicated this was not feasible for a reasonably sized multi-beam antenna. This is discussed in more detail in the radar section to follow.

Smaller orbit track separations can be obtained by considering patterns that repeat every 2 days, every 3 days, etc. The longer the cycle, the smaller the track separations will be. The pattern need not repeat in an integral number of days so that there are virtually an infinite number of repetition patterns with their corresponding altitudes to choose from. However, it is not necessary to consider all possibilities since consideration of patterns that repeat in an integral number of days yields a reasonably large number of possible orbits from which to choose and simplifies the analysis considerably.

Since the earth rotates 2π radians in one day the nodal rate of change due to the earth's rotation can be found from

$$\dot{\Omega}_a = \frac{2\pi \pm \frac{\dot{\Omega}_a}{D}}{N} \quad \text{rad/orbit}$$

or

$$\dot{\Omega}_a = \frac{2\pi D}{(DN \pm 1} \quad \text{rad/orbit} \qquad (11)$$

where D = number of days between pattern repetitions

N = approximate number of integer orbits/day (rounded to next highest integer orbits/day)

Note that although an integer is used for N to generate a set of $\dot{\Omega}_a$ the number of orbits actually completed in one day will not necessarily be an integer . Also, the plus sign in the formula gives a nodal precession (eastward movement) while the minus sign gives a nodal regression (westward movement).

As an example, suppose we want the orbit track pattern to repeat in a westerly direction every two days (D = 2) with N = 15 orbits/day. Then,

$$\dot{\Omega}_a = \frac{4\pi}{29} = 0.43332 \text{ rad/orbit}$$

Since the earth rotates 2π rad in 24 hours the required orbit period would be $0.43332 \times \frac{24}{2\pi} = 1.6552$ hours. The required altitude would be 725.630 km. For these conditions 14.5 orbits would actually be completed in 24 hours with 29 orbits being completed in 48 hours. The 30th orbit would exactly repeat the track of the 1st orbit and the cycle would be repeated. The separation distance between the 1st orbit and the 15th or between the 2nd and 16th and so on would be 0.21666 rad in longitude or about half of what it would be for 15 orbits/day repeated daily.

It should be noted here that since the orbits under consideration are required to be sun-synchronous they would have a small precession rate about the earth due to earth's oblateness. However, this precession rate does not affect the preceding calculations since it is accounted for by the motion of the earth about the sun. The length of the day is accordingly reckoned at 24 hours to account for this motion.

A partial map of sun-synchronous orbits is shown in figure 15 where orbit track separation in longitude is plotted versus altitude. Also indicated on the figure for some discrete points are the exact number of days before the orbit track pattern repeats itself and the number of the orbits completed in that time period.

In the case of surveillance and mapping of ice on the Great Lakes where the conditions being surveyed can be quite changeable due to current, winds, temperature, etc. it would be necessary to obtain a complete image of the region in as short a time as possible to effectively aid navigation and ice control operations. In fact short response time may be necessary for many applications (ocean state surveillance, pollution monitoring, etc.). Short response time infers wide swath width coverage. As mentioned earlier, however, the radar system would be limited in the maximum swath width achievable which at least rules out obtaining a complete image daily of an area the size of the Great Lakes from a sun-synchronous orbit. For example, if we consider an orbit track separation of .1 rad in longitude, the orbit track separation or swath width at the latitude of the Great Lakes would be about 450 km. If this were the maximum achievable swath width, from figure 15 this would limit the choice of orbits to those having a track repetition cycle of about 4 days or greater. However, the track separation distance at the equator will be about 45 percent greater than at a latitude of 45 deg. Thus, if the satellite were required to map any part of the globe, the equatorial separation distance would be the design point. If the maximum separation distance were limited to 450 km at the equator it would take about 6 days or more to obtain a complete image of the Great Lakes.

The separation between orbit tracks is a function of the orbit inclination, the longitudinal separation and the latitude being considered. The separation distance will be maximum near the equator and zero at the point at which the two orbit paths cross which will tend to be near the maximum latitude point of the orbits. In order to compute the separation distance as a function of latitude it is necessary to choose a specific sun-synchronous orbit. A method for calculating the separation distance between any two orbit tracks on the earth's surface displaced in longitude by an amount $\Delta\Omega$ is presented in Appendix B.

C. Equatorial Orbits

This class of orbits is of interest since it allows the earth scan velocity to be small by choosing an altitude somewhat below geosynchronous so that the satellite has some desired easterly velocity relative to the earth's surface. As will be discussed in the radar section this would enable the radar system to obtain high image

resolution while covering a large swath width with only a few or even a single beam. This type of orbit would experience no atmospheric drag which is a simplifying feature. Another advantage than an equatorial orbit would have over a sun-synchronous orbit is that areas can be scanned more than once per day. On the other hand, orbit eclipsing will be more prevalent than with the sun-synchronous orbits. Also, limitation on the radar beam incidence angle will preclude mapping the near equatorial region (angle too vertical) and the polar regions (angle too shallow) which may be a drawback for some applications. It may be possible to eliminate this problem by giving the orbit a slight inclination to allow the side-looking radar to periodically view the equatorial region while not significantly increasing the satellite's velocity with respect to the earth's surface. This was not investigated in this study but should be considered in any future, more detailed studies of this concept.

1. Orbit Eclipse

The geometry of a circular equatorial orbit with respect to illumination from the sun can be considered in basically the same way as for the sun-synchronous orbits discussed earlier. In this case, however, the orbit inclination is zero and there is no sun-synchronization. Maximum daily eclipsing will occur when the sun is crossing the equator on about March 21 and again six months later. Shown in figure 16 are plots of how the eclipse time varies throughout the year for a range of equatorial orbit altitudes from 10,000 km to 40,000 km. Geosynchronous altitude is 35,786.04 km.

2. Earth Coverage Patterns

Earth coverage from an equatorial orbit depends primarily on the satellite's velocity with respect to the earth's surface and the latitude being scanned. The relative angular velocity, ω_r, between the satellite

and the earth is

$$\omega_r = \omega_s + \omega_e$$

where ω_s is the satellite's angular velocity

ω_e is the earth's angular velocity

The relative velocity of an equatorial satellite with respect to a point on the earth's surface is

$$V_r = \omega_r \times R_e = \omega_r R_e \cos \lambda \qquad (12)$$

and is plotted versus altitude in figure 17 for various latitudes. For altitudes below geosynchronous, the difference between the satellite's and the earth's rotation will cause the satellite to "lap" the earth so that multiple daily scans may be achieved. Shown in figure 18 is the number of daily passes over an area on the earth's surface versus satellite altitude. It can be seen that areas to be scanned may be covered at least daily for altitudes below about 20,000 km (1/day occurs at 20,207.8 km).

The number of satellite eclipses encountered each day, N_e, will occur once more than the number of target passes per day. The longitudinal separation of these eclipses (center to center) would simply be $360/N_e$ deg. The longitudinal slice "blacked out" on each eclipse measured as a segment of earth's longitude would be

$$\frac{360\ f}{24}\ (24-P)\ \text{deg}$$

where P is the satellite's period (hours)

f is the fraction of the orbit in shadow (figure 16)

For example, for a 4/day coverage where h = 8062.8 km, P = 4.7974 hours and f = .1465 (max.) each eclipse would cover 42.2 deg of earth's longitude with each eclipse being separated (center to center) by 360/5 = 72 deg. The longitudinal location of the eclipses would depend on the initial relationship between the time of day and the longitudinal position of the satellite with respect to the earth. For an integral number of passes per day the eclipses would always occur at the same longitudinal positions. In the above example all longitudinal positions would see full sunlight at least three times per day.

For a satellite in equatorial orbit, the radar beam incident angle will depend on the orbit altitude and the latitude being mapped. This is illustrated in figure 19. If radar system performance were limited to incident angles of about .35 rad (20 deg) for instance, latitudes above 60 deg could not be mapped. However, even this amount of coverage would cover most of the world's shipping lanes, for example, suggesting an application for ocean state surveillance and ice imaging.

Of importance to the radar system is the rate at which the distance to a target varies with time in order to obtain a Doppler effect. This distance $r(\phi)$ is shown in figure 20 and $\dot{r}(\phi)$ may be found as follows:

From figure 20, beam position 1 lies in the plane of the subsatellite meridian at some latitude and represents the point at which $r(\phi)$ is minimum. Point 2 represents a beam position ahead of the satellite. As the

satellite moves in an easterly direction the radius from the satellite to position 2 will become shorter until it reaches the value represented by position 1 and then it would lengthen again as the satellite moves further eastward.

From the law of cosines

$$r^2 = R_s^2 + R_e^2 - 2 R_s R_e \cos\xi$$

where $\cos \xi = \cos \lambda \cos \phi$

Differentiating with respect to time we get

$$2r\dot{r} = 2 R_s R_e \dot{\phi} \cos \lambda \sin \phi$$

but $\dot{\phi} = \omega_r$

Then $$\dot{r} = \frac{R_s R_e}{r} \omega_r \cos \lambda \sin \phi \qquad (13)$$

where $r = (R_s^2 + R_e^2 - 2 R_s R_e \cos \lambda \cos \phi)^{1/2}$

3. Radiation Damage to Solar Cells

The existence of trapped, high energy electrons and protons and solar flare protons in the equatorial region about the earth can cause significant damage to unprotected solar cells and other electronic components. Electronic components can generally be shielded to protect them from radiation damage with some weight penalty. However, solar cells present a more difficult problem.

Calculations were made to determine the altitude and cover glass thickness necessary to achieve a five year lifetime with no more than a 25 percent degradation in solar array power. A nominal 10 Ω -cm n-on-p cell with a thickness of 12 mils and infinite back shielding was assumed. It was determined that an equivalent 1 MeV electron fluence of approximately

7×10^{14} e /cm^2 would reduce the cell power by 25 percent. Accordingly, for a five year mission the maximum annual fluence impinging on the cell that could be tolerated would be 1.4×10^{14} e /cm^2.

Equatorial orbit altitudes ranging from 1000 to 20,000 km were studied. For orbits below 11,000 km the trapped protons were the dominant damaging particles, while trapped electrons were predominant above 11,000 km. Solar flare protons made a significant contribution to the solar cell damage only at altitudes above 14,000 km. The solar flare model with the greatest proton fluence was chosen. It was concluded that a five year lifetime can be obtained only for orbital altitudes below 1200 km or above 11,000 km. The heart of the trapped proton belt lies between these altitudes and lifetimes less than a year would be expected. Outside these extremes, the effect of cover glass thickness was considered and it was concluded that a five year lifetime with no more than a 25 percent power degradation could be achieved with cover glass thicknesses less than 30 mils in all cases.

However, equatorial orbits below 1200 km are not practical since earth coverage would be severely limited by radar beam incident angle constraints at low altitudes. For example, at 1200 km, earth coverage would be limited to a narrow swath between 10-20 deg latitude. The region of interest for a solar array system would thus be confined to altitudes above 11,000 km. The altitude should be chosen no higher than necessary since the required RF power increases fairly rapidly with altitude. This will be discussed in more detail in the following section on Radar Considerations.

Within the 1200 to 11,000 km region another type of power system could conceivably be used such as an RTG (Radio-Isotope Generator). Other electronic components would need special radiation protection thus incurring some weight penalty. Such a system is judged to be more complex and costly than a solar array system operating outside this region. However, this approach would need more detailed study than can be given here to determine its feasibility.

RADAR CONSIDERATIONS

A. General

Preliminary results of the Lewis airborne SLR ice mapping program indicate that rapid coverage of the Great Lakes is necessary (ref. 2). Figure 21 shows typical imagery of Lake Erie obtained with that system. The figure shows a complete pass on February 22, 1973. The dark line through the center of the image is the blind ground track of the aircraft. A portion of the February 23, 1973 pass is also shown with a sketch of Lake Erie. Observe the February 23 pass and note the ice pack against the western edge of Pelee Point. On the 22nd this was relatively open water. Close scrutiny of these photographs will reveal many other striking changes.

This same phenomenon has been observed with ERTS-1 imagery an example of which is shown in figure 22. Note the change along the southern shore that occurred in one day.

Because the Great Lakes ice formation is a dynamic phenomenon, rapid coverage of the lakes is desired. Daily coverage would be desirable and more than 3-4 days separation would render the imagery useless if accurate navigational maps are required. However, these lakes span approximately 8° in latitude by 17° in longitude. This is an area of about 900 km by 1300 km. Rapid coverage of such a vast area will require very large swath widths. As a result of antenna dimensional limitations and signature constraints, spaceborne synthetic aperture radar (SAR) proposals to date limit expected swath widths to about 60-100 km. Rapid coverage of these lakes will require swath widths 4-10 times greater. Among the obvious ways of obtaining larger swath widths are: adjustment of the SAR look angle (angle from vertical as seen by the spacecraft) and/or using larger antennas.

Since target signatures are sensitive to look angle, a look angle favorable to large swath widths may not be favorable to target signature. Therefore, it is desirable to have flexibility in choosing the look angle.

Since the realizable swath width is proportional to the antenna azimuth dimension, using larger antennas is a conceptually simple alternative. Deployable antennas of 10 meters in dimension exist (ATS-F satellite) and larger antennas may be possible. A 10 meter antenna would allow a swath width of about 60-100 km at low altitudes ($\sim$ 1000 km) and for small incidence angles ($\sim$ 10°-40°). A 4-10 fold increase would imply a deployable antenna of 40-100 meters. Such a development for X-band (most favorable band for ice imaging) would be a formidable task. Hence it would be desirable to find other schemes.

A possible solution has been proposed (ref. 8) which will yield large swath widths with reasonable antenna size and no restrictions on look angle. Essentially the method employs independent SAR's in parallel to increase the realizable swath width. This section will present a simplified analysis of this scheme and use it to estimate spacecraft requirements for wide swath coverage.

B. Synthetic Aperture Radar

1. Single Beam Radar

The typical spaceborne SAR geometry appears as shown in figure 23. As the spacecraft moves along its trajectory, RF bursts are periodically directed at the ground. The period of the bursts and the spacecraft velocity relative to the ground target determine the separation, ΔX, between

transmit/receive locations as seen by the ground target. The beam strikes the ground to one side of the satellite radar and a portion of the reflection returns in the direction of the spacecraft. This side looking geometry is necessary for obtaining good range resolution since the targets on the ground can be discriminated according to time delay.

For example, the side view of figure 24 shows that the reflection along R_2 lags the reflection along R_1. If the transmitted pulse width is τ then the minimum resolvable target separation, Δr,

$$\Delta r \geq \frac{c\tau}{2\cos\theta}$$

where c is the velocity of propagation and θ is the local incidence angle. Therefore, resolution in range is a matter of choosing an appropriate pulse width and adjusting the transmitter and receiver bandwidths accordingly.

The transmit/receive locations along the trajectory offer different radar "views" of each target. If the returns at each point are recorded and later added together vectorially, the result is equivalent to the output of an array of antennas with the same spacing and total length. The apparent or synthetic length parallel to the flight path, d_{as}, and the dimension perpendicular to the flight path, D_r, form the synthetic aperture. The null to null azimuthal resolution of this SAR, Δa, is

$$\Delta a \geq \frac{\lambda}{d_{as}}$$

where λ is the wavelength of the incident radiation. The equality is obtained for uniform weighting of the radar pulses and perfect coherency

between successive pulses. Immediately, one can see a factor of two improvement over conventional arrays. This is an advantage obtained through coherent detection. However, other limitations arise which make the equality unattainable in certain applications. Cutrona (ref. 9) has shown that the curvature of the reflected waves produce phase errors which, when unaccounted for, limit the resolution. If unaccounted for, these phase errors limit the resolution to

$$\Delta a = \frac{\sqrt{\lambda R}}{2}$$

where R is the slant range to the target. However, if compensation is made for these phase errors the resolution is theoretically (ref. 9)

$$\Delta a = \frac{D_a}{2}$$

where D_a is the real antenna azimuth dimension. However, perfect coherency between pulses is not always possible and atmospheric variations become significant when d_{as} is long (ref. 10). Nevertheless, resolutions of 10's of meters are obtainable from altitudes of 1000's of km.

The performance of such antennas has been analyzed thoroughly and results can be found in the literature (refs. 11, 12, and 13). The gain of such an array is given by

$$G = N^2 G_o$$

where N is the number of RF bursts coherently summed and G_o is the real antenna gain. For non-uniform weighting some loss in gain can be expected but sidelobe suppression is achieved (ref. 12).

Conventional linear arrays have only a slight effect on the effective receiver noise temperature. SAR's do not have this advantage. The gain of the SAR is the result of adding many radar returns. Unfortunately, the noise added to each return by the receiver front-end will contribute to each summation. Consequently, as successive range returns are coherently added the signal power goes up as the square of the number of pulses and the noise power goes up proportional to the number of pulses. Therefore, the net improvement in signal to noise ratio only goes up proportional to the number of pulses. This effect will be accounted for when estimating the average SAR power requirements.

Since the generation of the synthetic aperture is periodic, major sidelobes occur at intervals of Ω_{maj} radians, where

$$\Omega_{maj} = \frac{\lambda}{2\Delta X}$$

These major sidelobes must be suppressed by the real antenna since the synthetic weighting, N^2, is the same at all major sidelobes. This places a restriction on the minimum size of the real antenna or maximum element spacing through the inequality,

$$\frac{\lambda}{2\Delta X} \geq \frac{\lambda}{D_a}$$

where D_a is the real antenna azimuth dimension. Clearly, the constraint is independent of wavelength and can be interpreted as

$$\Delta X \leq \frac{D_a}{2}$$

A plot of a typical receiver pattern is shown in figure 25. The dotted line indicates the response of the real antenna and the solid line is the

overall response. The location of the real antenna nulls and spurious lobes are indicated. Clearly, by adjusting the real antenna azimuth dimension or the synthetic array spacing, the major sidelobe can be moved to a minor response of the real antenna.

Therefore, by choosing an appropriate pulse width, τ , and synthetic aperture, d_{as}, a resolution cell

$$\Delta S = \Delta r \Delta a = \frac{R \lambda c \tau}{2 d_{as} \cos\theta}$$

is achieved (provided $\frac{R\lambda}{d_{as}} > \frac{D_a}{2}$ for a focused SAR and $\frac{R\lambda}{d_{as}} > \frac{\sqrt{\lambda R}}{2}$ for an unfocused SAR).

Processing techniques exist for generating the vector sum of N returns at all range intervals simultaneously. The favored technique presently is an optical process (refs. 14, 15, and 16) which reduces each of N range scans to a single scan of high resolution. The high resolution scans are then recorded side by side on photographic film to produce a high resolution radar image of the ground.

To avoid range and azimuth ambiguities, constraints must be placed on the radar system parameters. The azimuth ambiguity problem has already been mentioned. The requirement was finally interpreted as a restriction on element spacing

$$\Delta x \leq \frac{D_a}{2}$$

Since the element spacing is fixed by the radar pulse repetition frequency, prf, and spacecraft relative velocity, V_r , the above inequality can also be written

$$\text{prf} \geq 2 \frac{V_r}{D_a}$$

Therefore the minimum prf is established to avoid azimuth ambiguities.

2. Single Beam/Multiple Frequency SAR

As was mentioned before it is desirable to have as wide a swath width as possible. The swath width is fixed by the prf. This can be seen by examining figure 26. The reflection along R_2 lags the reflection along R_1. If the prf is high enough the reflection along R_2 for pulse p will interfere with the reflection of pulse p + 1 along R_1. This causes a range ambiguity which limits the prf to

$$\text{prf} \leq \frac{C}{2(R_2 - R_1)}$$

However, consider the case when successive pulses are transmitted at different frequencies. If these frequencies are spaced so that no interference occurs between carriers, then the above restriction only applies to each carrier individually. But if the overall pulse rate is prf then the pulse rate for each carrier is prf/m where m is the number of carriers. Therefore, the overall prf limitation for multifrequency operation becomes

$$\text{prf} \leq \frac{m\,C}{2(R_2 - R_1)}$$

The prf is then constrained by range and azimuth ambiguities to lie between

$$2\frac{V_r}{D_a} \leq \text{prf} \leq \frac{m\,C}{2(R_2 - R_1)}$$

3. Multifrequency/Multibeam SAR

Range discrimination can also be obtained by using several focused beams. The above restriction on prf would then apply to each beam. Sidelobe interference could be suppressed by using different bands of frequencies for each beam.

It is clear from the above equation that the widest possible swath occurs for

$$prf = \frac{2\ V_r}{D_a}$$

The largest possible unambiguous range difference is then

$$R_2 - R_1 = \frac{m\ C}{prf}$$

Referring back to figure 26 one can see the geometrical relationship between beamwidth, β , swath width, SW, and range difference, ΔR. For a given angle ϕ between nadir and the target the slant range is given by

$$R = R_e \sqrt{1 + \left(\frac{R_s}{R_e}\right)^2 - 2\left(\frac{R_s}{R_e}\right) \cos \phi}$$

where R_e = radius of the earth

R_s = spacecraft orbital radius

ϕ_1 is chosen to produce a favorable incidence angle, θ_1. Given a particular incidence angle, θ_1, ϕ_1 can be computed from

$$\phi_1 = \cos^{-1}\left(\frac{R_e}{R_s} \cos \theta_1\right) - \theta_1$$

Letting ϕ_1 be the smallest angle from nadir, then

$$R_1 = R_e \sqrt{1 + \left(\frac{R_s}{R_e}\right)^2 - 2\,\frac{R_s}{R_e} \cos \phi_1}$$

The range difference is obtained from the equation for prf

$$\Delta R = R_2 - R_1 = \frac{mc}{prf}$$

and therefore, $R_2 = R_1 + \Delta R$

The most extreme angle, ϕ_2, from nadir is then computed from

$$\phi_2 = \cos^{-1}\left\{\frac{1}{2}\left(\frac{R_s}{R_e} + \frac{R_e}{R_s} - \frac{R_2^2}{R_s R_e}\right)\right\}$$

The resultant swath width is then

$$SW = R_e(\phi_2 - \phi_1)$$

and the required antenna range beamwidth is

$$\beta = 2\sin^{-1}\left\{\sqrt{4\left(\frac{R_e}{R_1+R_2}\right)^2 \sin^2(\phi_2 - \phi_1) - \left(\frac{R_2 - R_1}{R_1+R_2}\right)^2}\right\}$$

Therefore, the required antenna range dimension is

$$D_r = \frac{2\lambda}{\beta}$$

For multiple beam operation the angular width of each beam is fixed by the antenna range dimension. The side looking geometry causes beams farther from nadir to cut wider swaths than those nearer nadir. Therefore, the range ambiguity problem is most severe at extreme ranges from nadir.

If D_r is chosen to suppress the range ambiguity at ranges distant from nadir, then the beam close in to nadir will be too narrow to realize the full unambiguous range interval. This effect can be compensated for by increasing the number of independent carriers in those beams extreme from nadir.

Letting SW_j be the swath width of the j th beam the total swath width is then,

$$SW = \sum_{j}^{b} SW_j$$

where b is the number of beams.

Assuming processing in all beams i synchronized so that the synthetic length, d_{as}, is the same for all beams, the azimuth resolution of the j th beam becomes

$$\Delta a_j = R_j \frac{\lambda}{d_{as}}$$

Choosing d_{as} to give a nominal resolution in some beam between j = 1 and j = b, say j = n, then the azimuth resolution in the j th beam can be written

$$\Delta a_j = \frac{R_j}{R_n} \Delta a$$

where Δ a is the nominal azimuth resolution and R_n is the slant range of the n th beam.

Assuming the radar pulse width is the same for all beams, the range resolution in the j th beam is

$$\Delta r_j = \frac{c\tau}{2\cos\theta_j}$$

where θ_j is the local angle of incidence of the jth beam (approximately the same across the beam for swath widths encountered in this study). Again, choosing τ to give a nominal range resolution, Δr, in the nth beam, the range resolution in the jth beam is then

$$\Delta r_j = \Delta r \frac{\cos \theta_n}{\cos \theta_j}$$

In the jth beam the received signal power can be written,

$$P_{r_j} = \frac{P_{t_j}}{L_j} G_{t_j} \left(\frac{\lambda^2}{4\pi R_j^2}\right) \left(\frac{\sigma_j \Delta a_j \Delta r_j}{4\pi}\right) \left(\frac{\lambda^2}{4\pi R_j^2}\right) G_{r_j}$$

where P_{r_j} is the received signal power in the jth beam

L_j is the RF losses in the jth beam

G_{t_j} is the transmit antenna gain in the jth beam direction

$\frac{\lambda^2}{4\pi R_j^2}$ is the space loss in the jth beam

σ_j is the scattering coefficient in the jth beam direction

G_{r_j} is the effective gain in the receive mode

This power must exceed the receiver noise power by the desired signal to noise ratio. Therefore,

$$\frac{P_{t_j}}{L_j} G_{t_j} G_{r_j} \left(\frac{\lambda^2}{4\pi R_j^2}\right)^2 \left(\frac{\sigma_j \Delta a_j \Delta r_j}{4\pi}\right) \geq \left(S/N\right) NKTB$$

where KTB is the effective receiver noise power

N is equal to the number of RF pulses used to generate the synthetic aperture

(S/N) is the desired signal to noise ratio

Substituting, $G_{tj} = 4\pi \frac{D_a D_r}{\lambda^2} \eta_t$

$G_{rj} = N^2 G_{tj}$

$\bar{P}_{tj} = P_{tj} \tau prf$

get, $$\bar{P}_{tj} = 4\pi \frac{R_j^4 L_j (S/N) KTB \tau prf}{D_a^2 D_r^2 \eta_t^2 \sigma_j \Delta a_j \Delta r_j N}$$

where $\bar{P}_{tj}$ = average transmitter power in jth beam

η_t = efficiency of real aperture

Making the additional substitutions,

$$\Delta a_j = \Delta a \frac{R_j}{R_n}$$

$$\Delta r_j = \Delta r \frac{\cos\theta_n}{\cos\theta_j}$$

$$N/prf = \frac{da_s}{V_r} = \frac{\lambda R_j}{\Delta a V_r}$$

$$\sigma_j = \sigma_o \sin\theta_j$$

$$B = \frac{1}{\tau}$$

the total required average power can be written

$$\bar{P}_t = \sum_{j=1}^{b} 4\pi \frac{R_n R_j^2 V_r L_j (S/N) KT \cot\theta_j}{D_a^2 D_r^2 \eta_t^2 \Delta r \lambda \sigma_o \cos\theta_n}$$

where b, the number of beams satisfies,

$$SW = \sum_{j=1}^{b} \Delta w_j$$

The RF bandwidth of the radar may vary from beam to beam since some beams may have multiple carriers. The video bandwidth is assumed to be the same for each beam and this was used in estimating the average power requirements. However, the radar front end and the data link must pass all beam returns simultaneously. Therefore the RF bandwidth of each radar beam is

$$BW_j = \frac{2 m_j \gamma}{\tau}$$

where m_j is the number of carriers in the beam and γ is a factor accounting for any guard bands used. The data link requirements are not included in this study.

C. Application of Multifrequency/Multibeam SAR to Equatorial and Polar Orbits

The relatively small swath widths of conventional orbital SAR's is a result of the high velocity required to orbit. When a target comes into the field of view of the real beam pattern, it produces a doppler shifted return depending on the length of the synthetic aperture and the relative approach velocity toward the target. The faster the spacecraft the higher the frequency. The sampling theorem dictates that sampling of the doppler frequency must exceed twice the doppler frequency. Thus the prf increases as the spacecraft velocity increases. A high prf reduces the obtainable swath width through the range ambiguity. Therefore, as the velocity increases the obtainable swath width decreases. This property is displayed in figure 27. The incidence angle limit contour represents the distance from nadir to a 10° incidence angle. The swath width for lower velocities encounter this limit. However, for orbital velocity the obtainable swath width is far below this limit.

1. Equatorial Orbits

Orbital velocity decreases as the spacecrat altitude increases. In equatorial orbits the angular velocity of the earth subtracts from the angular velocity of the satellite creating an apparent low orbital velocity. Hence, more improvement in swath width should occur for equatorial orbits than for polar orbits.

Unfortunately, striking improvements are not obtained until very high altitudes are used as shown in figure 28. These contours were generated for a target at 48° latitude (northern extreme of the Great Lakes) and an X-band SAR. Two azimuth dimensions were used. For a 10 meter azimuth dimension the solid line results. At each altitude the antenna range dimension is set equal to that required to eliminate the range ambiguity. For altitudes below approximately 11,500 km, a 10 meter range dimension is insufficient to eliminate the range ambiguity. Two frequency operation is required to enlarge the range interval to a value controllable with a 10 meter range dimension. We are interested in the maximum obtainable swath width so the range dimension is reduced to the minimum necessary to eliminate the range ambiguity. Above 11,500 km, the 10 meter range dimension limitation is sufficient to eliminate the range ambiguity and multifrequency operation is not required. For a 15 meter azimuth dimension, single frequency operation is realized over the full altitude range. The limiting contour on the left side of the figure is the 10° incidence angle limit. The limiting contour at the top of the figure is an arbitrary 900 km limit built into the design procedure. 900 km is sufficient to span the five Great Lakes in a north-south direction and a larger swath is not necessary.

At these high altitudes severe requirements are placed on the spacecraft power supply. The required average power is shown in figure 29. For a 10 meter azimuth dimension, the required range dimension for multi-frequency operation below 11,500 km is small and causes a large increase in required power. Above 11,500 km, there is a drop in the unambiguous range interval and a corresponding increase in the antenna range dimension. Therefore, the required power drops. With a 15 meter azimuth dimension the required power is monotonic to about 24,000 km. Between 11,500 km and approximately 24,000 km there is very little difference in the required power for the two antennas. However, as was shown in figure 28, the swath width is 50% larger for the 15 meter antenna.

At altitudes near synchronous, a "hole" in the power requirement occurs. In generating the data of figures 28 and 29 an arbitrary limit of 900 km was placed on the swath width. At altitudes above 28,000 km, the single frequency range ambiguity exceeds this limit for either antenna. Therefore, the prf was increased to fix the range ambiguity at the 900 km limit. Normally the prf would be chosen as small as possible to maximize swath width. In this case the swath width is limited by another constraint. The extra returns can then be used to increase the SAR gain and less power is required. This reduction is most noticeable near synchronous where the relative velocity of the spacecraft approaches very low velocities. The required synthetic aperture is fixed by the resolution requirement and remains approximately constant. The prf remains fixed to specify the 900 km range ambiguity. Because of the decreasing velocity more and more excess returns are available. Consequently, the resultant increase in SAR gain causes the power requirement to experience a rapid drop near synchronous altitude.

As synchronous altitude is approached, the orbiting time of the spacecraft becomes very long and the rate of coverage so low as to make such a scheme impractical for surveillance of the Great Lakes. Another serious weakness of these orbits is the required stability of the SAR local oscillator. Figure 30 depicts the rapid rise in the required long term stability as the spacecraft approaches synchronous orbit. Stability in excess of 1 part in 10^{12} places a very severe restriction on the local oscillator.

An examination of figures 28 and 29 reveal that a single pass coverage of the Great Lakes (900 km swath) from equatorial orbit has a very demanding power requirement. However, it is interesting to note that for equatorial orbits every pass is a potential imaging pass. Thus, by constructing a mosaic of five consecutive passes, for example, a daily map of the Great Lakes ice cover is obtainable with an X-band SAR at an altitude of approximately 6400 km. If a 15 meter antenna is used, single frequency operation is sufficient with an expenditure of about 370 watts per pass. For a 10 meter antenna, two frequency operation is necessary with an expenditure of 1.2 kw per pass. Clearly, development of a 15 meter X-band antenna would be a tremendous asset to such a system. In either case, the local oscillator stability requirements are modest and approximately 2 parts per 10^{10}. It should be noted that at 6400 km altitude, latitudes to 50° are accessible with a 10° incidence angle (figure 19).

The question arises as to the applicability of such a system at lower latitudes. At lower latitudes the incidence angle is greater and for 100 meter resolution, the required pulse length must be smaller. This requires

a corresponding increase in receiver bandwidth and hence, transmitted power. Simultaneously, the achievable swath width increases requiring a corresponding decrease in the antenna range dimension. This reduces the gain of the antenna and the required power is further increased. This trend is depicted in figure 31.

If the achievable swath width at the lower latitudes is greater than required, a higher prf and larger antenna range dimension can be used to reduce the required power. For example, the achievable swath width at 10° latitude for an X-band SAR at 6400 km altitude (figure 31) is 409 km. The required power is 7 kw. Quadrupling the prf reduces the swath width to 100 km. The antenna range dimension goes from 1.06 meters to 4.24 meters. The required power is reduced by a factor of 16 to 426 watts.

Both the Great Lakes application and low power low latitude applications could conceivably be satisfied by using an antenna with multiple beams. That is, a large number of beams could be used at the lower latitudes with a smaller number (down to a single beam) used at the higher latitudes. This would be equivalent to having an antenna with adjustable range coverage.

The multibeam antenna approach would allow tailoring of the SAR characteristics to optimize power and performance at each latitude. Hence, the equatorial SAR would be applicable to the lower latitudes as well as the latitude range of the Great Lakes.

While an altitude of 6400 km for an equatorial orbit appears to be a reasonable compromise between the power required, achievable swath width, antenna size and frequency of coverage, the satellite would be in the midst

of the most intense trapped proton radiation belt. As discussed earlier in section III.C.3, a power supply other than solar cells (e.g., an RTG) would be required. In addition other electronic components would need special radiation protection thus incurring some weight penalty. The feasibility of this approach would need more detailed study than can be given here.

An alternate approach would be to select a higher equatorial orbit outside the most intense radiation region where solar cells would be adequately protected. The problem is that as the altitude is increased the required power also increases rapidly (figure 29) while the rate of coverage decreases (figure 18). A reasonable compromise appears to be an altitude of about 14,000 km. At this altitude the required average power would be about 2.5 kw (figure 29) and the satellite would "lap" the earth twice daily. A 10 meter antenna could achieve a swath width of about 280 km at the latitude of the Great Lakes while a 15 meter antenna would afford a swath width of about 420 km (figure 28). In either case, however, daily coverage of the Great Lakes would not be possible as was the case at 6400 km altitude without going to impractically large antennas (greater than 30 meters in the range dimension).

2. Polar (Sun-Synchronous) Orbits

For polar orbits little is gained by going to high altitudes. The coverage rate is low, power required is excessive, and image distortion (refs. 17, 18) results because the doppler shift produced by the rotation of the earth is comparable to the shift produced by the orbital velocity of the spacecraft.

At low altitudes (400-1000 km) the swath width for single frequency operation is on the order of 50-100 km. Rapid coverage of the Great Lakes from polar orbit therefore requires multifrequency/multibeam techniques. Typical power requirements as a function of incidence angle for single beam/single frequency operation are shown in figure 32.

The curve must be interpreted carefully. The antenna range dimension is constantly changing as indicated to suppress the range ambiguity. This change is in a direction to increase the antenna gain at low incidence angles. Hence, a decline in power requirement results at low incidence angles. Also, at low incidence angles larger width radar pulses are sufficient to obtain the required range resolution. The attendant bandwidth reduction allows for a further reduction in power. However, these effects only delay the inevitable. At 10° incidence the required antenna range dimension is 8.5 meters and increases rapidly as the incidence angle decreases further. The maximum practical antenna size is quickly encountered and no further power reduction is possible. Also the scattering coefficient decreases very rapidly at these low angles and eventually it must dominate and cause the power to rise again.

For polar orbits the swath width falls along the east-west span of the Great Lakes. This east-west span is approximately 1300 km. It is reasonable to assume that at least four and possibly six beams could be synthesized with the type antenna needed for this application. At 20° incidence this would require four to six X-band multiple feeds to illuminate a 10 x 3 meter antenna with the displacement of the beams along the minor axis.

Although figure 32 showed the required power to rise rapidly as the incidence angle increased, in the range of 10° to 40° this rate is relatively slow. In the vicinity of 20°, say ±2° the required power could be approximated with an average value. Then superimposing several beams over this area and adding the required powers based on the above average value will not be much in error. Using this approach, the swath at 20° can be increased in multiples of 109 km and 97 watts required power. Four beams would then span 436 km with a required 388 watts of power. This swath would be sufficient to span the Great Lakes in three days. Six beams would imply two day coverage with 582 watts. The approximate required power versus coverage period is shown in figure 33.

SYSTEM SELECTION

From the foregoing discussion it appears that daily coverage could perhaps be achieved from an equatorial orbit at about 6400 km altitude. The 6400 km equatorial orbit "laps" the earth five times daily thus allowing a daily image to be constructed from a mosaic of five consecutive passes. Radar beam swath widths on the order of 250 km are achievable at the latitude of the Great Lakes with such an equatorial satellite so that an area the size of the Great Lakes (about 900 km north to south) could be mapped in five or even four passes. The average power required would be about 400 watts. However, because of the intense radiation at this altitude (due mostly to trapped protons) a power source other than solar cells (e.g., an RTG) would be required. Other electronic components would need radiation protection, thus incurring a weight penalty. Such a system is judged to be relatively complex and costly and does not appear to be an attractive solution. However, this approach would need more detailed study than can be given here to adequately assess its feasibility.

An alternate approach is to select a higher equatorial orbit (above 11,000 km) where solar cells can be adequately shielded but at the expense of daily imaging. An altitude of about 14,000 km appears to be a reasonable choice. At this altitude, solar cells can be adequately protected with a fused silica glass cover of reasonable thickness. A thickness of about 20 mils would limit power degradation to 25 percent at the end of five years. At 14,000 km the required average power for imaging at the latitude of the

Great Lakes would be about 2.3 kw. The satellite would "lap" the earth twice daily. At the latitude of the Great Lakes, swath widths of 280-420 km could be achieved with antenna range dimensions of 10-15 meters respectively. Daily coverage of the Great Lakes would not be possible since it would require an impractically large antenna (greater than 30 meters in the range dimension).

Some pertinent parameters for the two equatorial orbits discussed above are listed in the following table:

Equatorial Orbits for Great Lakes Imaging

Altitude, km	6410.82	13916.91
Period, hours	3.998	7.993
Inclination, deg	0	0
Average power, watts	400	2500
Area scan repetition period , hours	4.8	12
Latitude coverage, deg	41-49	41-49
Respective beam incidence angles, deg	26-12	34-24
Achievable swath width at 50 deg latitude, km	250	420
Antenna size, meters	12 x 15	6 x 15
Resolution, meters	100 x 100	100 x 100
Receiver effective noise, °K	500	500
Primary power source	RTG	Solar

Conventional single-beam/single-frequency technology is adequate for covering the Great Lakes from an equatorial orbit. However, development of a deployable 12 meter x 15 meter or 6 meter x 15 meter antenna would be required. This appears to be technically feasible in light of the successful development of a 10 meter (approximately) deployable antenna for ATS-F.

To create a mosaic, the radar beam would have to be moved on each pass. This could be done by either changing the satellite attitude or steering the beam. Steering the beam would be the preferred approach to minimize the satellite attitude control requirements. For the small steering angle involved (about 6 deg at 6400 km and 1.5 deg at 14,000 km) the beam could probably be electronically steered. Otherwise a slewed antenna would be required which would add to the satellite's attitude control requirements.

Eclipsing of the satellite by the earth would occur six times daily for the 6400 km orbit and three times daily for the 14,000 km orbit. The eclipsing would have no direct effect on the power system design for the 6400 km orbit since solar cells would not be used. For the 14,000 km orbit, eclipsing would occur about nine months of the year with a maximum of about 10.5 percent of each orbit (about 50 minutes). In terms of earth coverage each eclipse would cover about a 25 deg slice in longitude at intervals (center to center) of 120 deg. Any one area could be scanned only once daily with the satellite in full sunlight, thus requiring three days to cover an area the size of the Great Lakes (420 km swath each day). By

providing battery backup, both of the daily passes over the target area could be utilized for imaging, thus halving the time required to 1.5 days. However, because of the large amount of eclipsing involved, battery backup is impractical. For instance, at least 250 pounds of Ni-Cad batteries would be required to provide this backup capability. The batteries would also be required to undergo a daily charge/discharge cycle for about nine months each year.

For radar imaging over a range of latitudes from an equatorial orbit a slewed antenna would be required. Earth coverage would be restricted to latitude bands on either side of the equator. Limiting the radar beam incidence angle to a range from 10 to 70 deg, for instance, would limit the latitudes to bands from about 10 to 50 deg for the 6400 km orbit and about 14 to 62 deg for the 14,000 km orbit. Degradation in performance will occur at the lower latitudes because of the change in incidence angle. Using the 6400 km orbit as an example, with no change in the radar system the swath width would decrease from 250 km at 50 deg latitude to 50 km at 10 deg latitude. The range resolution would be proportionately degraded from 100 meters to 500 meters. Conceivably, this problem could be circumvented by using a variable mode radar which would switch to multiple beams and shorter pulse widths at the lower latitudes. This would require the development of a multibeam/multifrequency synthetic aperture radar which may require a substantial technology development effort. As an indication of the difficulty involved, the Goodyear Aerospace Corporation has estimated that for the EOS (Earth Observatory Satellite) radar, which is a single beam/single frequency system, there is only a 50 percent likelihood of obtaining 5000 hours or about 200 days of operation. The chances of obtaining a similar operational capability, much less operations on the

the order of several years, with a multibeam/multifrequency synthetic aperture radar would appear to be quite small at this time. Considerable technology development work is indicated in this area.

An important point to remember is that the required average power is a strong function of the target latitude (or beam incidence angle). This is illustrated in figure 31 for the 6400 km orbit. Note that while less than 400 watts is required at 50 deg latitude about 7 kw would be required at 10 deg latitude to utilize the full unambiguous range interval of the system. In other words, figure 31 assumes a constant resolution as latitude is varied and the antenna range dimension is decreased to match the growth in unambiguous range interval. The latitude range covered would thus be considerably less than indicated earlier in order to limit the power required to a practical value.

For the sun-synchronous orbit case, the relatively modest power requirement allows us to choose an altitude high enough (around 1000 km) to completely avoid atmospheric drag and the attendant complexities of a drag compensation system. A reasonable choice seems to be the case having a three-day coverage pattern and requiring about 400 watts of average power. A two-day coverage requiring about 600 watts is also considered practical. Daily coverage would require about 1.2 kw which is not as attractive as the two-day coverage case in terms of the power required.

Wide swath coverage from sun-synchronous orbit will also require the development of a multibeam/multifrequency synthetic aperture radar. The number of beams required for the three-day, two-day and daily coverage cases would be 4, 6 and 12 respectively. From a practical point of view,

12 beams is not consistent with the required antenna range dimension of about 3 meters, thus ruling out daily coverage.

The three-day and two-day coverage cases are summarized below for a resolution of 100 meters x 100 meters and a receiver effective noise temperature of 500°K.

Sun-Synchronous Orbits

Coverage Period	3-day	2-day
Altitude, km	1011.5441	1072.2403
Period, hours	1.75610	1.77778
Inclination, deg	99.5310	99.8105
Average power, watts	400	600
Orbits per 24 hours	13-2/3	13-1/2
Earth track separation in longitude, deg	8.7805	13.3333
Earth track separation at equator, km	952.0	1443.5
Earth track separation at 45 deg latitude, km	655.5	995.2
Beams required	4	6
Total achievable swath width, km	436	654
Antenna size, length x width, meters	10 x 3	10 x 3

For sun-synchronous orbits, beam steering is not required since all targets eventually come into view resulting in global coverage. This is not possible with the equatorial orbits. With global coverage possible, more applications for this system would likely result.

It should also be noted that the average power levels quoted for the sun-synchronous orbits are for a mean incidence angle of 20 deg. Unlike the equatorial orbits, the incidence angle can remain nominally fixed while still achieving global coverage, thus avoiding the increase of power at lower incidence angles that the equatorial orbits experience.

For a sun-synchronous orbit normal to the sunline at about 1000 km altitude, solar eclipsing will occur for a period of about two months (roughly mid-May to mid-July) reaching a maximum of about 11 percent of the orbit period (about 12 minutes). Battery backup power could be provided if imaging is required during this period. About 10-15 pounds of Ni-Cad batteries would suffice. Otherwise, batteries would only be required for housekeeping functions.

CONCLUSIONS

Applications involving dynamic phenomena such as ice imaging, ocean state surveillance, and pollution monitoring require short response time (image turnaround time) which in turn implies wide swath width coverage.

Equatorial orbits are not a practical solution. Daily coverage from equatorial orbit requires an altitude of about 6400 km which is in the heart of the trapped proton radiation belt thus precluding the use of solar array power. Orbits above the most intense part of the radiation belt such as the case investigated at 14,000 km do not allow daily coverage and result in considerably higher power requirements. Battery backup power does not appear practical.

Equatorial orbits do not allow global coverage thus limiting other potential applications. Coverage of a range of latitudes would require a multibeam/multifrequency synthetic aperture radar and a slewed antenna. In addition, coverage at the lower latitudes would result in high radar beam incidence angles and increased power requirements up to the multi-kilowatt range.

Sun-synchronous orbits around 1000 km altitude appear to be the best approach to obtaining wide swath coverage. However, a multibeam/multifrequency synthetic aperture radar system will need to be developed. Daily coverage of an area the size of the Great Lakes does not appear practical since the

large number of beams required (approximately 12) is not consistent with the required antenna range dimension of about three meters. Coverage at two-day or three-day intervals appears feasible. This would require six beams and four beams respectively. The average power required would be about 600 and 400 watts respectively.

Sun-synchronous orbits can obtain global coverage, thus allowing potentially more applications than an equatorial orbit. Antenna slewing would not be required since all targets eventually come into view.

Future studies are needed to define this system in more depth. Particular attention should be given to assessing the feasibility of a multibeam/multifrequency synthetic aperture radar and the possibility of using a large number of beams such as 12 to allow daily coverage of an area the size of the Great Lakes. In addition, studies are needed to identify other potential users and to determine what applications are practical. The costs and benefits associated with these applications need to be defined along with the capabilities of alternate approaches such as aircraft, in situ observations, etc. to adequately assess the merits of a radar imaging satellite.

APPENDIX A

Derivation of Ψ as a Function of Time for a Decaying Orbit

The angle Ψ is defined as the longitudinal relation between the sunline and the orbit perpendicular, $\Psi = \alpha - \Omega$. Thus, Ψ as a function of time can be expressed as

$$\Psi = \int (\dot{\alpha} - \dot{\Omega}) \, dt + K \text{ (constant)} \qquad \text{(A-1)}$$

Since the orbit is taken to be initially sun-synchronous, $\dot{\alpha} = \dot{\Omega}$ for $h = h_o$ and $I = I_o$ in equation (1) of the main text. Note that $\dot{\Omega} = \dot{\Omega}_a$. As the satellite decays, $\dot{\Omega}$ varies with h according to equation (1) with $I = I_o$.

Thus,

$$\Psi = K - \sqrt{\mu} \; J R_e^2 \cos I_o \int \left[(R_e + h_o)^{-3.5} - (R_e + h)^{-3.5} \right] dt \qquad \text{(A-2)}$$

Assuming $h << R_e$

$$\Psi = K + 3.5 \sqrt{\mu} \; J R_e^{-2.5} \cos I_o \int (h_o - h) \, dt \qquad \text{(A-3)}$$

The integral of h dt must now be determined. Using h from equation (8) of the main text,

$$\int h \, dt = \frac{86400}{\beta} \int \ln \left[- 86400 \; B \left(\frac{t}{W/C_D A} \right) + e^{\beta h_o} \right] dt \qquad \text{(A-4)}$$

where dt is reckoned in days.

Let

$$Z = \left[- 86400 \; B \left(\frac{t}{W/C_D A} \right) + e^{\beta h_o} \right] \quad \text{so that} \quad dZ = \frac{-86400 \; B}{(W/C_D A)} \, dt$$

Substituting into equation (A-4),

$$\int h \, dt = \frac{(W/C_D A)}{\beta B} \int - \ln Z \, dZ = - \frac{(W/C_D A)}{\beta B} \left[Z(\ln Z - 1) \right] \qquad \text{(A-5)}$$

By substituting equation (A-5) and Z into equation (A-3) and rearranging,

$$\Psi - K = 3.5\sqrt{\mu}\ J\ R_e^{-2.5}\ (W/C_DA)\cos I_o \left[\left\{\frac{-86400}{\beta}\left(\frac{t}{W/C_DA}\right) + \frac{e^{\beta h_o}}{\beta B}\right\}\left\{\ln\left[-86400B\left(\frac{t}{W/C_DA}\right) + e^{\beta h_o}\right] - 1\right\} + 86400\ h_o\left(\frac{t}{W/C_DA}\right)\right] \quad \text{(A-6)}$$

It should be remembered that t is in days and W is in Kgf in equation (A-6).

The constant K may be determined by evaluating equation (A-6) at t = 0 when $h = h_o$ and $\Psi = \Psi_o$.

$$K = \Psi_o - 3.5\sqrt{\mu}\ J\ R_e^{-2.5}\ (W/C_DA)\cos I_o\left[\frac{e^{\beta h_o}(\beta h_o - 1)}{\beta B}\right] \quad \text{(A-7)}$$

Combining equations (A-6) and (A-7) we may plot $\frac{\Psi_o - \Psi}{W/C_DA}$ versus $\frac{t}{W/C_DA}$ for various initial sun-synchronous orbits (see figure 8).

APPENDIX B

Separation Distance Between Earth Tracks of Two Circular Orbits Separted in Longitude by $\Delta\Omega$

Consider a circular orbit about the earth with a given retrograde inclination. As the satellite moves along its orbital path the sub-satellite point (along radius vector to center of earth) will describe a track on the earth's surface. As the earth rotates beneath the satellite orbit the resulting successive tracks will move westward across the earth's surface. Although the orbit itself describes a great circle about the center of the earth the track on the earth's surface will not because of the earth's rotation. This fact complicates but does not preclude obtaining a closed form approximate solution for the separation distance between the tracks. The approach here is to first derive an approximate solution based on assuming the tracks are great circles and then refining this solution for the actual geometry.

If we assume that the tracks are great circles, the computation of the separation distance involves utilizing a fairly simple set of trigonometric formulae. Consider sketch B1 showing two orbit tracks as great circles separated in longitude by $\Delta\Omega$ and having an inclination, I.

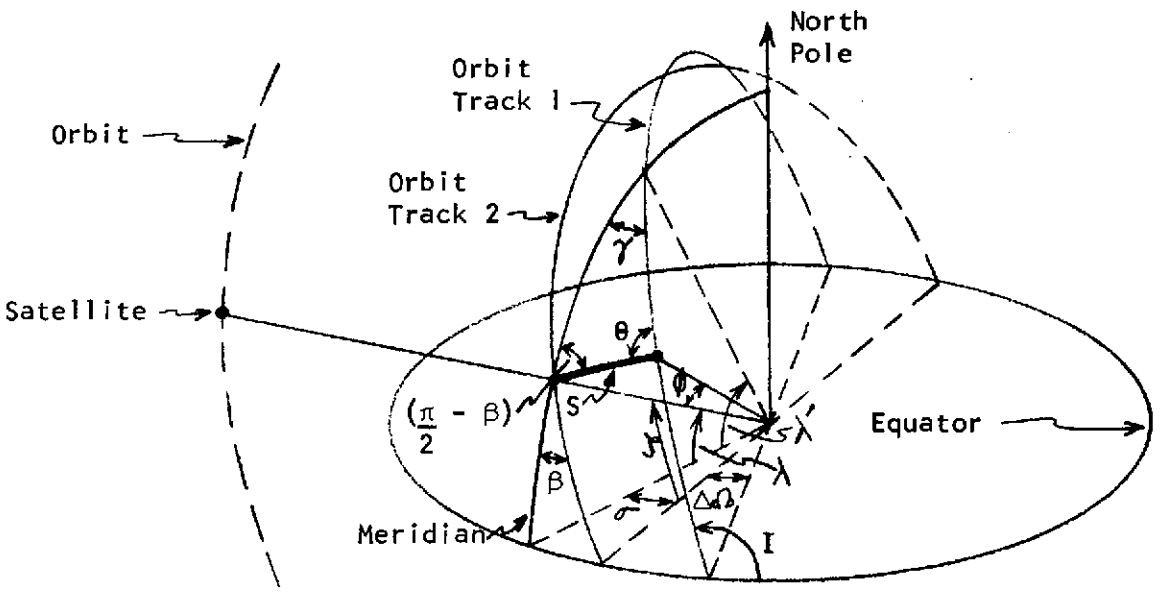

Sketch B1

Let us define the separation distance, S, as measured along a great circle on the surface of the earth from the subsatellite point at some latitude, λ, normal to the current orbit track (orbit track 2), to the preceding orbit track (orbit track 1).

It should be remembered that the geometry in sketch B1 does not represent the actual case. In reality the orbit track is continuous as the satellite orbits the earth and not a set of discrete circles as is depicted. To an observer on the surface of the earth the track would appear to cross the equator with an inclination greater than the orbit inclination due to the rotational velocity of the earth. However, the northernmost position of the orbit track would still reach a latitude consistent with the orbit inclination, i.e., $\pi - I$. The resulting orbit tracks thus will not be great circles due to the earth's rotation. However, each succeeding track will be skewed or displaced in the same way so that for a first approximation we can neglect the earth's rotation in calculating separation distance.

Consideration of sketch B1 and the relationships of spherical trigonometry lead to the following series of expressions:

$$\sin \gamma = \frac{\sin \lambda}{\sin I} \tag{B-1}$$

$$\tan \sigma/2 = \tan\left(\frac{\gamma + \lambda}{2}\right) \frac{\cos\left(\frac{3}{4}\pi - \frac{I}{2}\right)}{\cos\left(\frac{I}{2} - \frac{\pi}{4}\right)} \tag{B-2}$$

$$\sin \beta = \frac{\sin \sigma}{\sin \gamma}, \quad \lambda \neq 0 \text{ or } \beta = I - \frac{\pi}{2}, \quad \lambda = 0 \tag{B-3}$$

$$\cos \gamma = \sin I \cos (\sigma + \Delta\Omega) \tag{B-4}$$

$$\sin \lambda' = \frac{\sin I \sin (\sigma + \Delta\Omega)}{\sin \gamma} \tag{B-5}$$

$$\cos \theta = -\cos \gamma \cos\left(\frac{\pi}{2} - \beta\right) + \sin \gamma \sin\left(\frac{\pi}{2} - \beta\right) \cos (\lambda' - \lambda) \tag{B-6}$$

$$\sin \phi = \sin \gamma \sin (\lambda' - \lambda) \tag{B-7}$$

The separation distance, S, can then be found from

$$S = R_e \phi \tag{B-8}$$

where R_e is the radius of the earth and may be computed for an oblate earth from

$$R_e = \frac{ab}{(b^2 + (a^2 - b^2) \sin^2 \lambda)^{1/2}} \tag{B-9}$$

where a (equatorial radius) = 6378.160 km

b (polar radius) = 6356.775 km

One way of considering theeffect of earth's rotation on the orbit track and thus on the computation of the separation distance is to consider the instantaneous direction of motion at any point along the orbit track and to imagine that this resulted from an orbit with the appropriate inclination about a stationary earth. Thus the orbit track is assumed to be a great circle at any instant caused by an appropriately inclined orbit and the solution essentially reduces to the one just derived. The problem is to compute an instantaneous pseudo-inclination for any point along the orbit track. The longitudinal displacement of the track caused by earth's rotation affects all tracks equally and thus does not affect the separation distance.

Consider the orbit track as it crosses the equator. As indicated earlier, the earth's rotation will cause the track to have a greater inclination than the orbit itself. This may be seen by considering the linear velocity vector diagram in sketch B2.

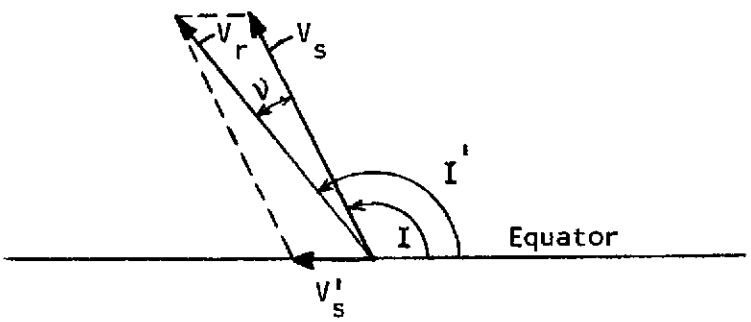

Sketch B2

V_s is the satellite's inertial orbital velocity. V'_s is the velocity of the satellite relative to the earth caused by the relative motion in longitude between the earth and the satellite's orbital plane. This relative longitudinal motion results from the rotation of the earth and the

precession (or regression) of the orbital plane due to oblateness. If the angular rotation of the earth is ω_e and the nodal precession of the orbit is $\dot{\Omega}_a$, then the resulting relative angular motion is

$$\omega' = \omega_e - \dot{\Omega}_a$$

and $$V_s' = \omega' R_e$$

Thus, from sketch B2, the resultant velocity of the satellite relative to the surface of the earth is

$$V_r = (V_s^2 + V_s'^2 - 2 V_s V_s' \cos I)^{1/2}$$

and

$$\nu = \cos^{-1}\left[\frac{(V_r^2 + V_s^2 - V_s'^2)}{2 V_s V_r}\right]$$

so that at the equator,

$$I' = I + \nu$$

For the computation of S at the equator then, equations (B-1) through (B-9) developed earlier can be used with I' substituted for I.

For locations other than the equator, imagine that the velocity diagram of sketch B2 is simply translated to the subsatellite point at some latitude, λ, (refer to sketch B1). The geometry is basically the same with the plane of the velocity vectors normal to the radius vector. V_s lies in the direction of the orbit plane and V_s' is normal to the meridian plane. Referring to sketch B1, the angle between the two would be $(\frac{\pi}{2} - \beta)$ where β can be solved from the previous series of expressions.

In this case,

$$V_r = \left[V_s^2 + V_s'^2 - 2 V_s V_s' \cos\left(\beta + \frac{\pi}{2}\right) \right]^{1/2} = (V_s^2 + V_s'^2 + 2 V_s V_s' \sin\beta)^{1/2}$$

ν is computed as before and from spherical trigonometry.

$$I' = \pi - \cos^{-1}\left[\sin(\beta + \nu)\cos\lambda\right]$$

Here again, I' would be substituted for I in equations (B-1) through (B-9).

REFERENCES

1. Larrowe, B. T.: Fine Resolution Radar Investigation of Great Lakes Ice Cover Rept. 1900-1-F, Radar and Optics Laboratory, The University of Michigan, 1971.

2. Jirberg, R. J.; Schertler, R. J.; Gedney, R. T.; and Mark, H.: Application of SLAR for Monitoring Great Lakes Total Ice Cover. NASA TM X-71473, 1973.

3. Ramler, James R.: Low-Thrust Orbit Raising in Continuous Sunlight While Thrusting in a Plane Perpendicular to the Earth-Sun Line. NASA TN D-4104, 1967.

4. Karrenberg, H. K.: Eclipse Fractions for Sun-Synchronous Orbits. SSD-TDR-64-100; TDR-269 (4550-10)-10, Aerospace Corp., (AD-603152), 1964.

5. Anon.: U.S. Standard Atmosphere, 1962. Prepared under sponsorship of NASA, USAF, and U.S. Weather Bureau for the U.S. Committee on Extension to the Standard Atmosphere, Dec. 1962.

6. Billik, B.: Survey of Current Literature on Satellite Lifetimes. ARS Jour., vol. 32, no. 11, Nov. 1962, pp. 1641-1650.

7. Hunter, Robert E.; Bartlett, Robert O.; Worlock, Robert M.; and James, Edmund L.: Cesium Contact Ion Microthruster Experiment Aboard Applications Technology Satellite (ATS)-IV. Jour. Spacecraft and Rockets, vol. 6, no. 9, Sept. 1969, pp. 968-970.

8. Greenberg, J. S.: A Systems Look at Satellite-Borne High-Resolution Radar. RCA Review, vol. 28, Dec. 1967, pp. 679-709.

9. Cutrona, L. J.; and Hall, G. O.: A Comparison of Techniques for Achieving Fine Azimuth Resolution. IRE Trans. on Military Electronics, vol. Mil-6, Apr. 1962, pp. 119-121.

10. Porcello, Leonard J.: Turbulence-Induced Phase Errors in Synthetic-Aperture Radars. IEEE Trans. on Aerospace and Electronic Systems. vol. AES-6, no. 5, Sept. 1970, pp. 636-644.

11. Brown, William M.: Synthetic Aperture Radar. IEEE Trans. on Aerospace and Electronic Systems, vol. AES-3, no. 2, Mar. 1967, pp. 217-229.

12. Heimiller, R. C.: Theory and Evaluation of Gain Patterns of Synthetic Arrays. IRE Trans. on Military Electronics, vol. Mil-6, Apr. 1962, pp. 122-129.

13. McCord, H. L.: The Equivalence Among Three Approaches to Deriving Synthetic Array Patterns and Analyzing Processing Techniques. IRE Trans. on Military Electronics, vol. Mil-6, Apr. 1962, pp. 116-119.

14. Cutrona, L. J.; Leith, E. N.; Polermo, C. J.; and Porcello, L. J.: Optical Data Processing and Filtering Systems. IRE Trans. on Information Theory, vol. IT-6, no. 3, June 1960, pp. 386-400.

15. Cutrona, L. J.; Leith, E. N.; Parcello, L. J.; and Vivian, W. E.: Coherent Optical Processing Techniques to Synthetic-Aperture Radar. IEEE Proc., vol. 54, no. 8, Aug. 1966, pp. 1026-1032.

16. Vander Lugt A.: Operational Notation for the Analysis and Synthesis of Optical Data-Processing Systems. IEEE Proc., vol. 54, no. 8, Aug. 1966, pp. 1055-1063.

17. Mims, James H.; and Farrell, James L.: Synthetic Aperture Imaging with Maneuvers. IEEE Trans. on Aerospace and Electronic Systems, vol. AES-8, no. 4, July 1972, pp. 410-418.

18. Raney, Keith R.: Synthetic Aperture Imaging Radar and Moving Targets. IEEE Trans. on Aerospace and Electronic Systems, vo. AES-7, no. 3, May 1971, pp. 499-505.

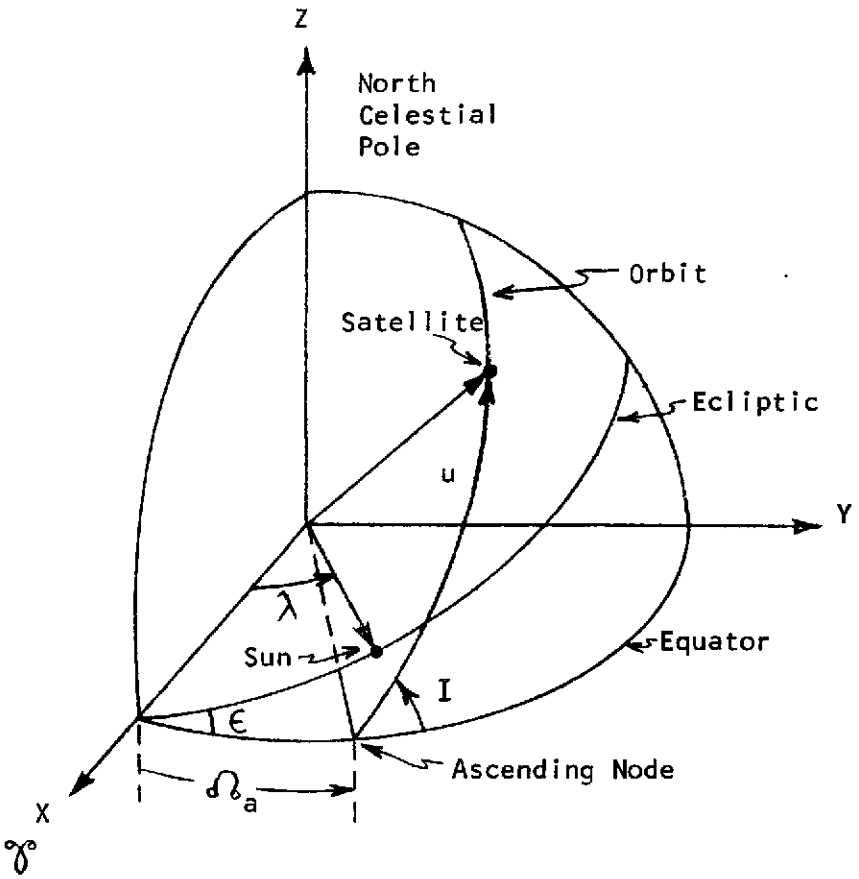

Figure 1 - Earth, Sun, Satellite Geometry

Figure 2 - Orbit Inclination Versus Altitude For Sun-Synchronous Orbits

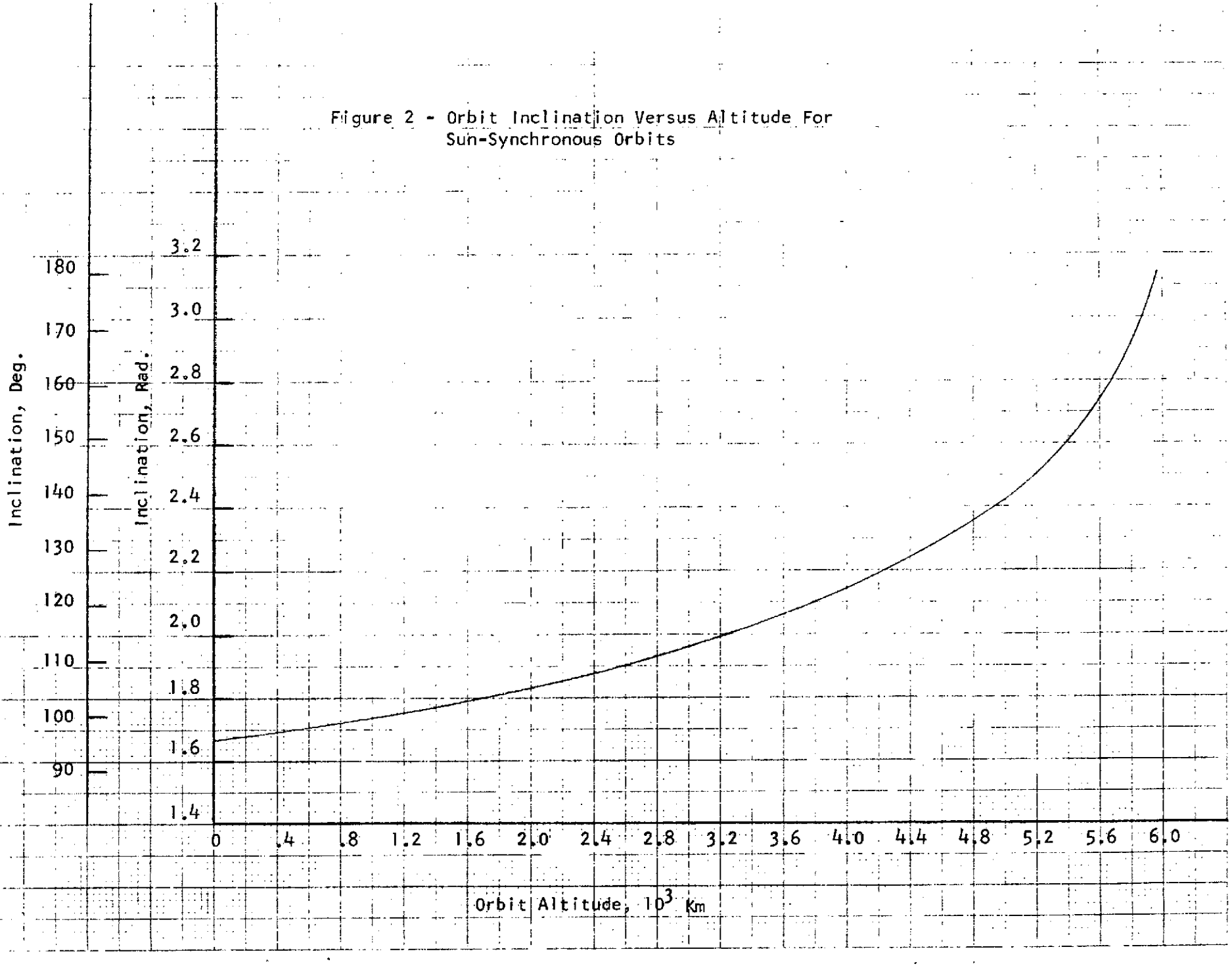

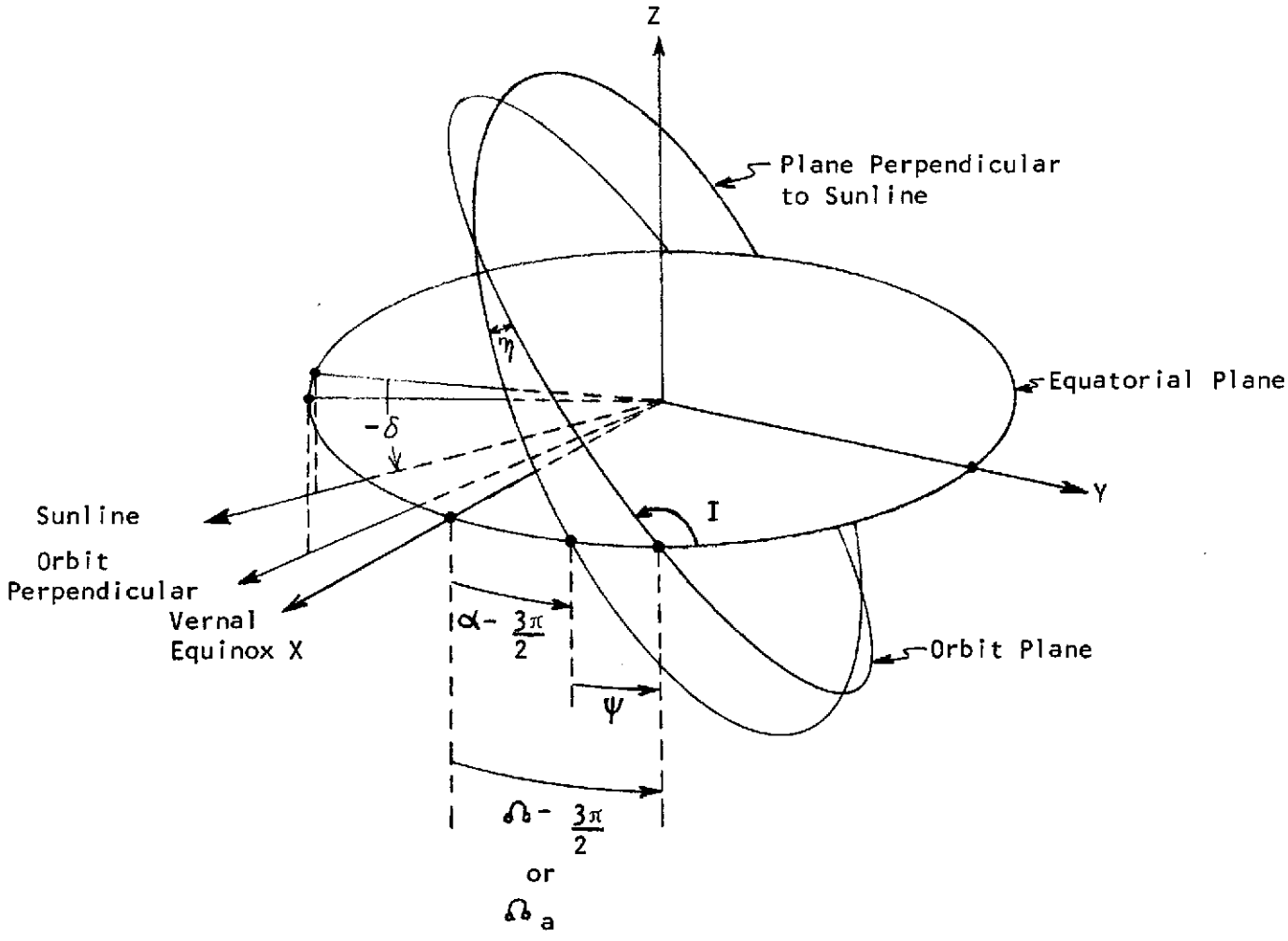

Figure 3 - Sun-Orbit Geometry for Sunline on Same Side of Orbit Plane as Orbit Perpendicular (Angular Velocity Vector)

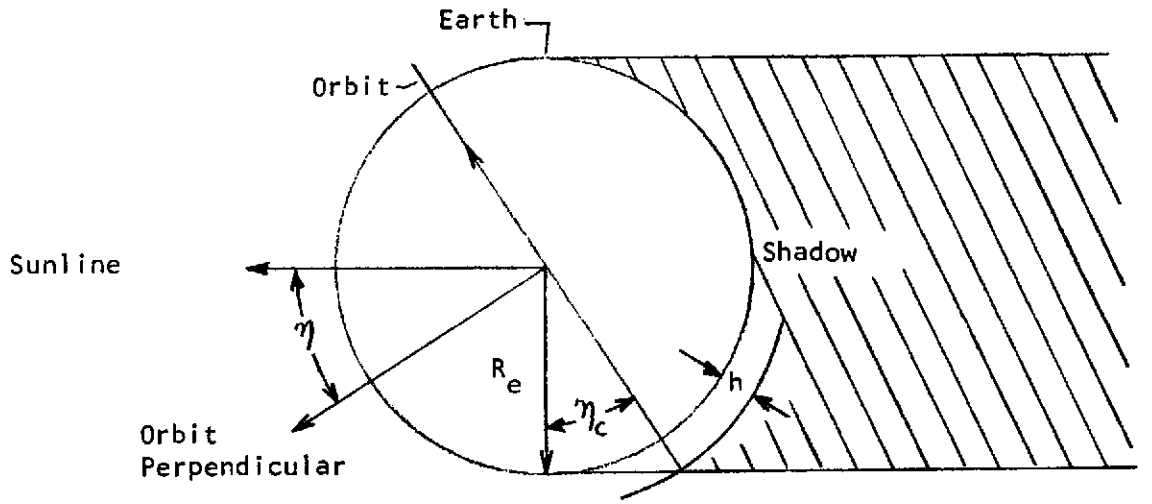

The plane of the figure is the plane containing the sunline and the orbit perpendicular.

Figure 4 - Orbit Shadow Geometry

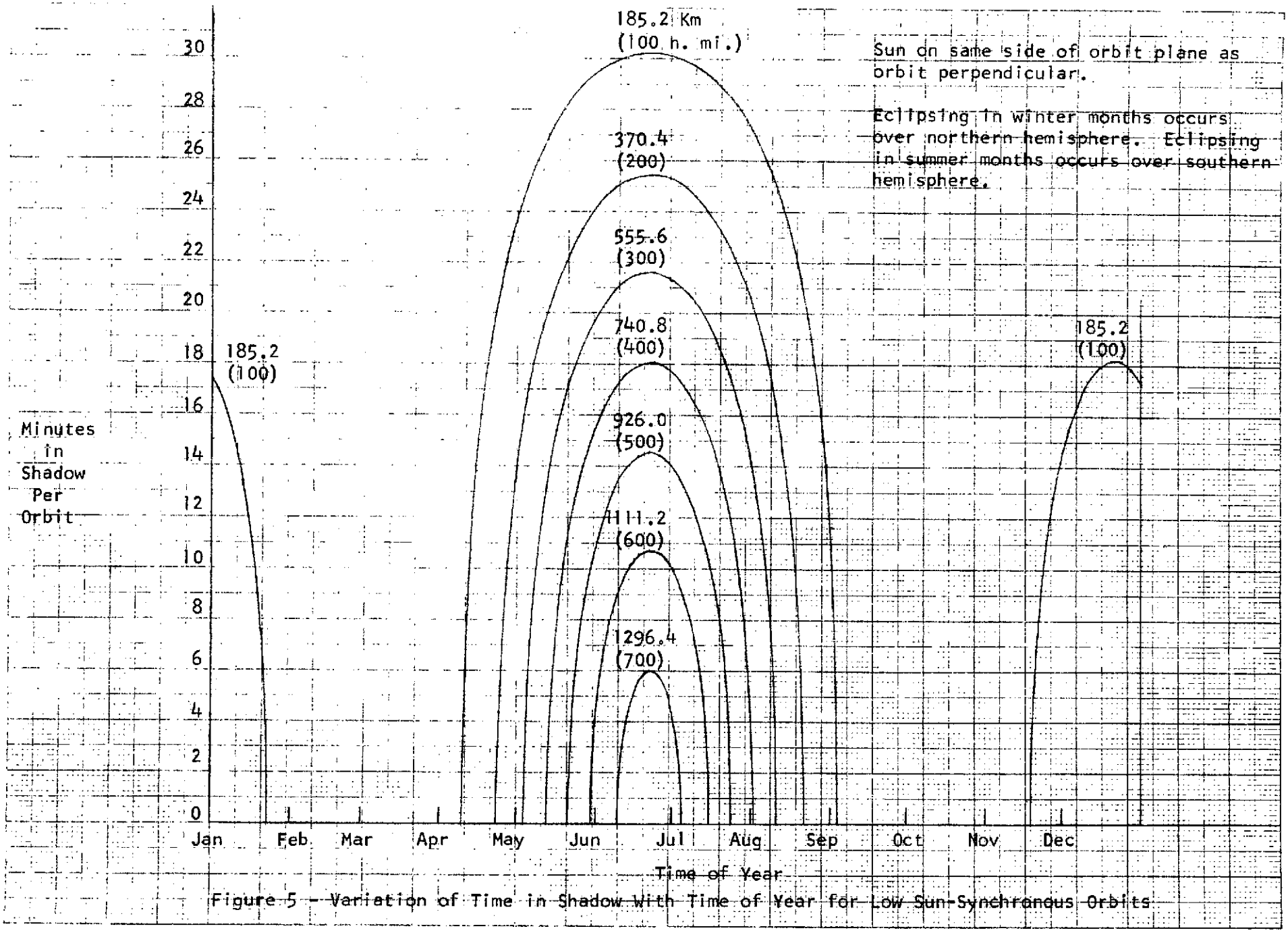

Figure 5 - Variation of Time in Shadow with Time of Year for Low Sun-Synchronous Orbits

Figure 6 - Atmosphere Density as a Function of Altitude

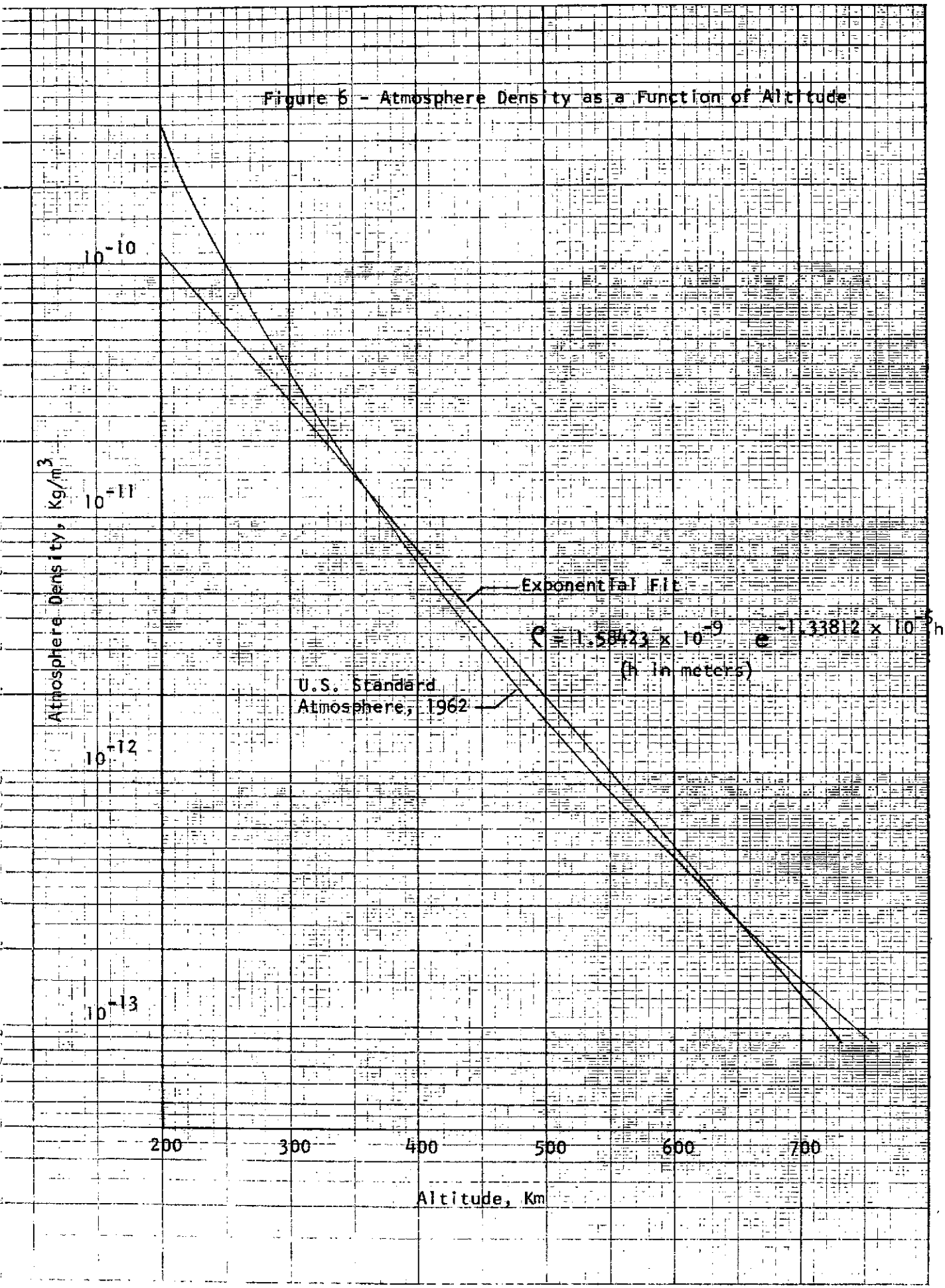

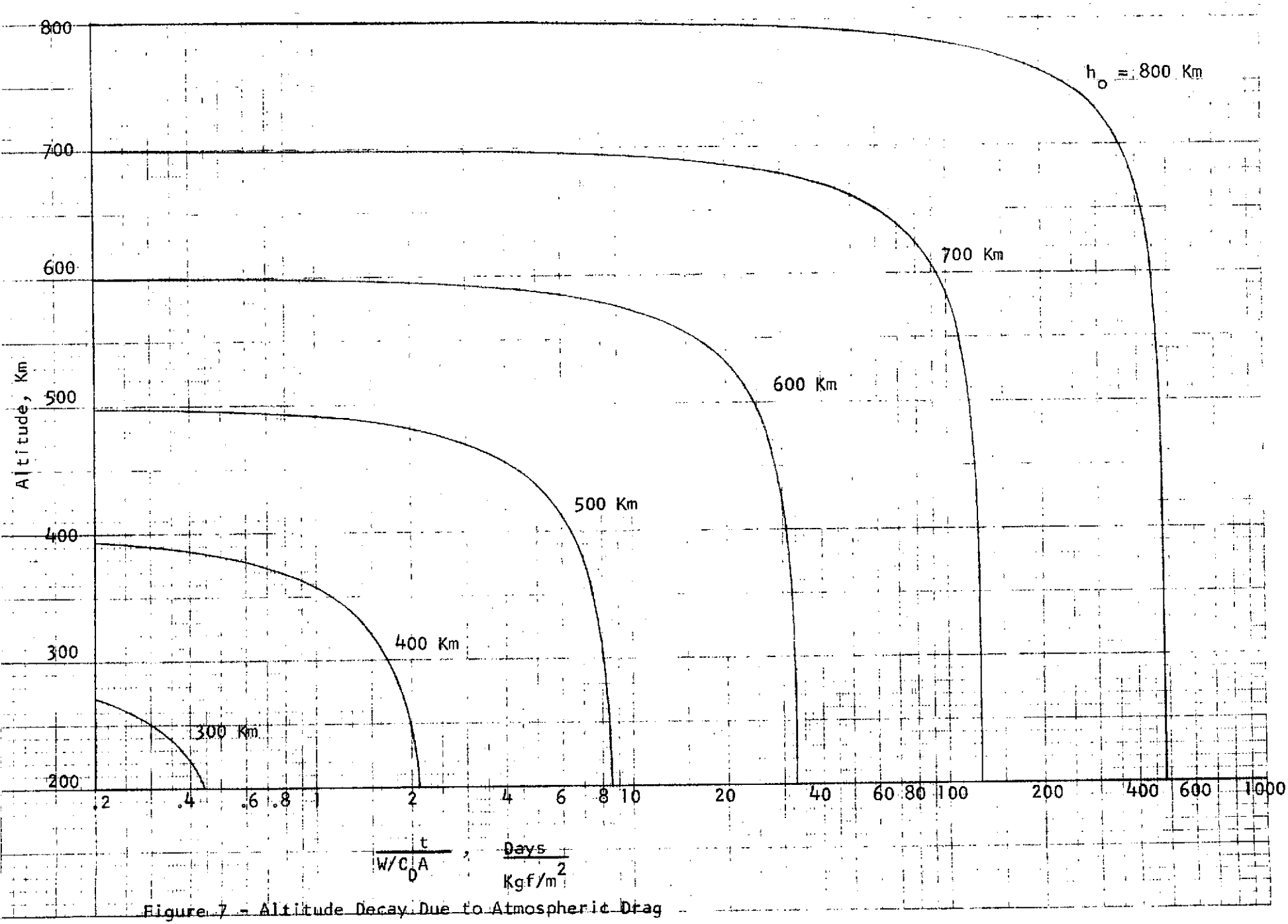

Figure 7 - Altitude Decay Due to Atmospheric Drag

Figure 8 - Effect of Altitude Decay on ($\Psi_o - \Psi$) as a Function of Time for Various Initial Altitudes.

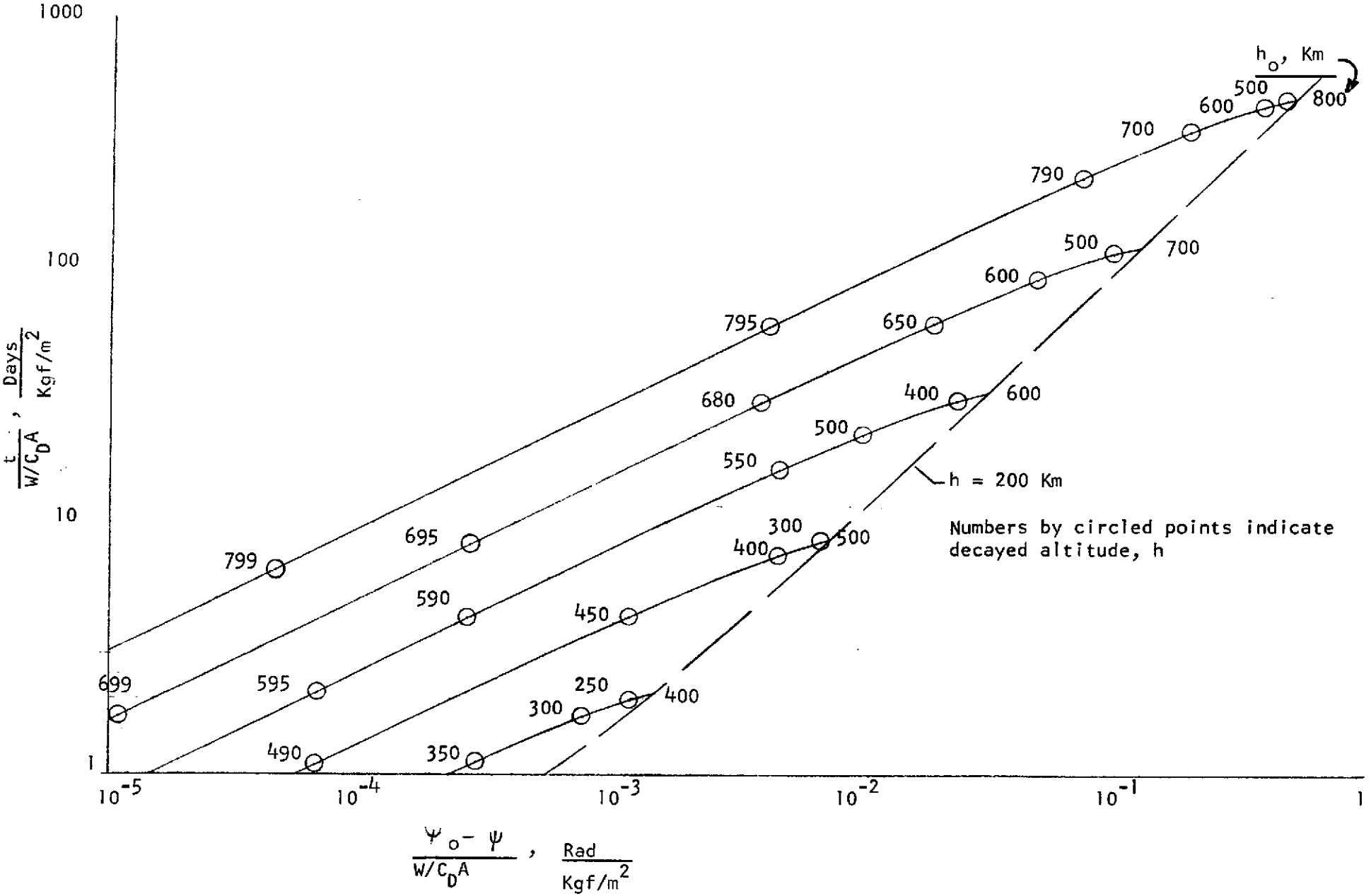

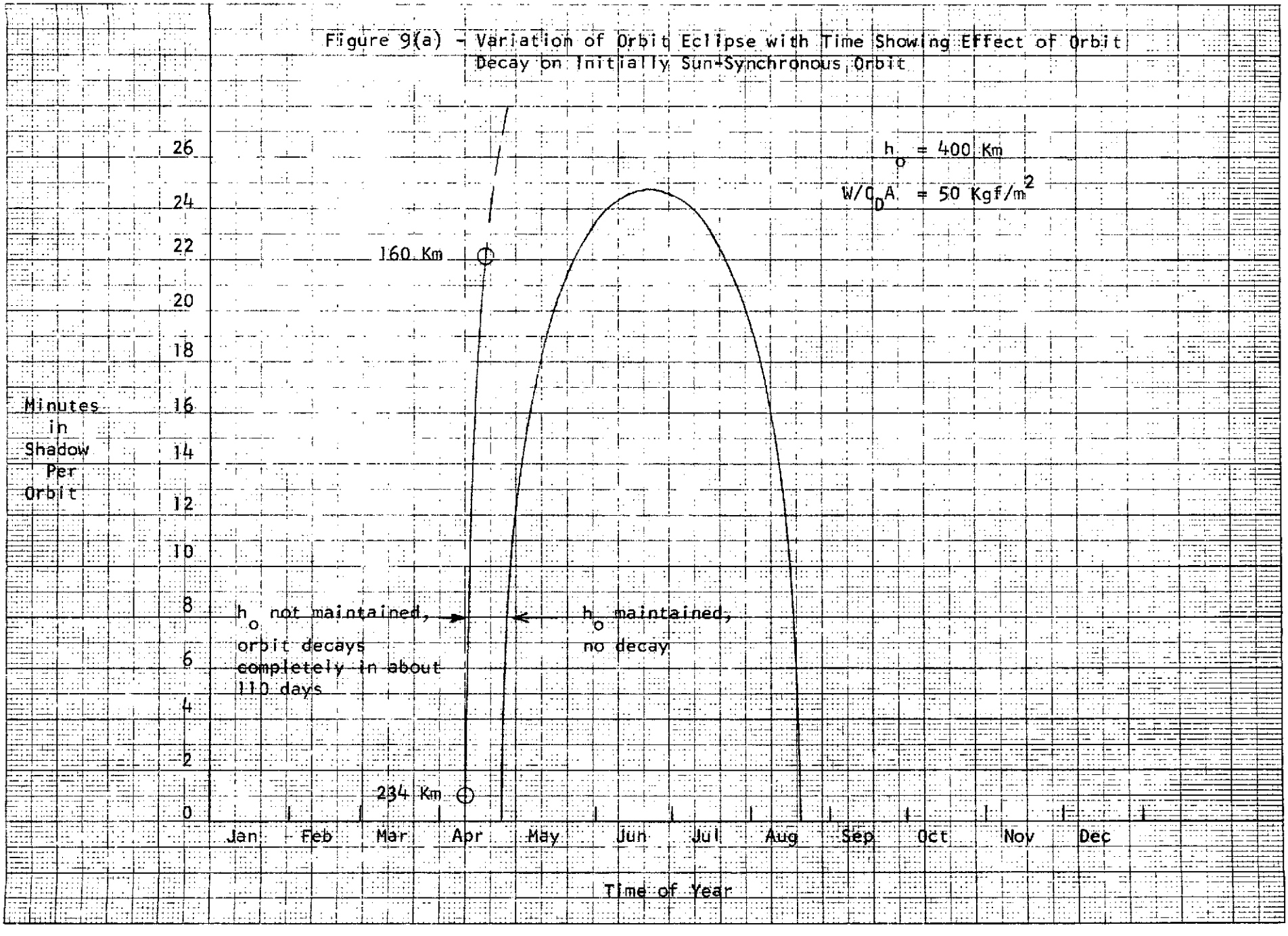
Figure 9(a) - Variation of Orbit Eclipse with Time Showing Effect of Orbit Decay on Initially Sun-Synchronous Orbit
h_o = 400 Km
$W/C_D A$ = 50 Kgf/m^2
160 Km
234 Km
h_o not maintained, orbit decays completely in about 110 days
h_o maintained, no decay
Minutes in Shadow Per Orbit
26
24
22
20
18
16
14
12
10
8
6
4
2
0
Jan
Feb
Mar
Apr
May
Jun
Jul
Aug
Sep
Oct
Nov
Dec
Time of Year

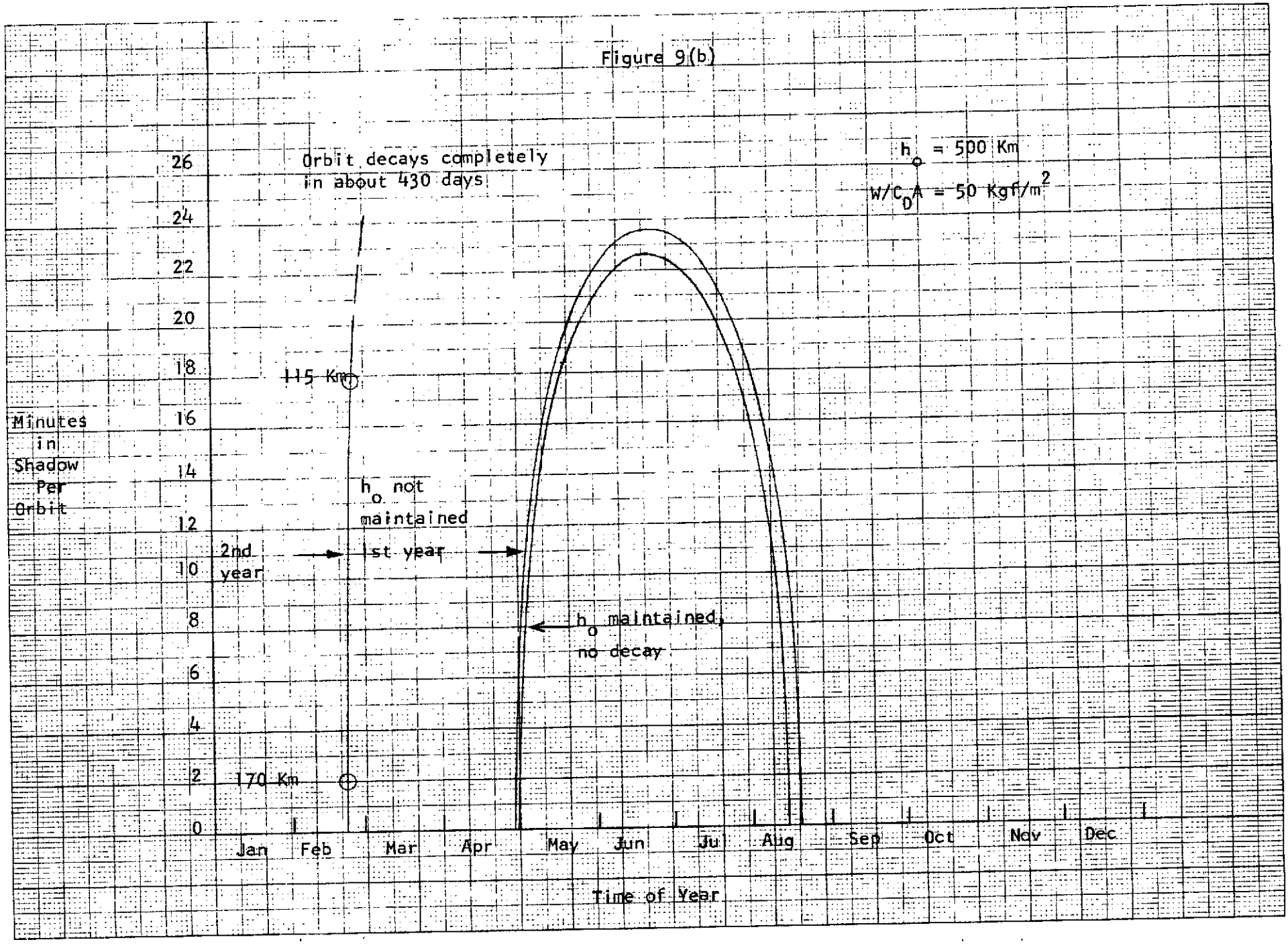
Figure 9(b)
Orbit decays completely in about 430 days
h_o = 500 Km
$W/C_D A$ = 50 Kgf/m^2
115 Km
170 Km
h_o not maintained
2nd year
1st year
h_o maintained, no decay
Minutes in Shadow Per Orbit
26
24
22
20
18
16
14
12
10
8
6
4
2
0
Jan
Feb
Mar
Apr
May
Jun
Ju
Aug
Sep
Oct
Nov
Dec
Time of Year

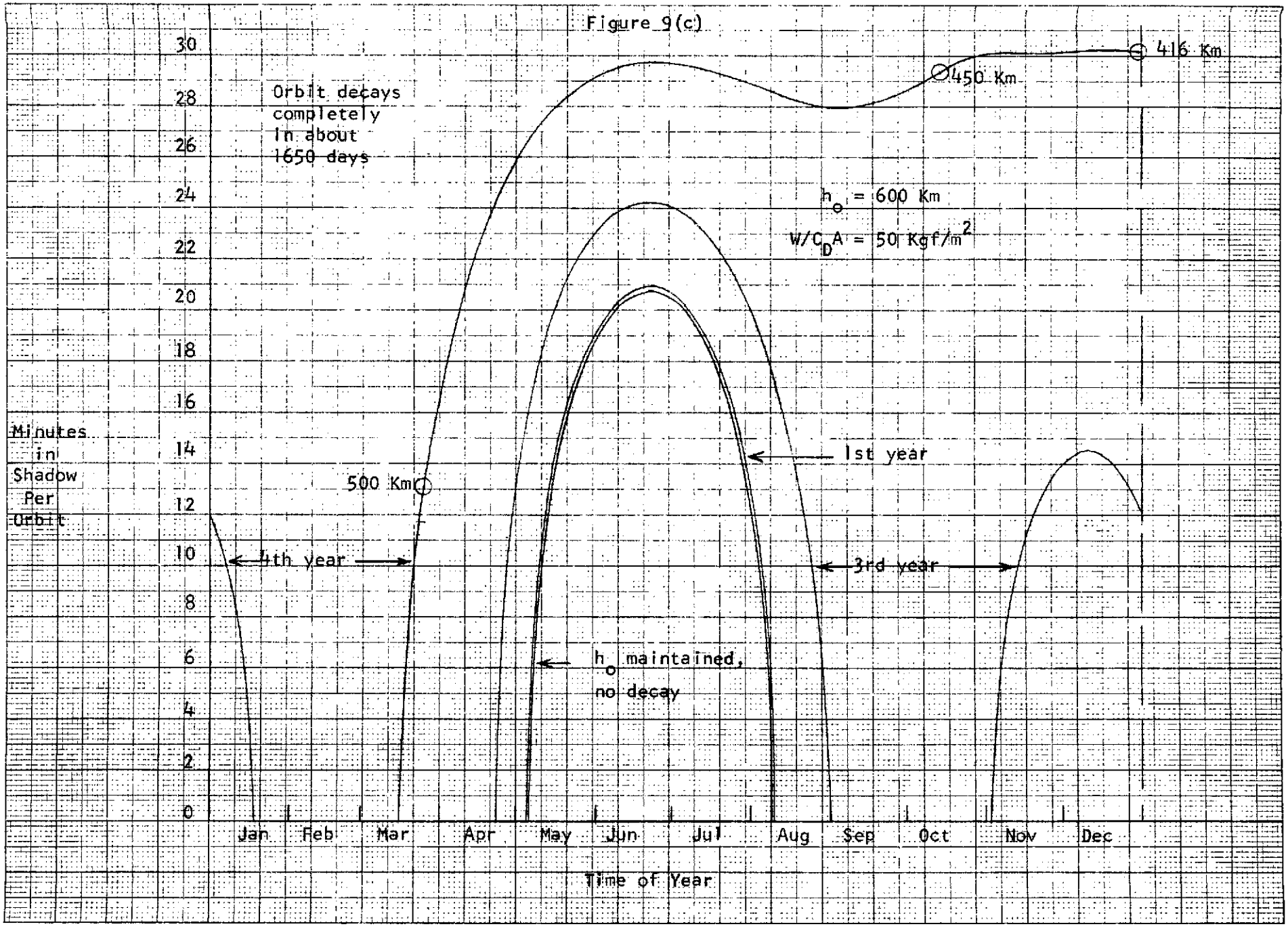
Figure 9(c)
Orbit decays completely in about 1650 days
416 Km
450 Km
h_o = 600 Km
$W/C_D A$ = 50 Kgf/m^2
500 Km
1st year
4th year
3rd year
h_o maintained, no decay
Minutes in Shadow Per Orbit
30
28
26
24
22
20
18
16
14
12
10
8
6
4
2
0
Jan
Feb
Mar
Apr
May
Jun
Jul
Aug
Sep
Oct
Nov
Dec
Time of Year

Figure 9(d)

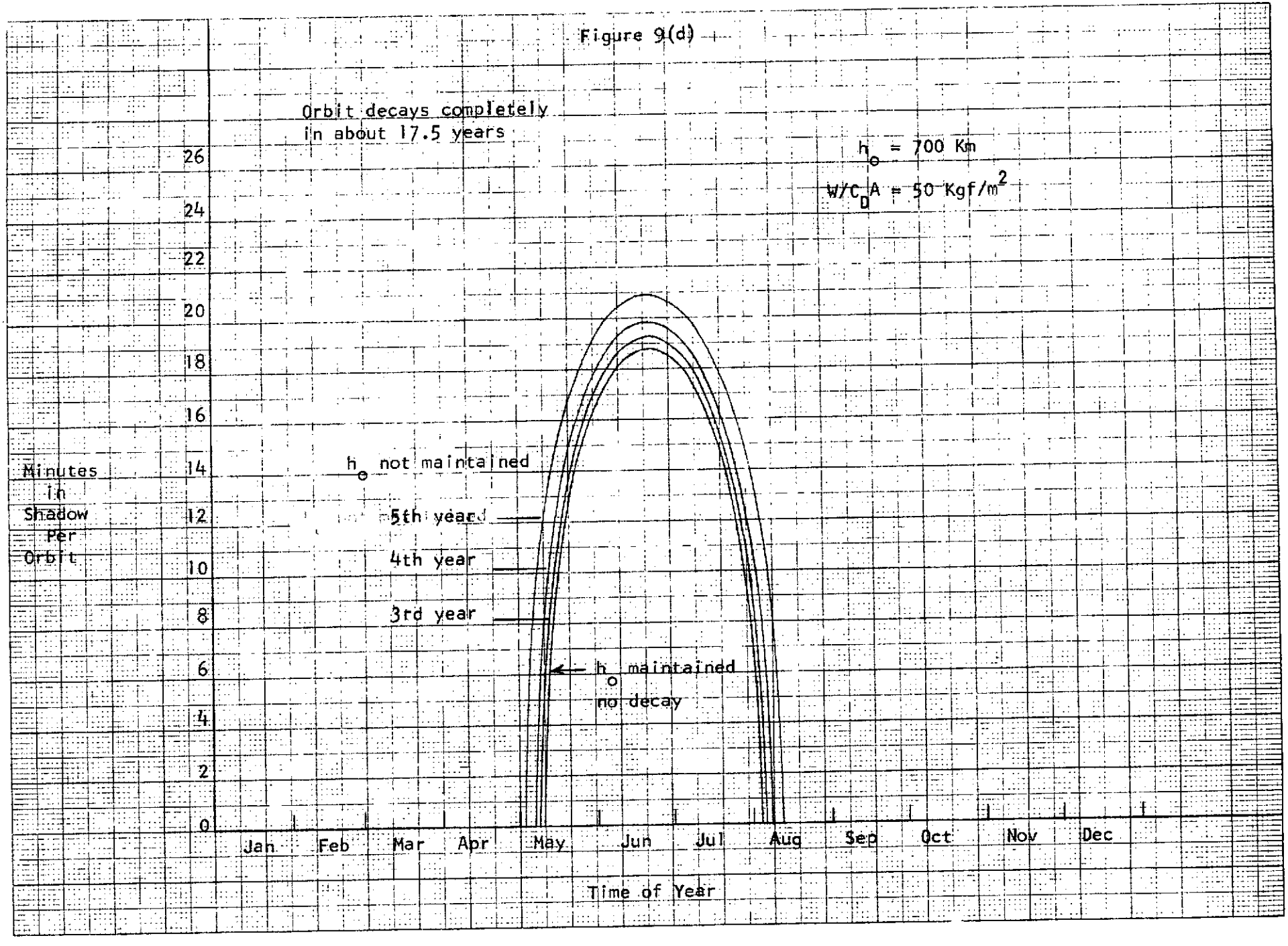
Orbit decays completely
in about 17.5 years
h_o = 700 Km
$W/C_D A$ = 50 Kgf/m^2
Minutes in Shadow Per Orbit
26
24
22
20
18
16
14
12
10
8
6
4
2
0
h_o not maintained
5th year
4th year
3rd year
h_o maintained
no decay
Jan
Feb
Mar
Apr
May
Jun
Jul
Aug
Sep
Oct
Nov
Dec
Time of Year

Figure 9(e)

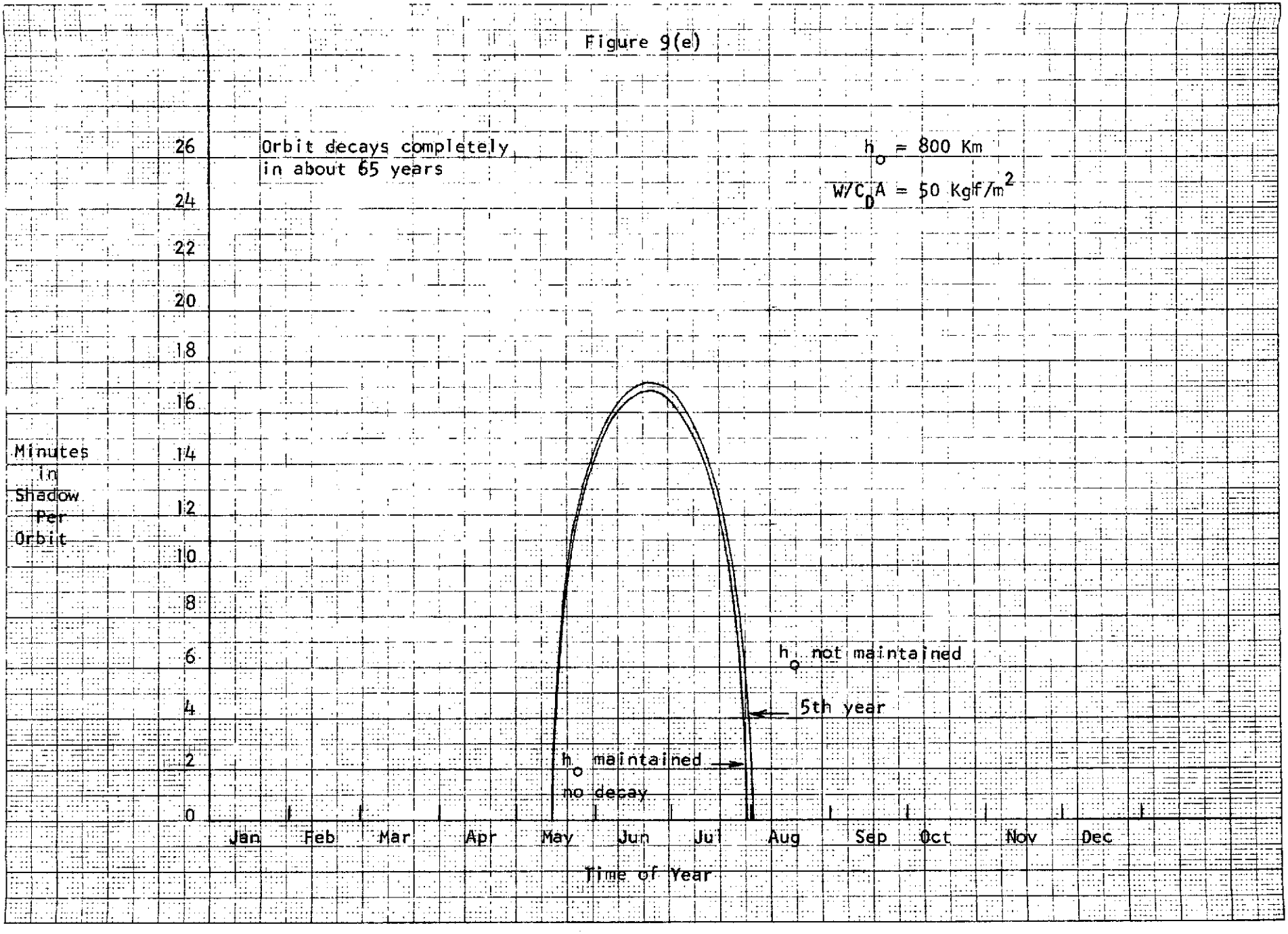
Orbit decays completely in about 65 years
h_o = 800 Km
$W/C_D A$ = 50 Kgf/m^2
Minutes in Shadow Per Orbit
26
24
22
20
18
16
14
12
10
8
6
4
2
0
h_o not maintained
5th year
h_o maintained
no decay
Jan
Feb
Mar
Apr
May
Jun
Jul
Aug
Sep
Oct
Nov
Dec
Time of Year

Figure 10 - Velocity Requirements for Orbit Sustaining Using Continuous Electric Propulsion

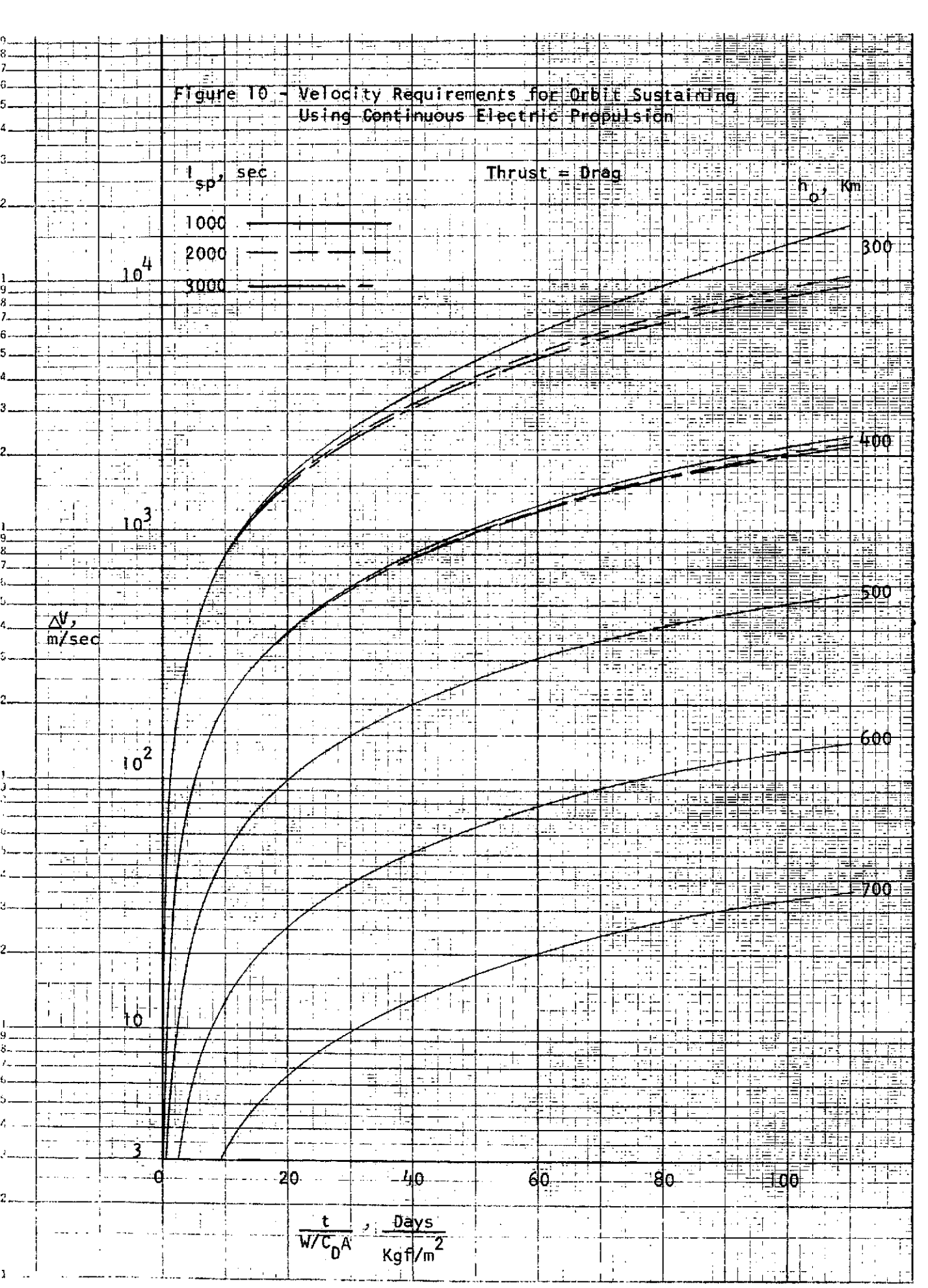

Figure 11 - Thrust and Propellant Required for Drag Cancellation (Continuous Thrusting)

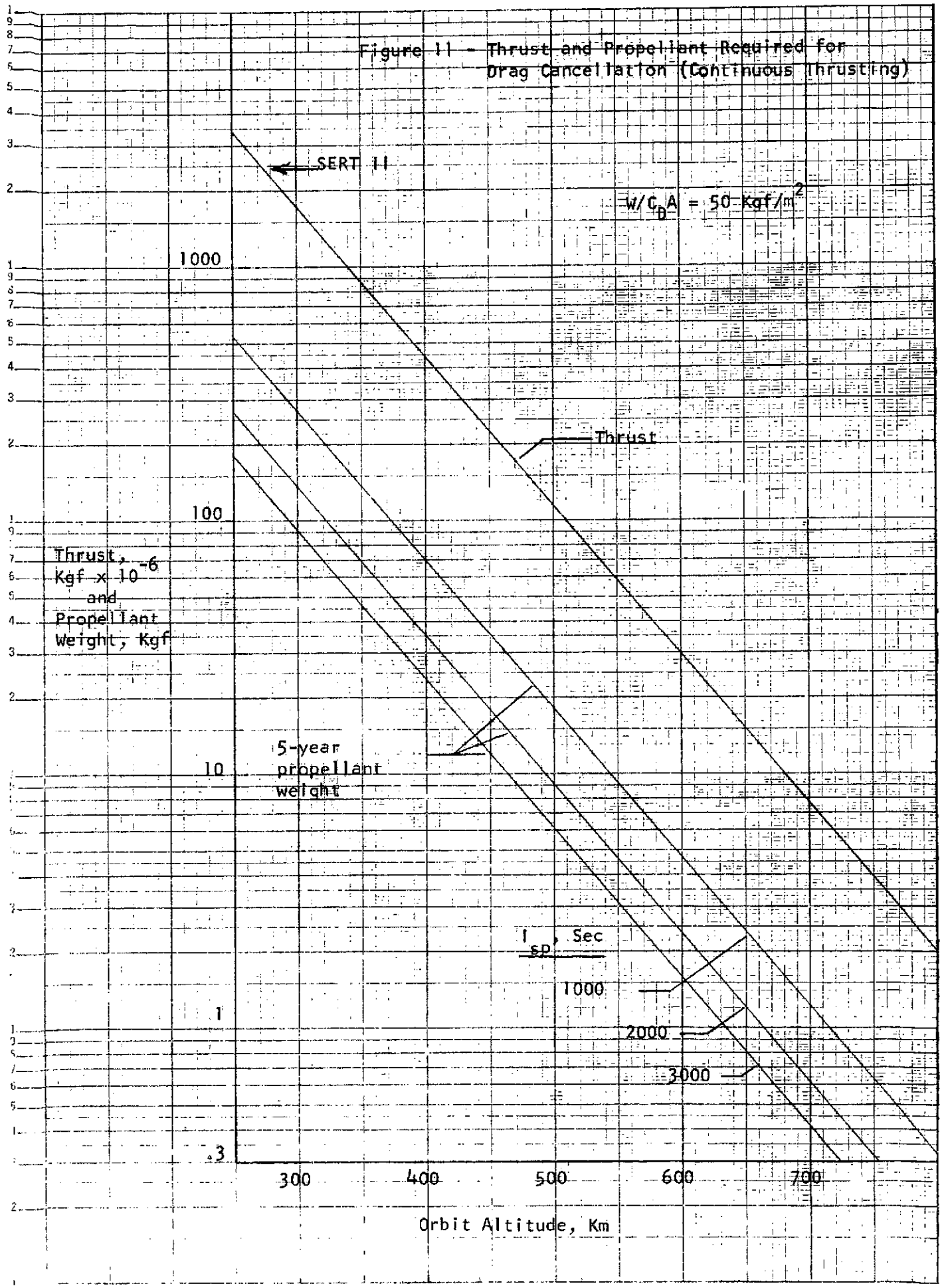

Figure 12(a) - Velocity Requirements for Orbit Sustaining Using Impulsive Thrust Hohmann Transfers

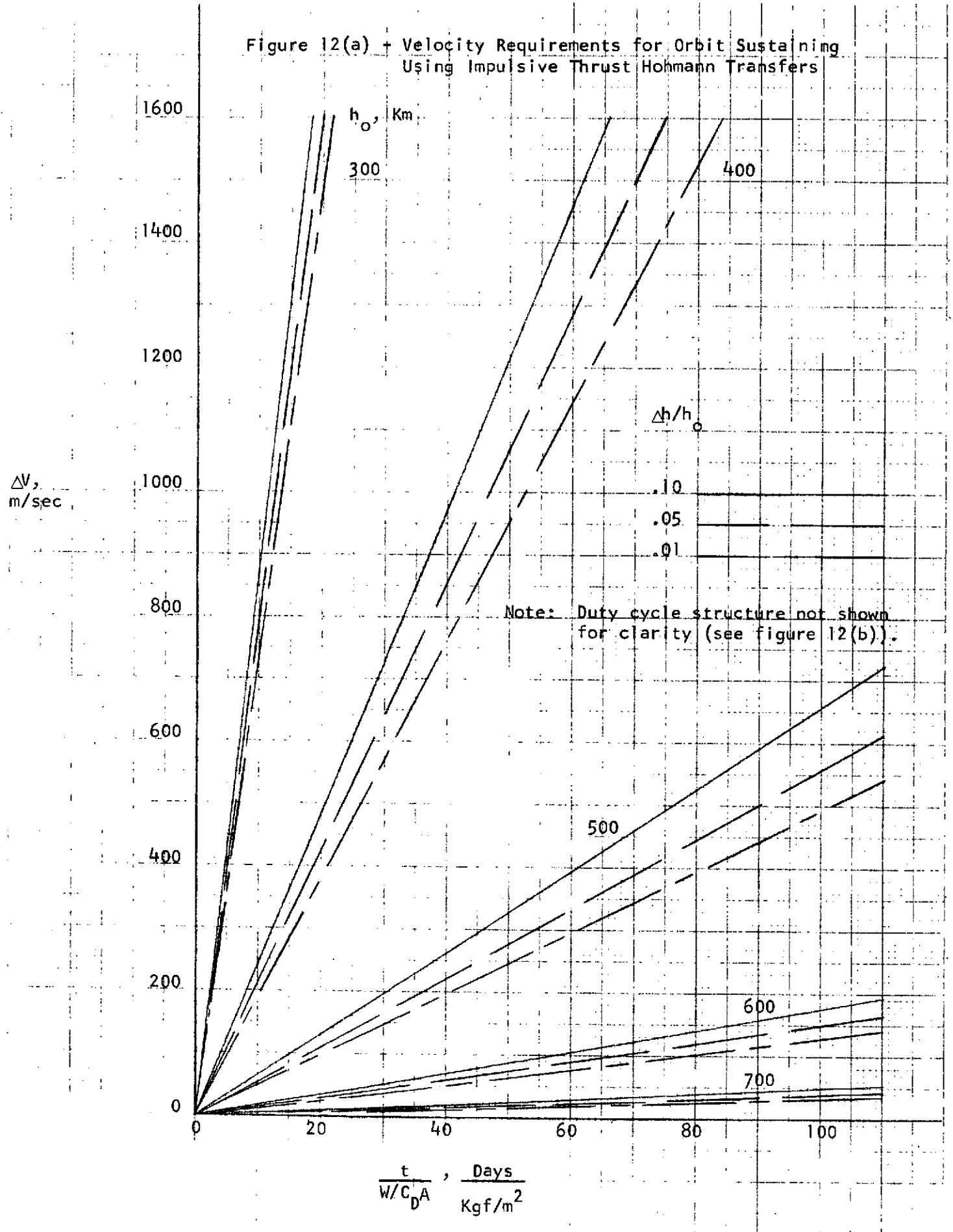

Figure 12(b) – Duty Cycle for Orbit Sustaining Using Impulsive Thrust Hohmann Transfers

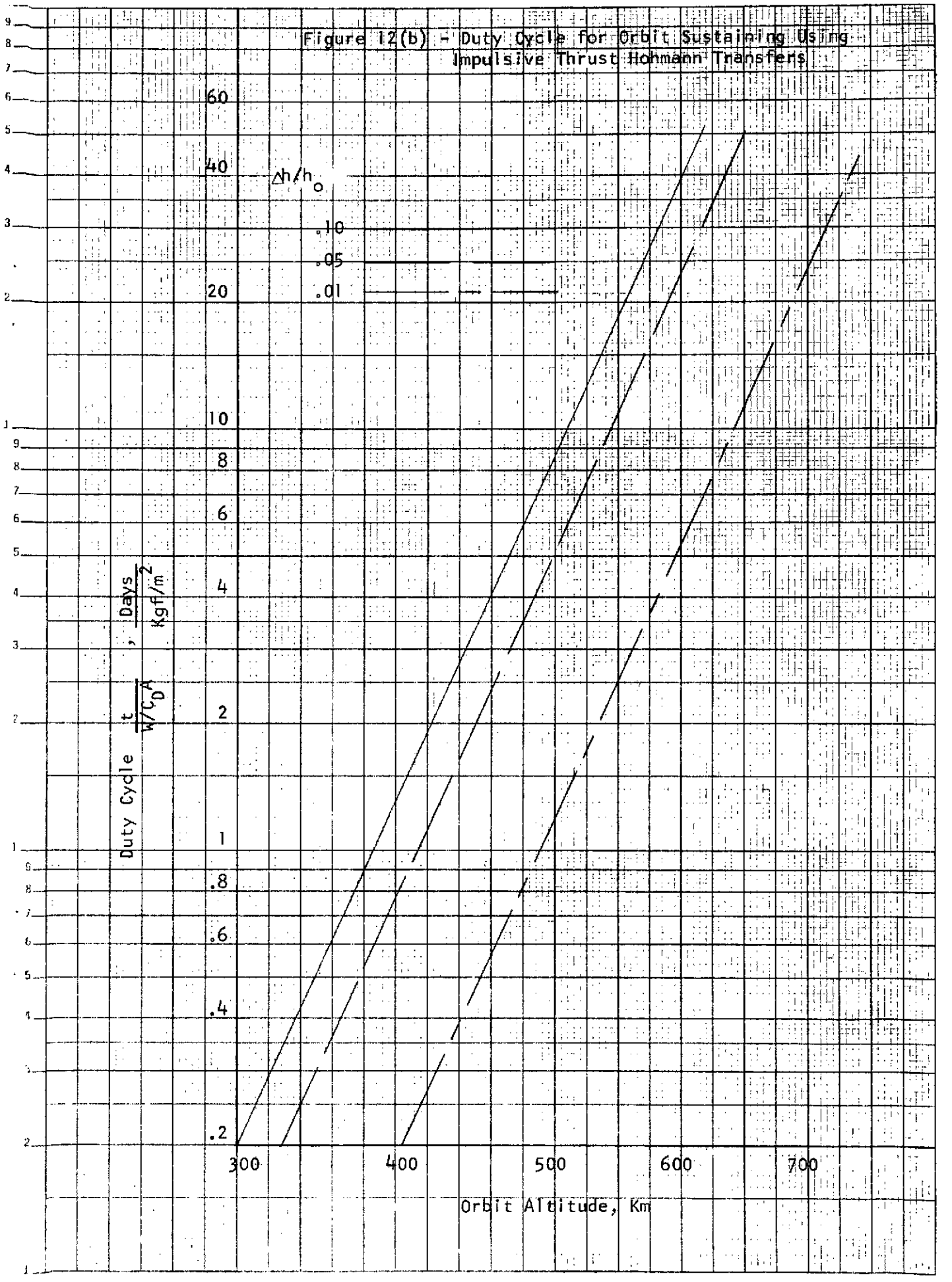

Figure 13 - Propellant Weight Required for Drag Cancellation (Impulsive Thrusting)

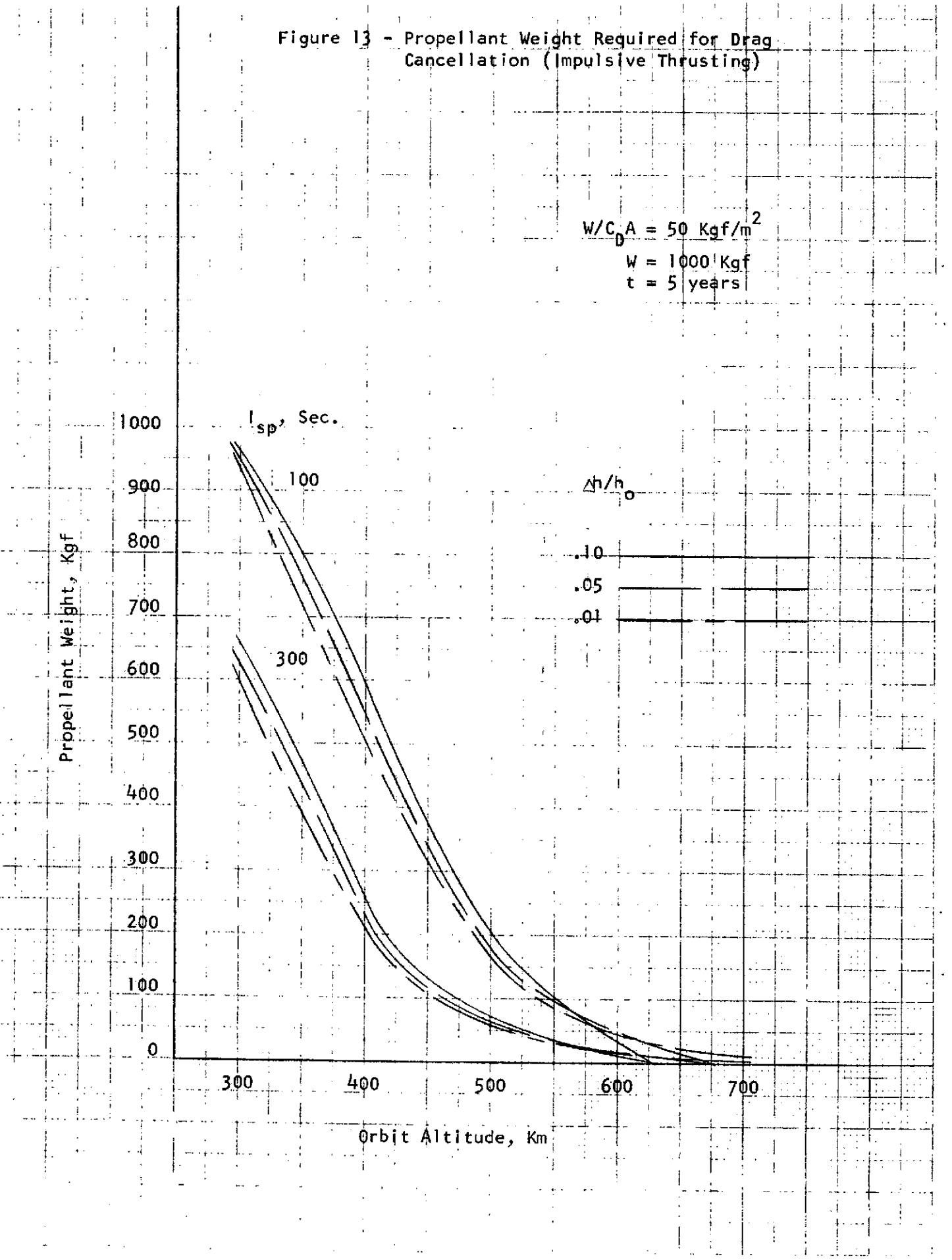

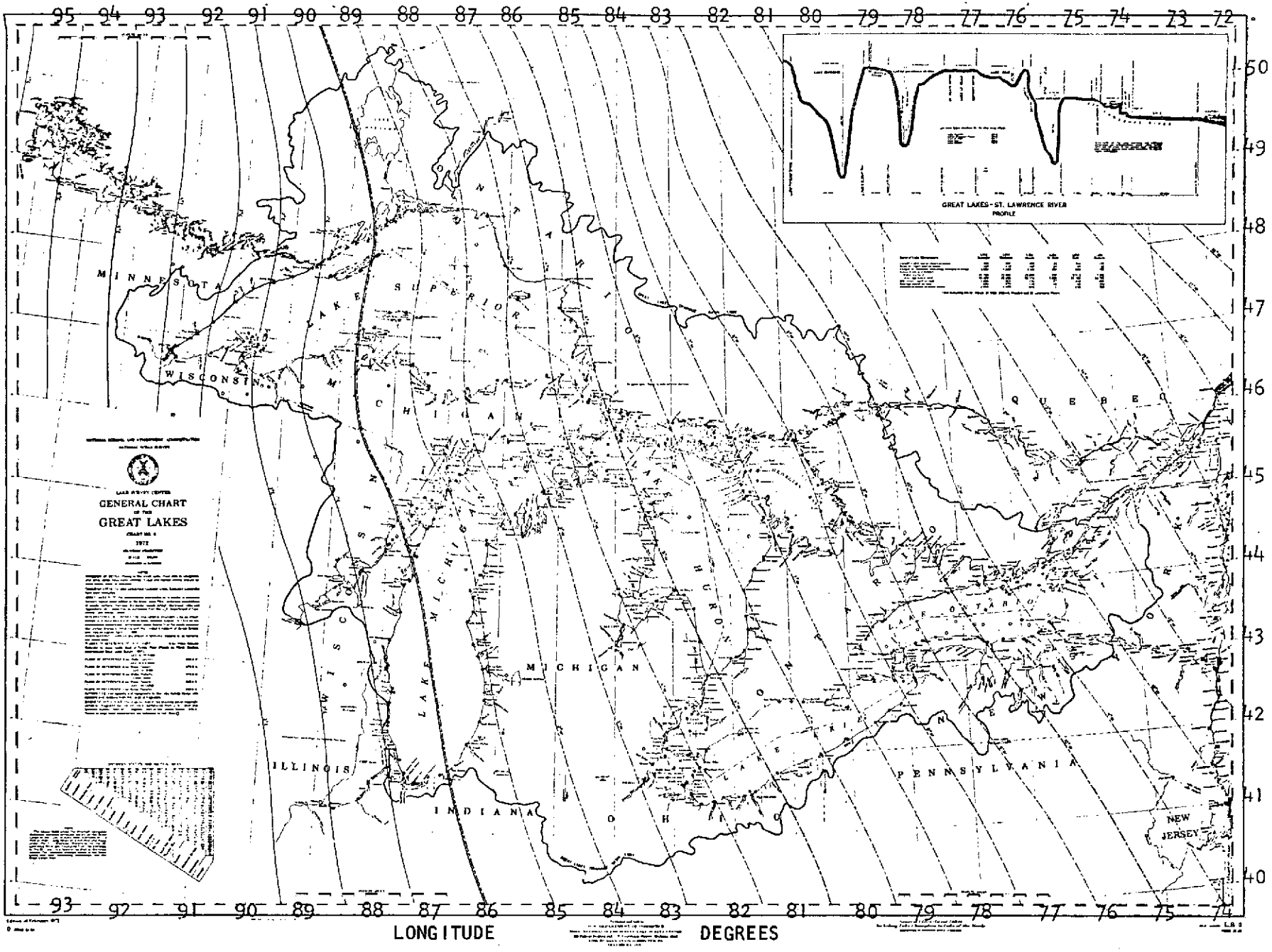

Figure 14 - Chart of the Great Lakes

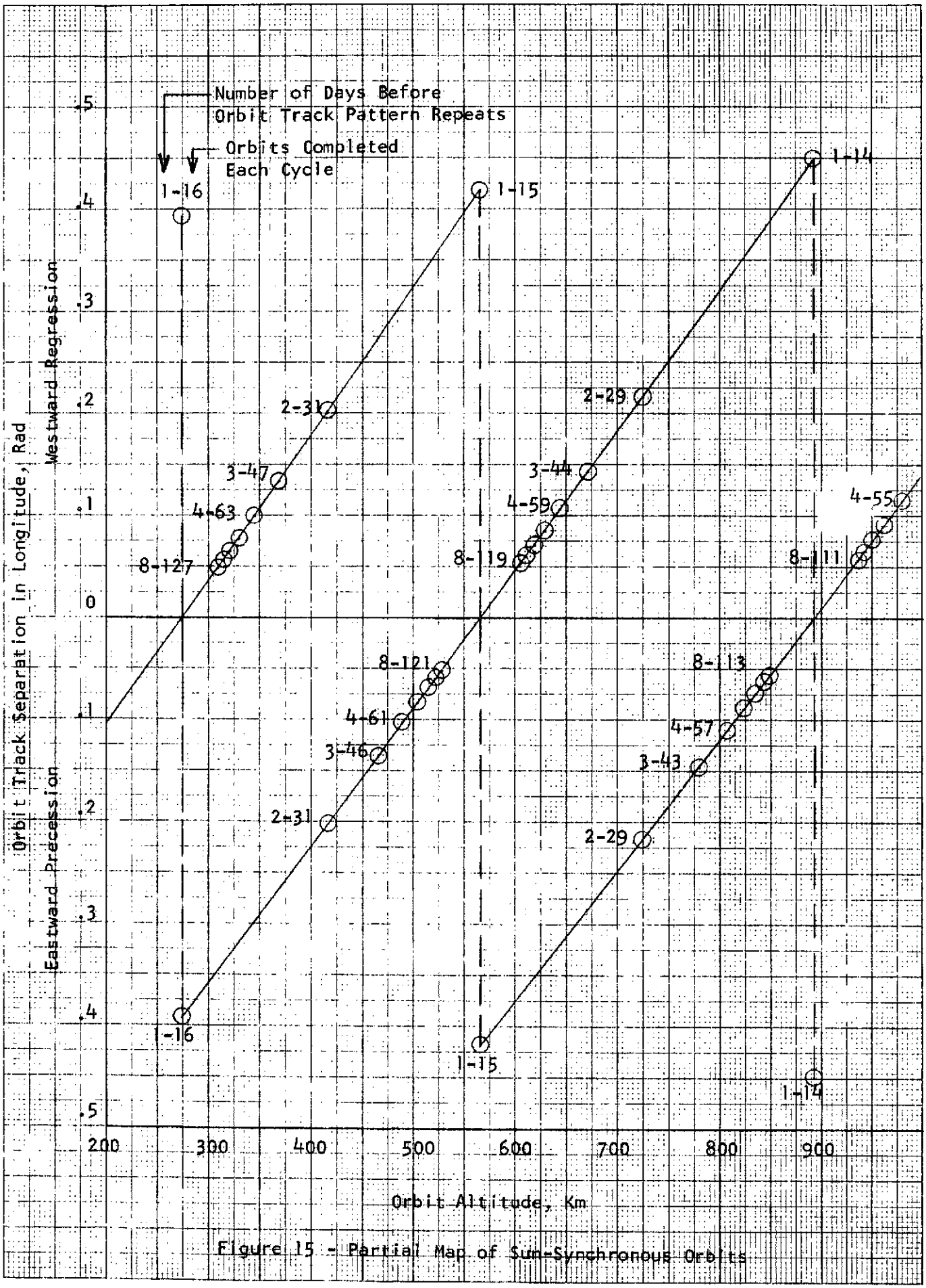

Figure 15 - Partial Map of Sun-Synchronous Orbits

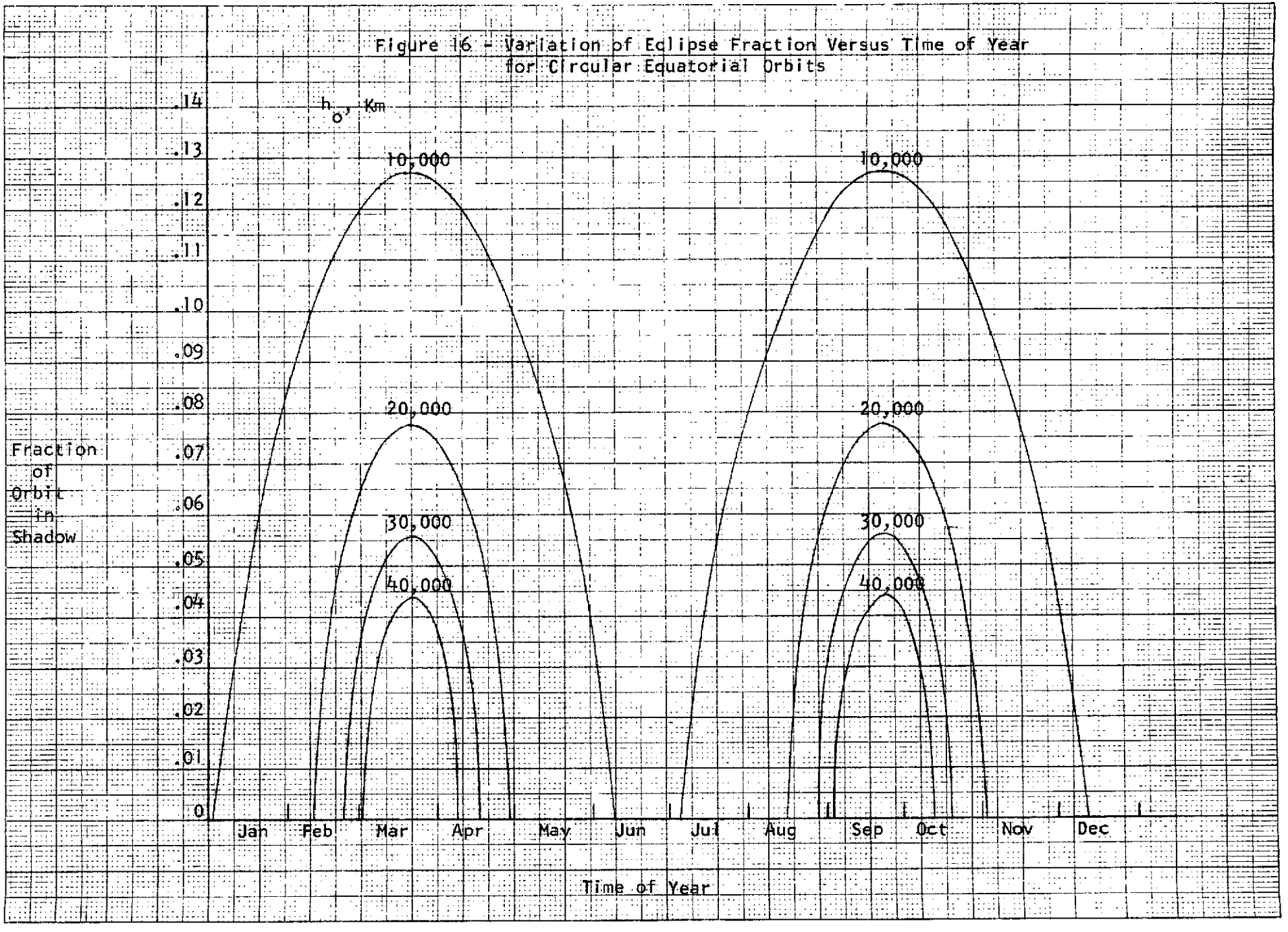
Figure 16 - Variation of Eclipse Fraction Versus Time of Year for Circular Equatorial Orbits
h_o, Km
10,000
20,000
30,000
40,000
10,000
20,000
30,000
40,000
Fraction of Orbit in Shadow
.14
.13
.12
.11
.10
.09
.08
.07
.06
.05
.04
.03
.02
.01
0
Jan
Feb
Mar
Apr
May
Jun
Jul
Aug
Sep
Oct
Nov
Dec
Time of Year

Figure 17 - Relative Velocity of Satellite in Equatorial Orbit with Respect to Earth's Surface

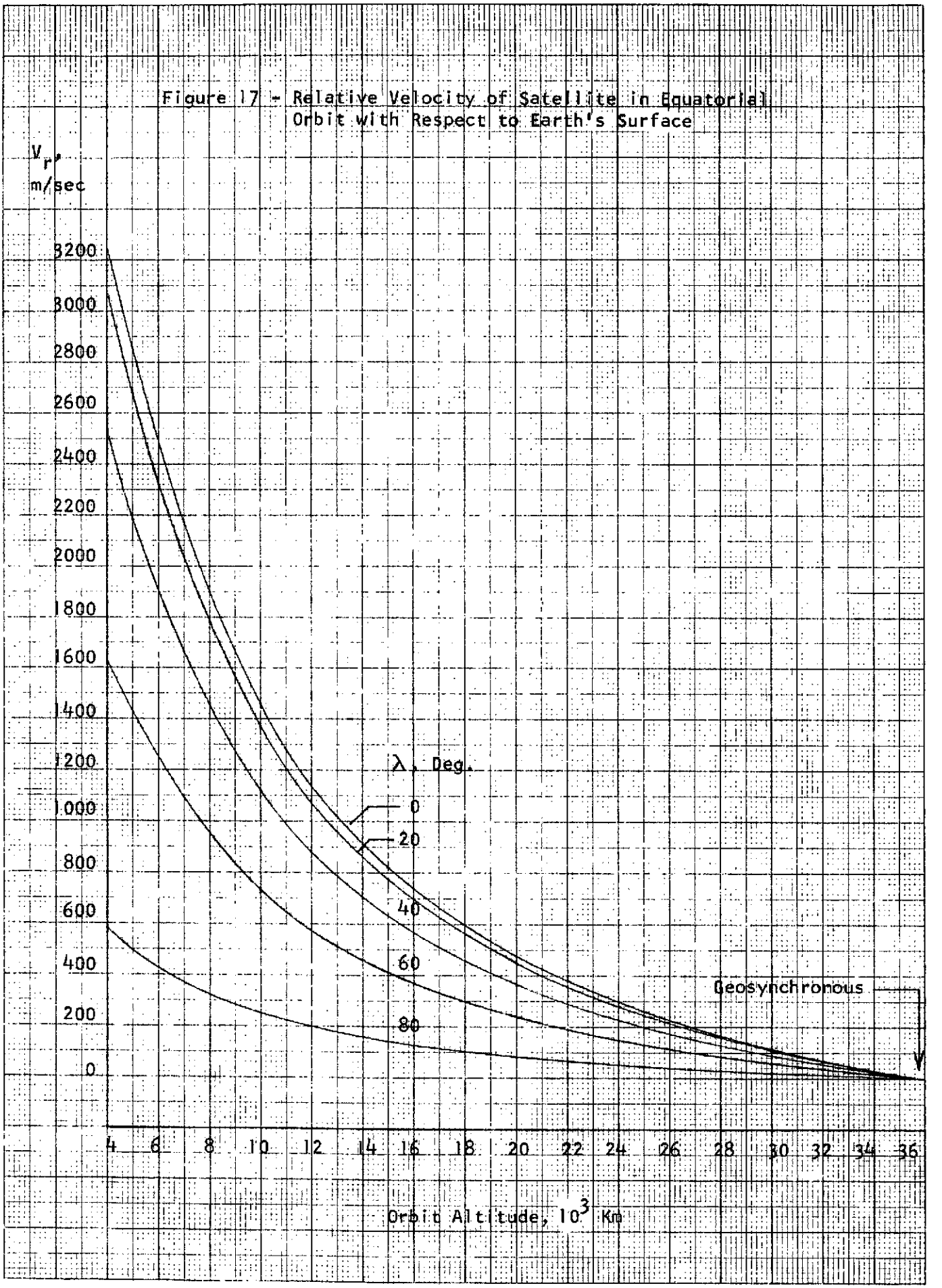

Figure 18 - Variation of Number of Target Passes Per Day Versus Altitude for a Satellite in Equatorial Orbit

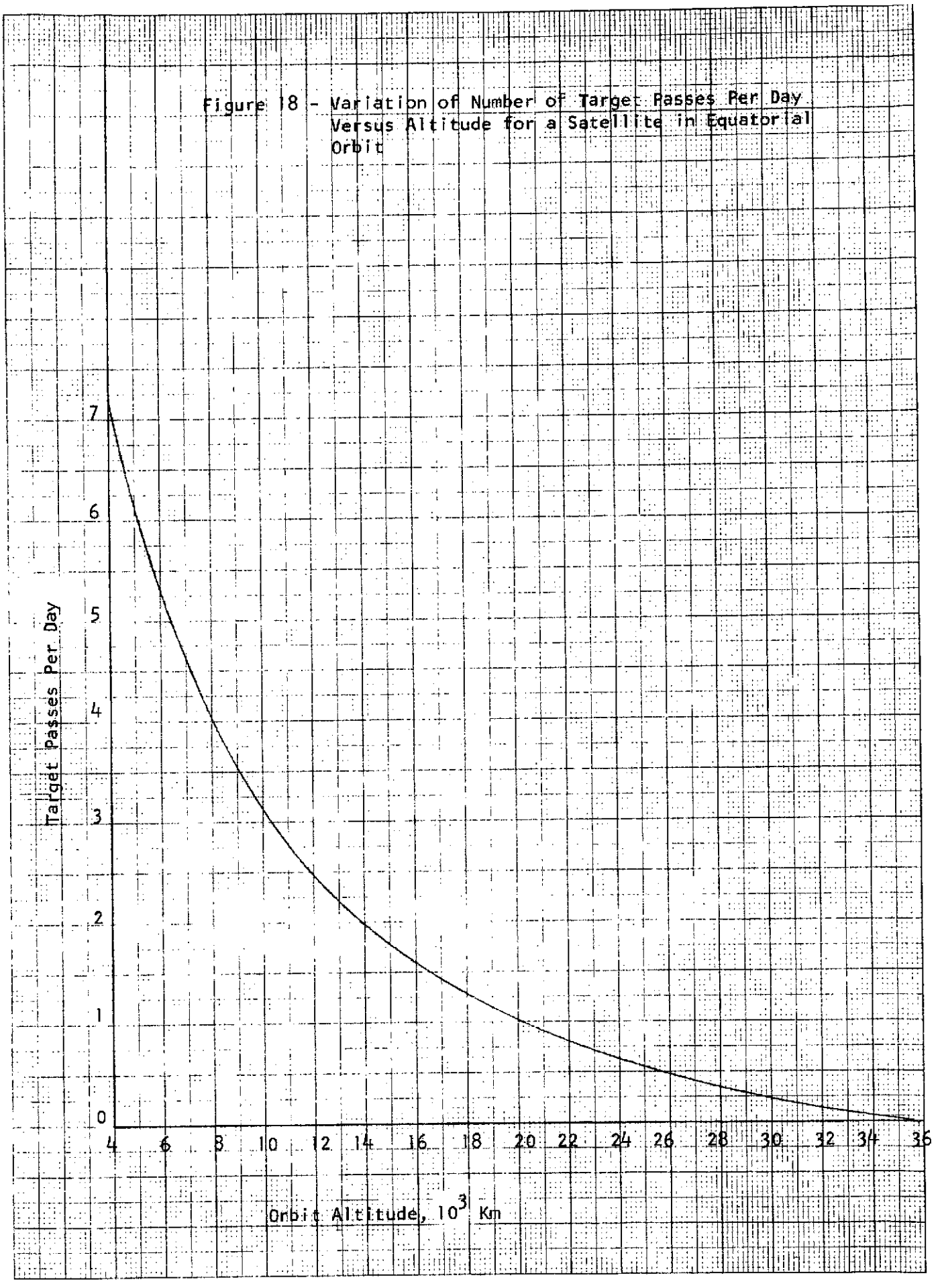

Figure 19 - Incident Angle with Earth's Surface of Radar Beam in Meridional Direction from Satellite in Equatorial Orbit

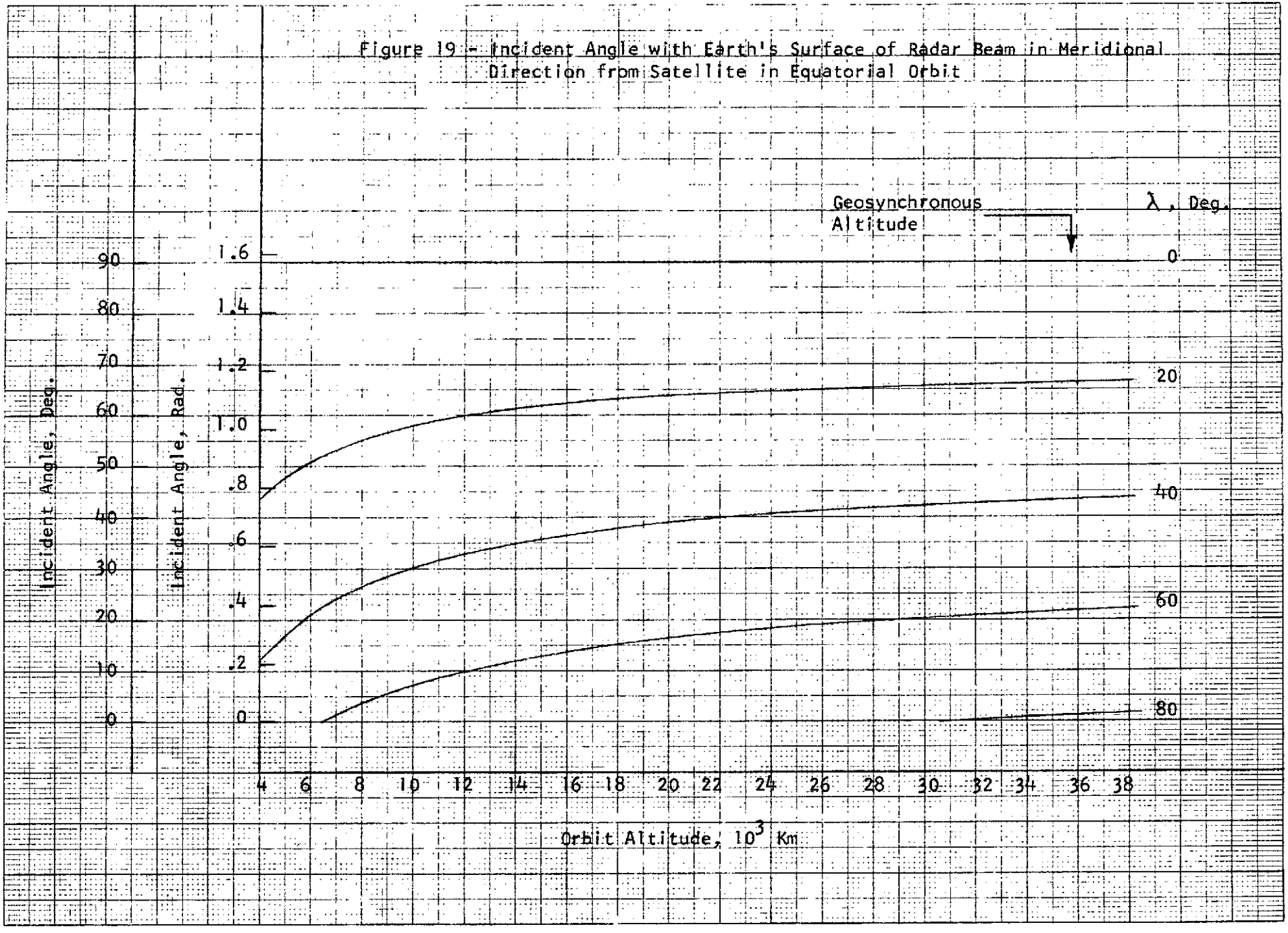

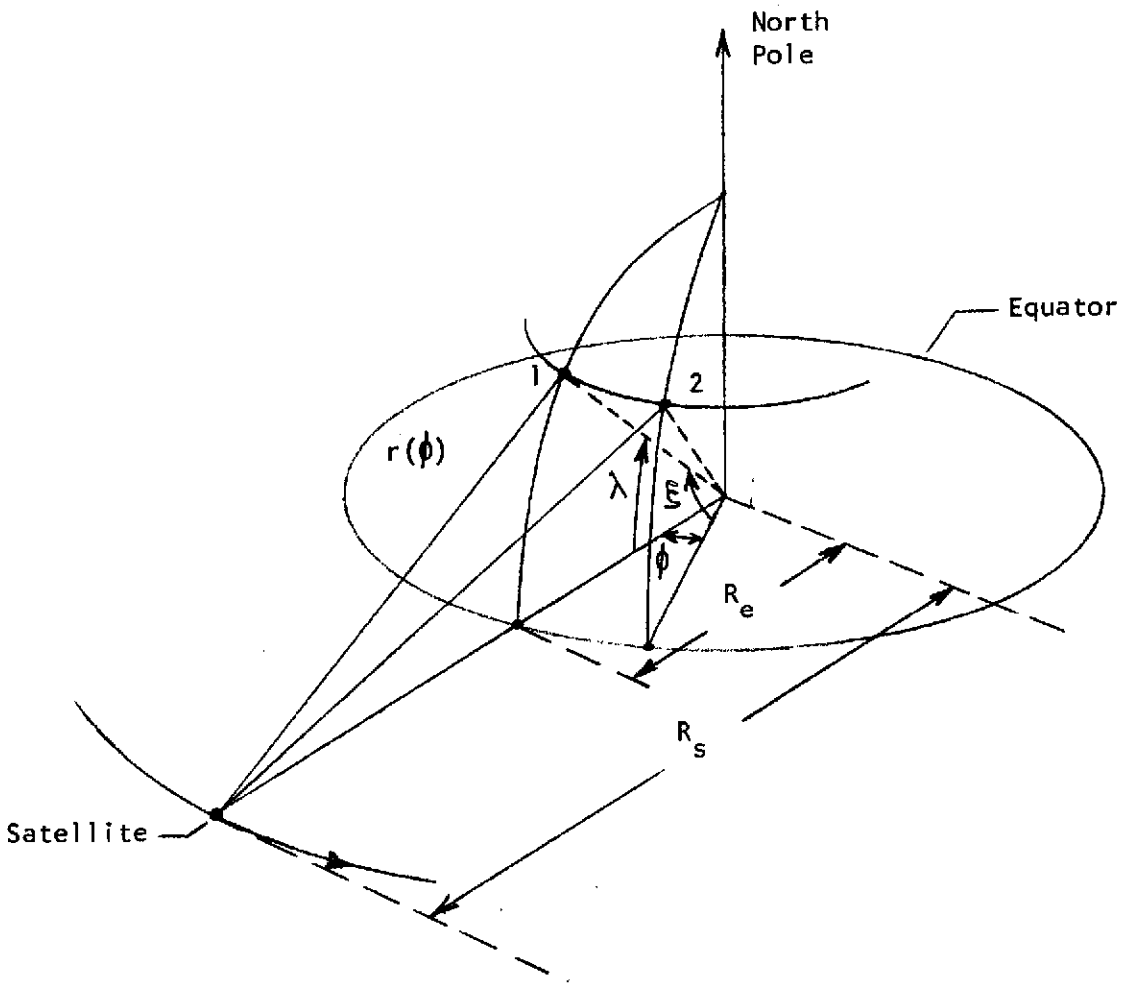

Figure 20 - Geometry of Distance from Satellite to Earth Target Point

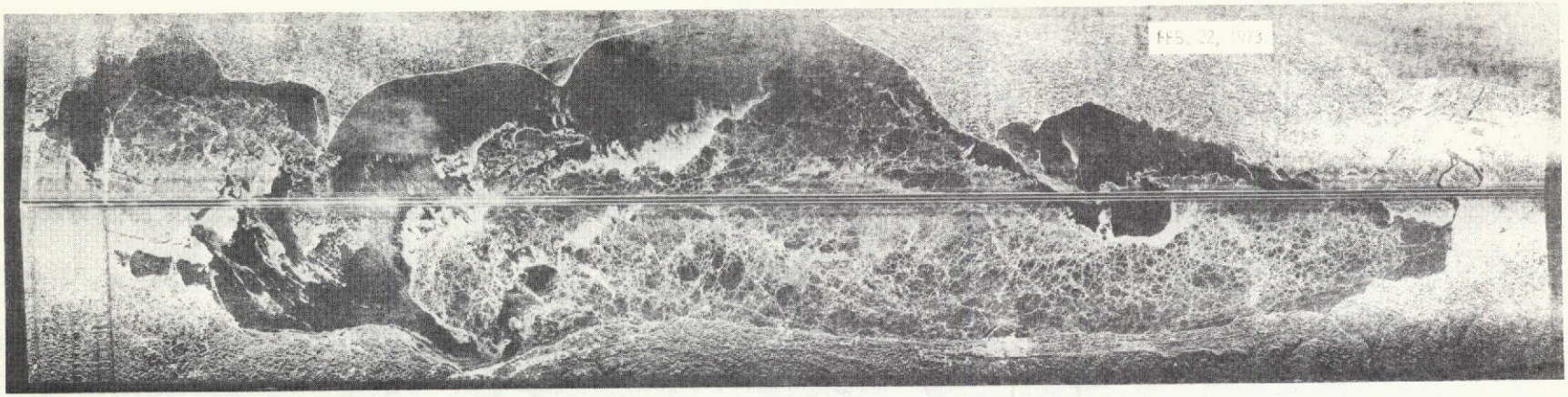

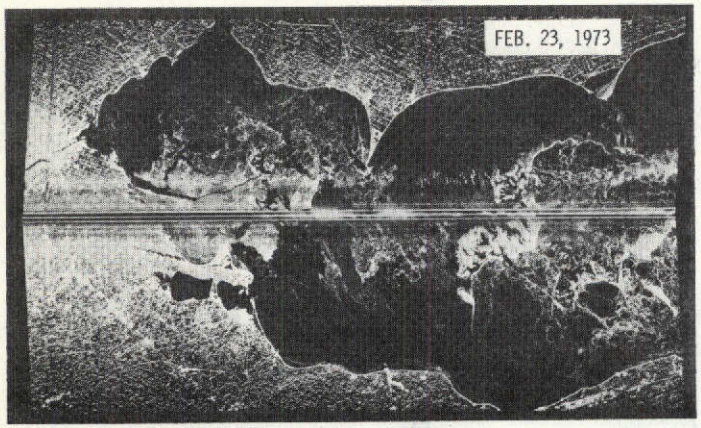

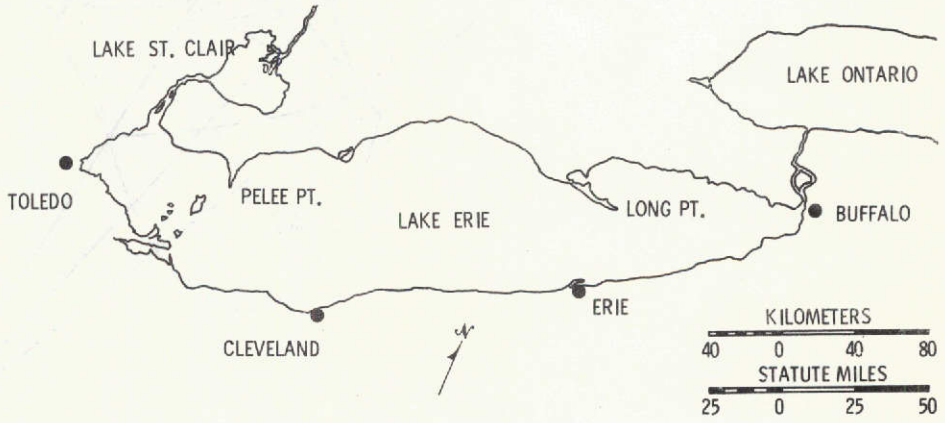

CS-68693

Figure 21. - Radar images of Lake Erie ice cover on February 22 and 23, 1973. Time of flight over the lake was approximately 70 minutes. The center line of the image is the blind ground track of the aircraft.

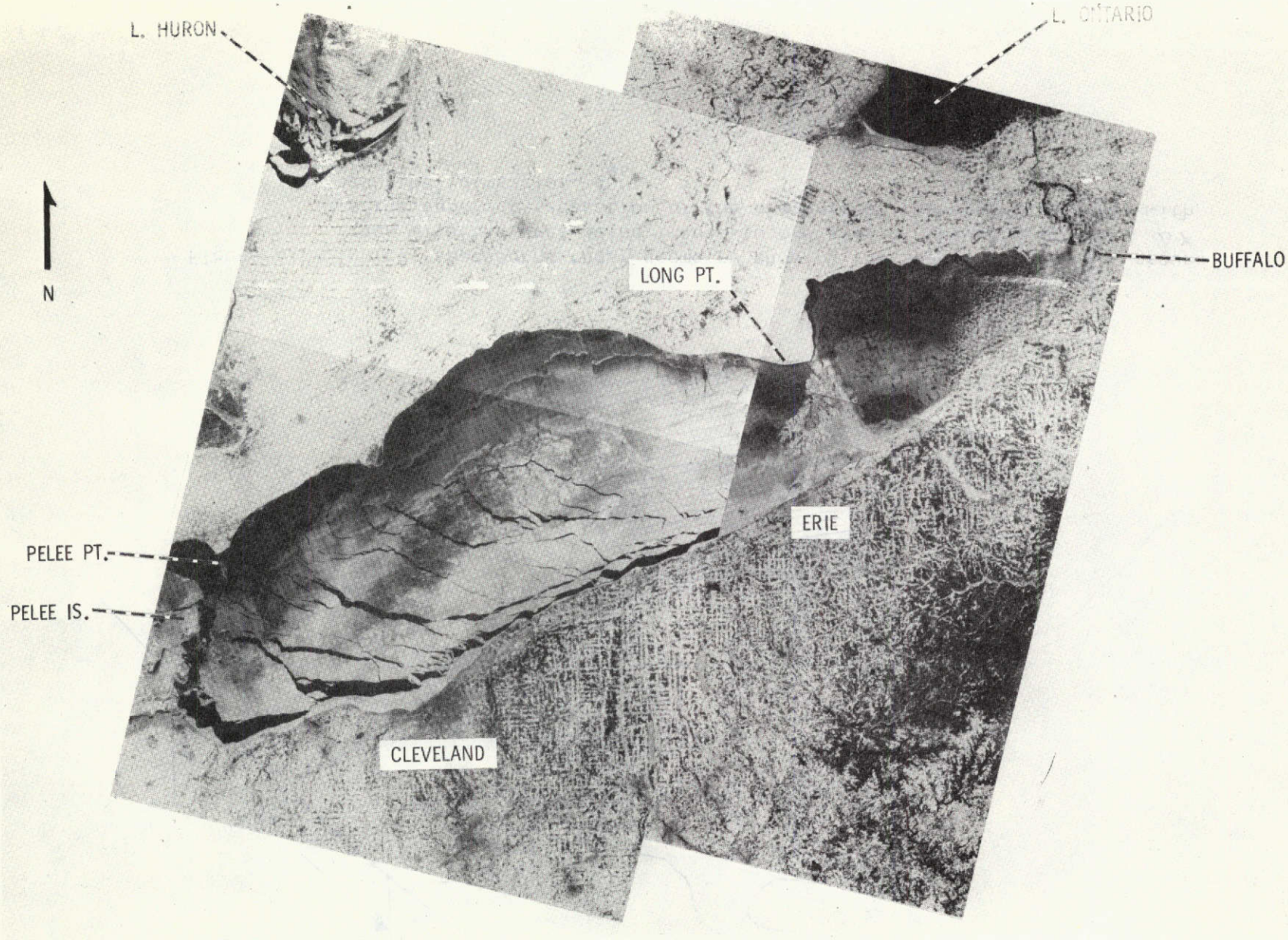

Figure 22. Photomosaic of ERTS-1 satellite imagery from band 4 showing Lake Erie ice cover on Feb. 17 (eastern basin) and Feb. 18, 1973 (central basin). Note the ice movement that occurred in one day along the southern shore.

CS-68689

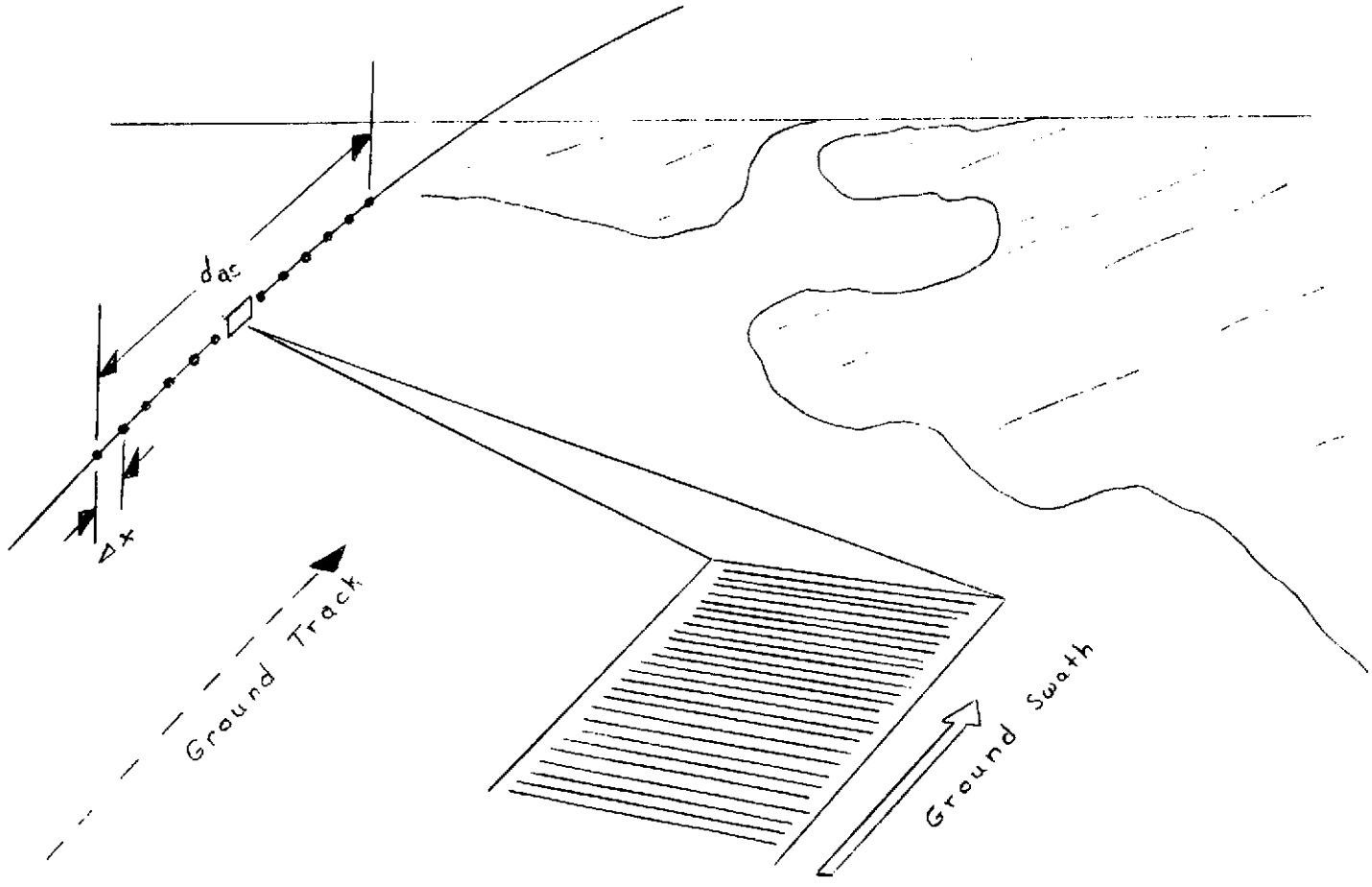

Figure 23 - Typical spaceborne radar geometry showing the spacecraft and its ground track with the area being imaged to one side of the ground track. ΔX is the apparent separation of the elements of the synthetic array with azimuthal dimension, d_{as}.

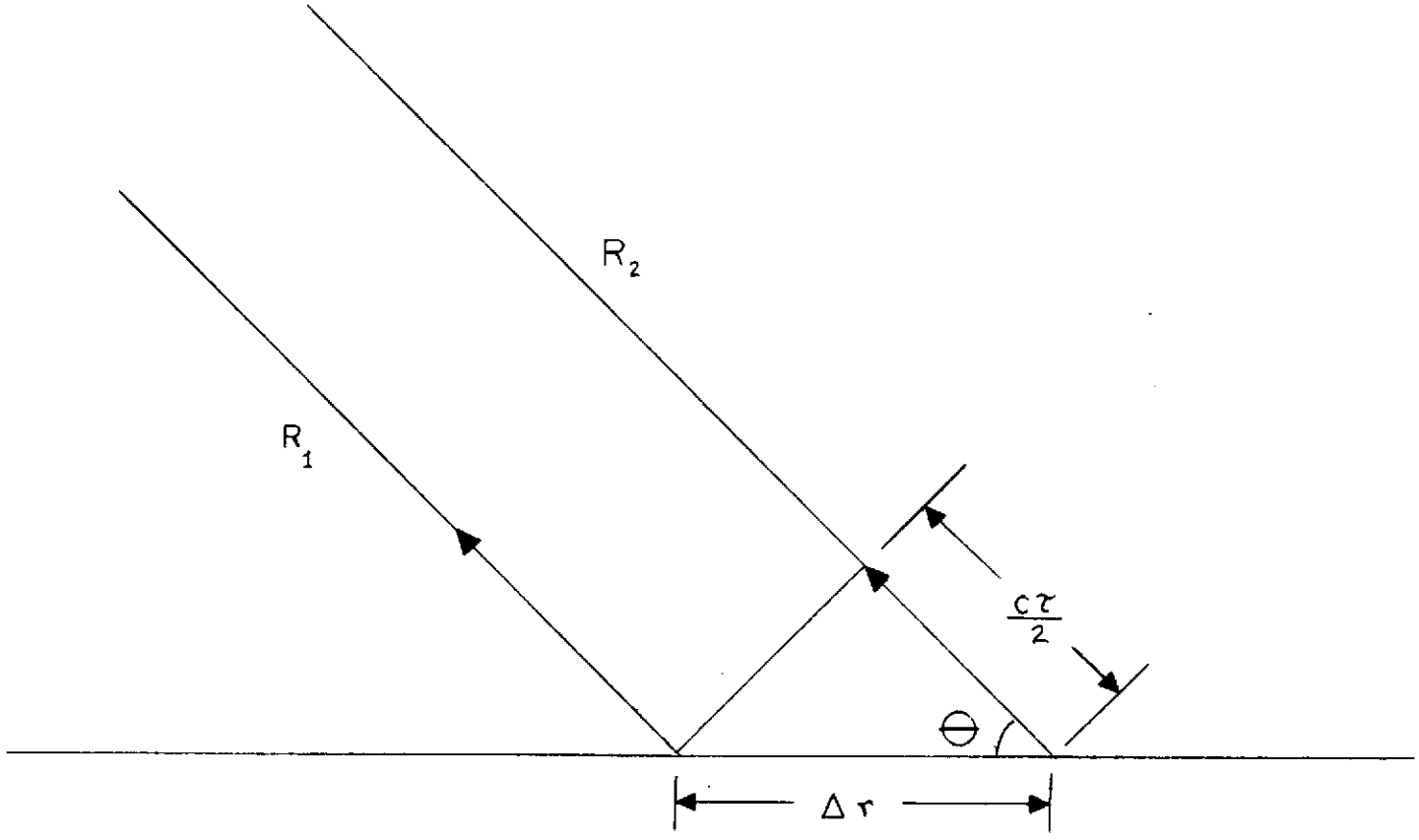

Figure 24 - Geometry showing relationship between incidence angle, θ , pulse width, τ , and range resolution on ground, Δr .

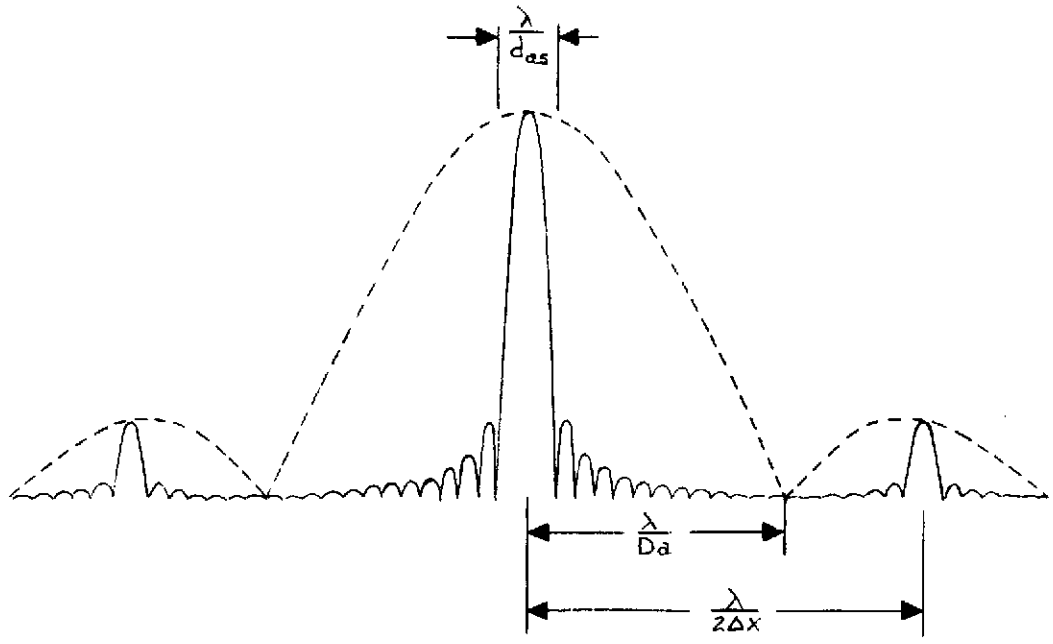

Figure 25 - Overall receive pattern for a typical synthetic array. The dotted contour is the real antenna pattern and the solid contour is the resultant pattern after synthesis.

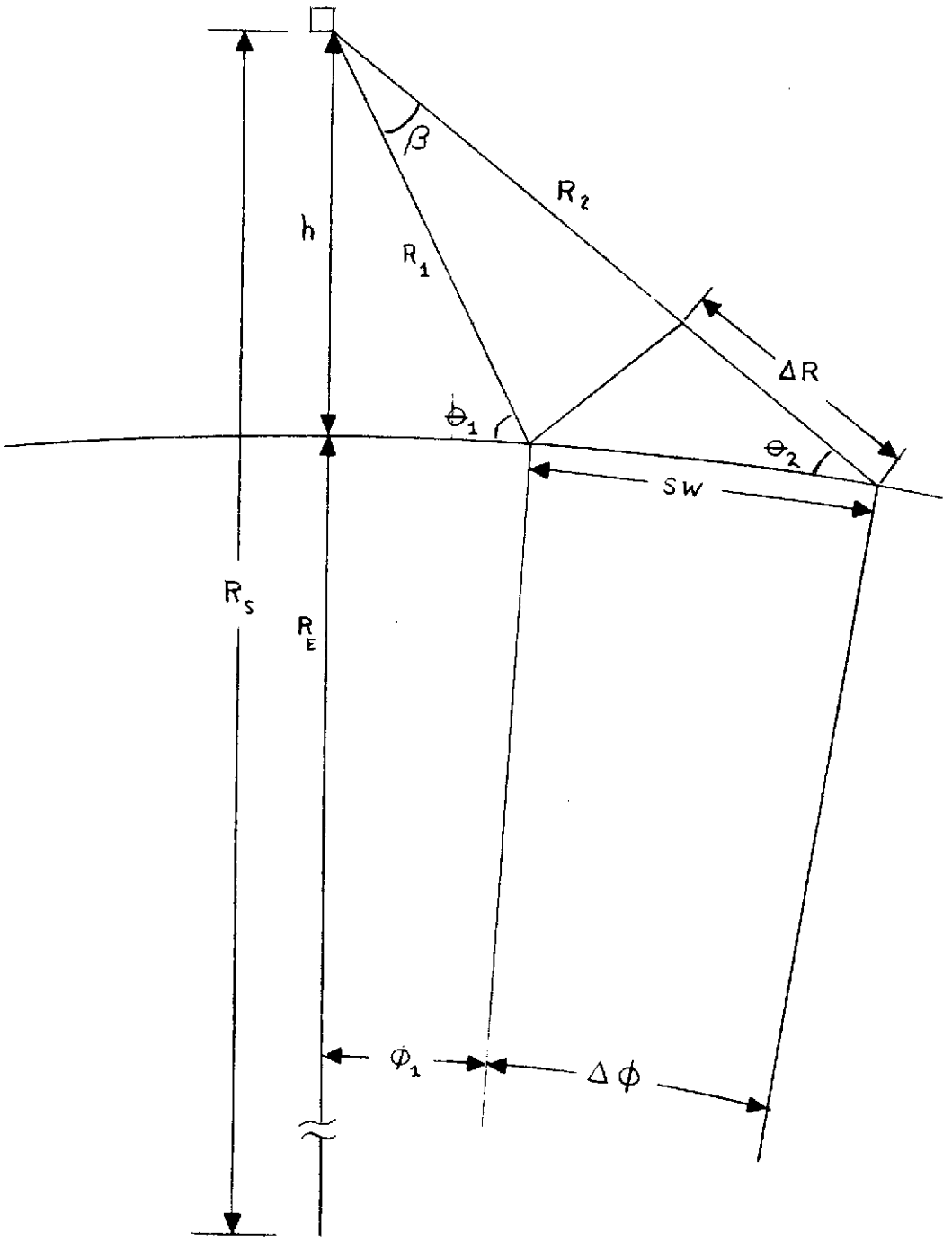

Figure 26 - Orbital geometry for SAR showing unambigious range interval, ΔR, the resultant swath width and required beam width, SW and β, the equivalent increment in longitude or latitude, $\Delta\phi$, for a particular incidence angle θ_1, θ_2 and altitude h. R_E is the earth's radius and R_S is the orbital radius.

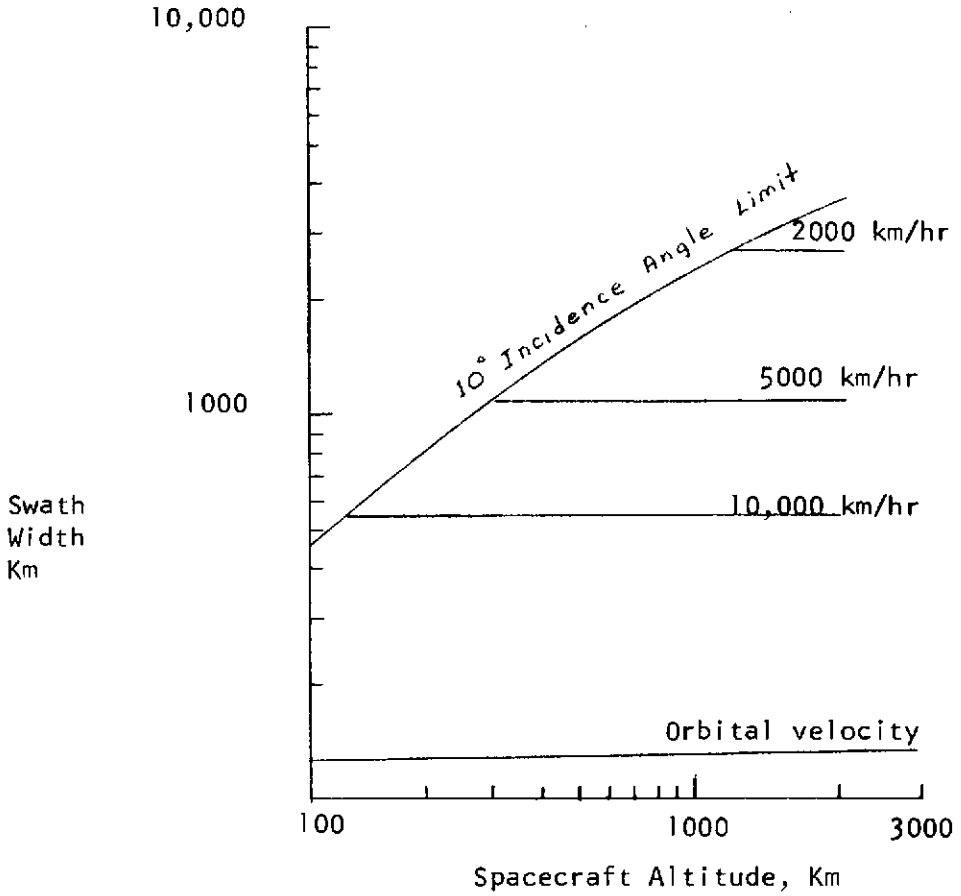

Figure 27 - SAR swath width as a function of SAR altitude with SAR velocity as a parameter.

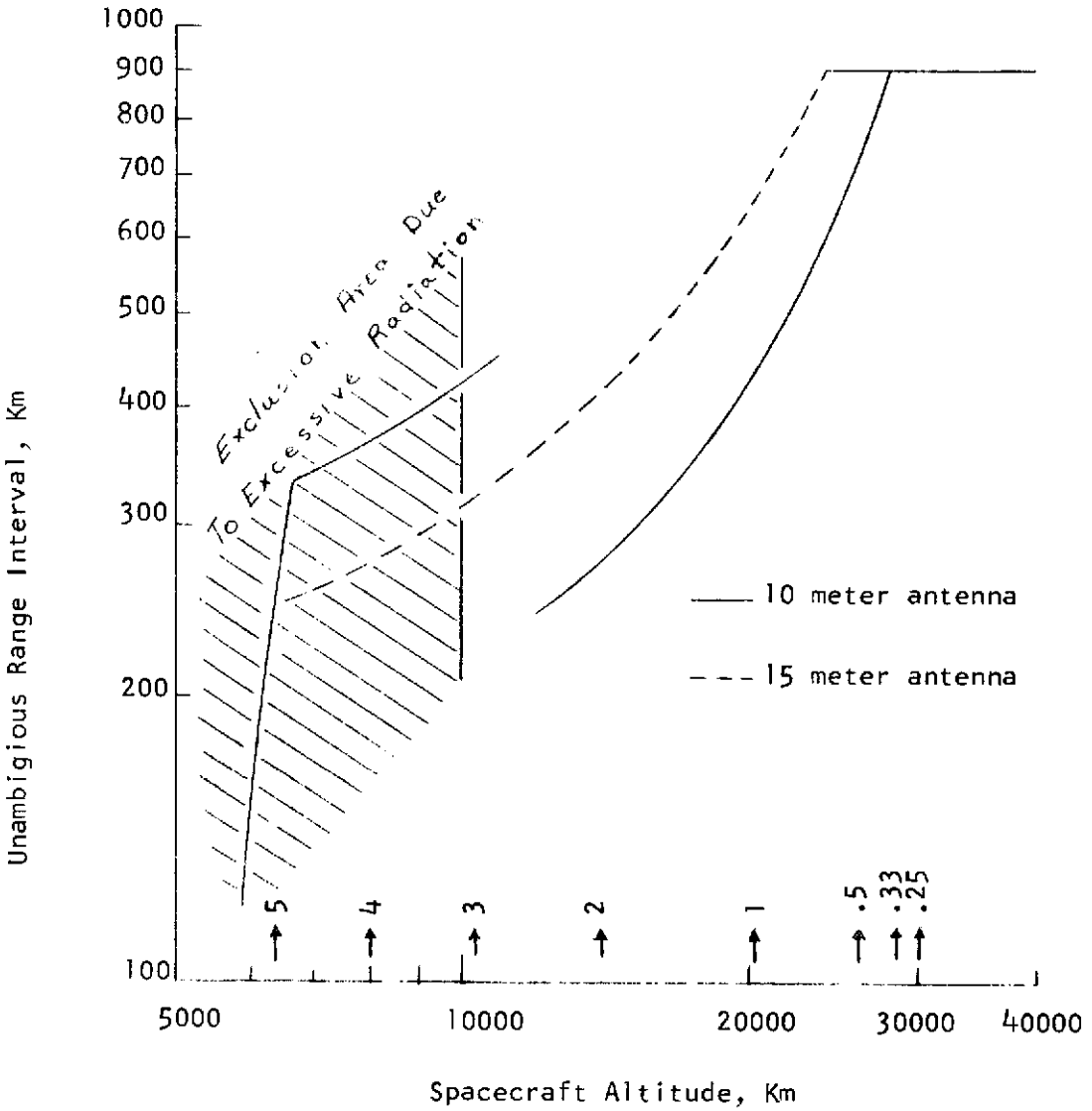

Figure 28 - Unambigious range interval versus spacecraft altitude for X band SAR in equatorial orbit. Target latitude 48° Maximum interval was fixed at 900 km to span the Great Lakes. Also shown are the number of passes daily over this target.

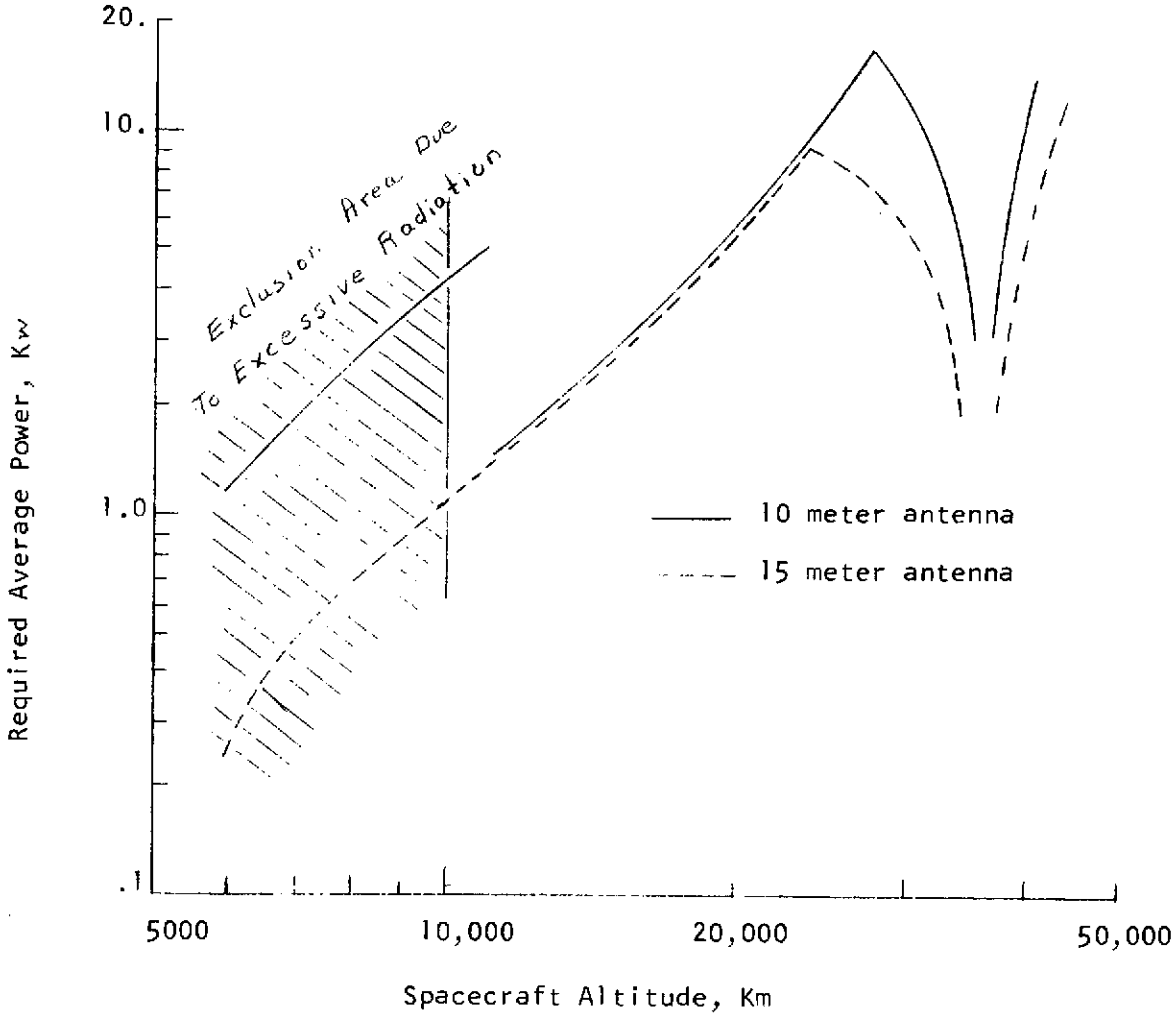

Figure 29 - Required average power versus orbit altitude for X band SAR in equatorial orbit. Target latitude 48°.

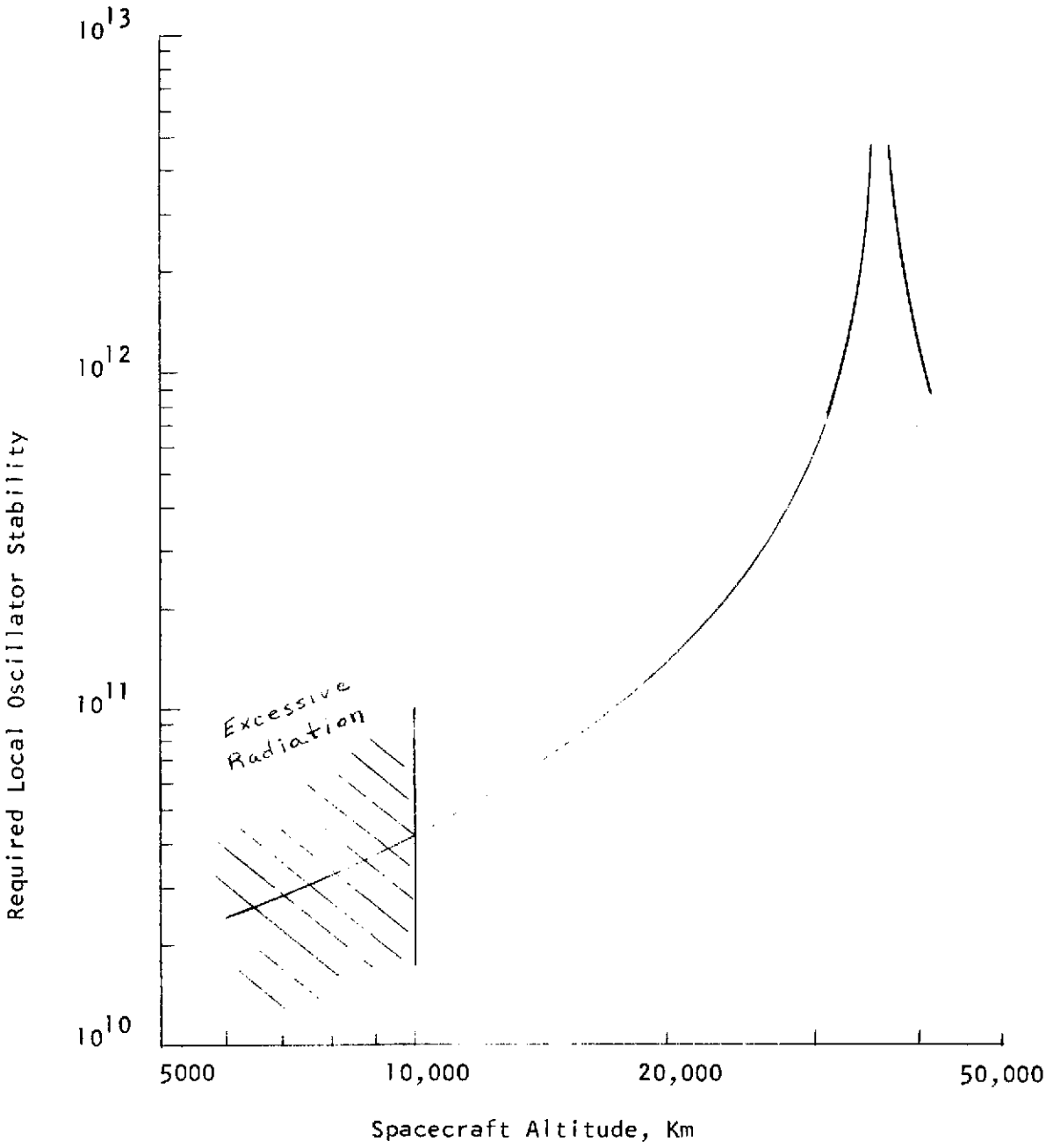

Figure 30 - Required local oscillator stability versus spacecraft altitude for X band SAR in equatorial orbit. Target latitude 48°.

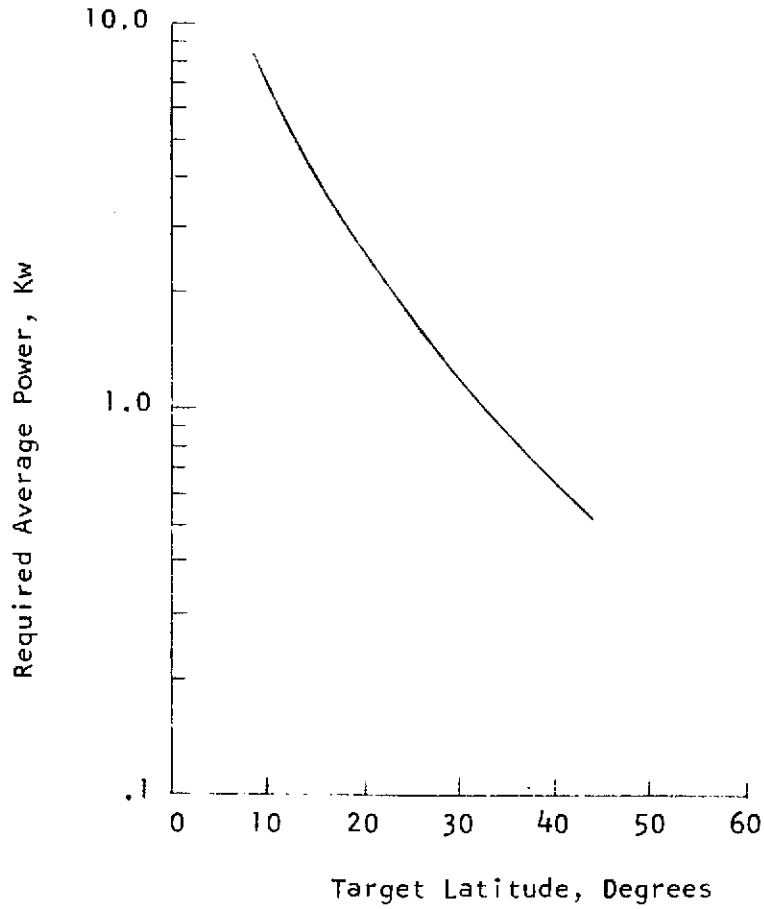

Figure 31 - Required average power to utilize full unambigious range interval for X band SAR at 6400 Km equatorial orbit versus target latitude.

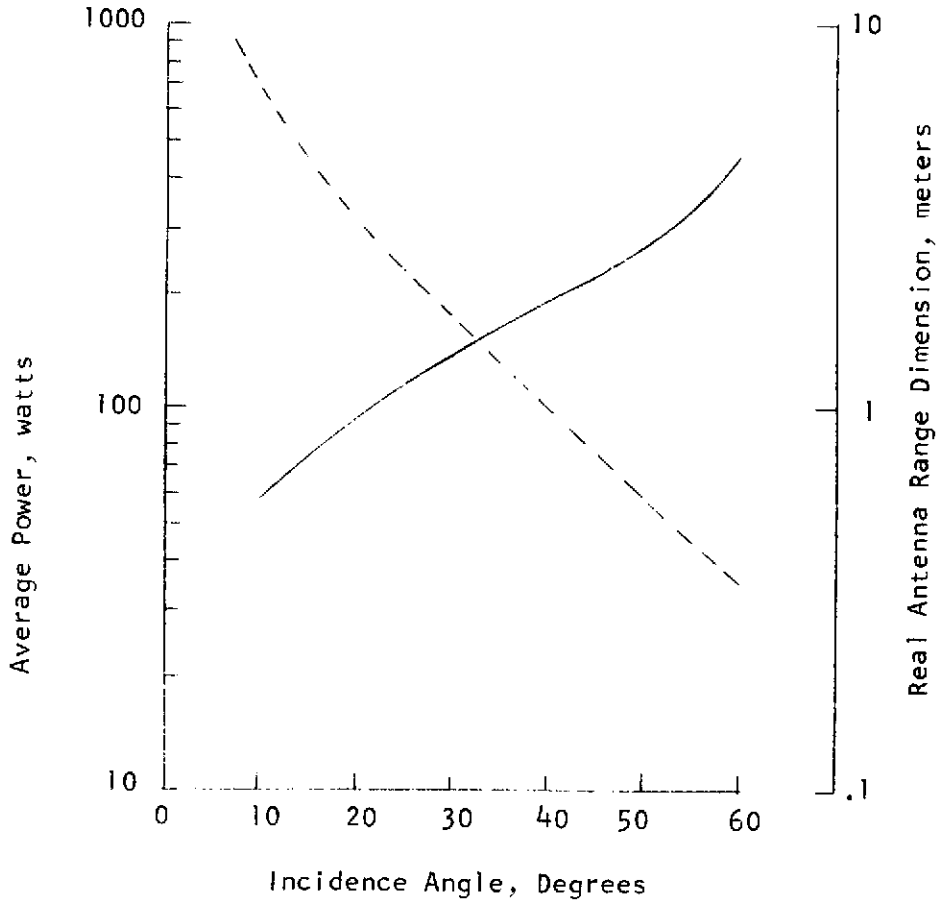

Figure 32 - Required average power and antenna range dimension for X band SAR in 1000 km altitude polar orbit as a function of incidence angle.

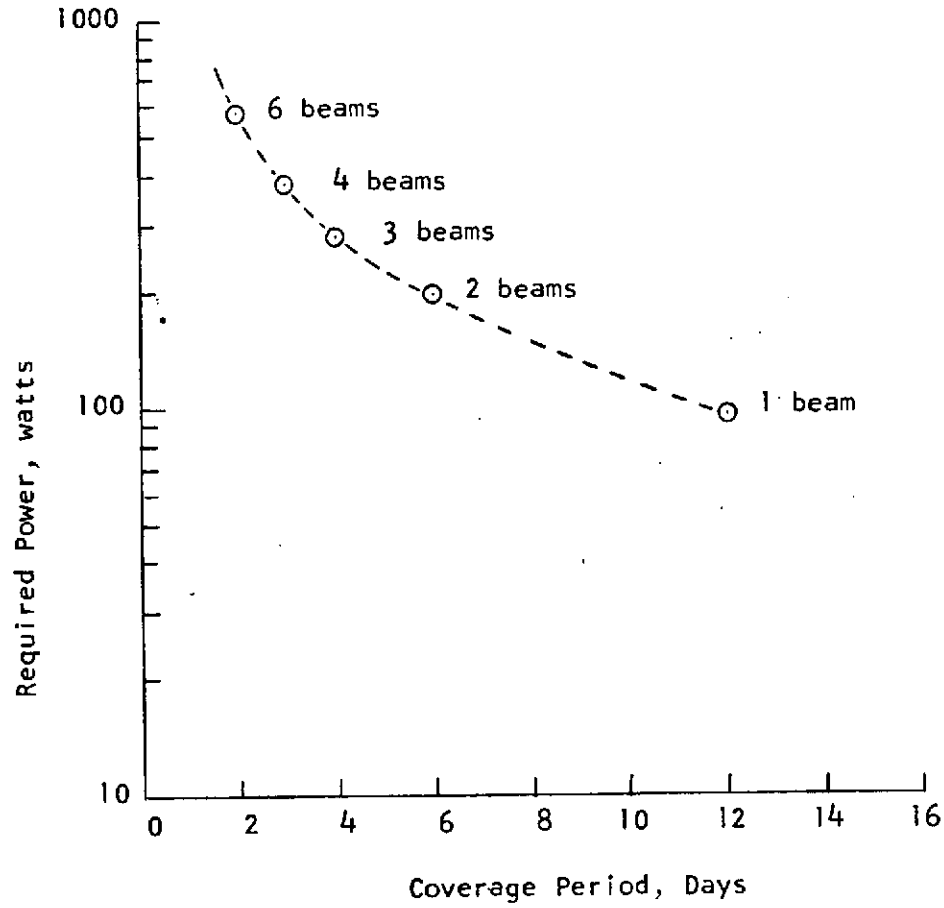

Figure 33 - Required average power for X band SAR in 1000 km polar orbit versus coverage period. Powers are approximate only. Mean incidence angle 20°.